International Atomic Energy Agency

INDC(CCP)-16/L

INDC INTERNATIONAL NUCLEAR DATA COMMITTEE

COLLECTION OF USSR REPORTS ON NUCLEAR DATA TOPICS

Compiled by the IAEA
Nuclear Data Section

July 1971

IAEA NUCLEAR DATA SECTION, KÄRNTNER RING 11, A-1010 VIENNA

PREFACE

This document contains six translations of USSR reports on reactor theory and nuclear data topics, some of which have been presented at the British-Soviet Seminar on Nuclear Constants for Reactor Calculations held in June 1968 at Dubna, and at the Dutch-Belgian-Soviet Seminar held at Melekess in February 1970. This document does not presume to represent the proceedings of these two meetings. It is hoped that the methods of treating resonance self-shielding for fast reactors and of comparing microscopic evaluated data with the results of critical facility experiments as developed particularly at the Institute of Physics and Energetics at Obninsk and presented in these reports will be of interest to reactor physics and nuclear data groups outside the USSR. This document was compiled, partly edited, and published by the IAEA Nuclear Data Section (NDS) in agreement with the authors and the Obninsk Nuclear Data Centre.

TABLE OF CONTENTS

METHODS AND PROGRAMMES FOR FAST REACTOR CALCULATION

Nickolayshvili Sh.S., Zolotukhin V.G.,
Markelov I.P., Blyskavka A.A.

Institute of Physics and Power Engineering
Obninsk, USSR

Translation made at Obninsk

§ 1. General outlines of the Problem.

1. A Number of reactor calculation problems involve the homogeneous equation:

$$L\varphi = \lambda \frac{\chi(E)}{4\pi} Q(r) \tag{1.1}$$

$$L\varphi = \vec{\Omega}\nabla\varphi + \Sigma_t\varphi - \frac{1}{4\pi}\int_0^\infty dE'\Sigma_s(\vec{r},E')\int_{|\vec{\Omega}|=1} d\vec{\Omega}' W(\vec{r},\vec{\Omega},\vec{\Omega}',E,E')\varphi(\vec{r},\vec{\Omega},E') \tag{1.2}$$

$$Q(\vec{r}) = \int_0^\infty dE\,\nu(\vec{r},E)\Sigma_f(\vec{r},E)\int_{|\vec{\Omega}|=1}\varphi(\vec{r},\vec{\Omega},E)\,d\vec{\Omega} \tag{1.3}$$

with an additional condition

$$\varphi(\vec{r},\vec{\Omega},E) = 0\ ,\quad (\vec{\Omega},\vec{n}) < 0 \tag{1.4}$$

at the reactor external boundary, where $\vec{n}$ is the unit outside normal to the surface of the boundary.

The function $\varphi(\vec{r},\vec{\Omega},E)$ is the unknown quantity equal to $v \times n(\vec{r},\vec{\Omega},E)$, where v is the velocity of a neutron with energy E, and $n(\vec{r},\vec{\Omega},E)$ is neutron density in the phase space $R \times \Omega \times \mathcal{E}$, R is three-dimendional Euclidean space of points $\vec{r}$, Ω - a set of all the points for the unit sphere corresponding to the all possible directions of neutron flight $\vec{\Omega}$, and $\mathcal{E}$ - a set of all possible values for neutron energies E. The function $Q(r)$ determined by the equation (1.3) is called a distributionfunction of secondary fission neutrons or fission neutrons.

$\Sigma_t(\vec{r},E)$ is the total macroscopic cross section for E-energy neutrons at the $\vec{r}$-point, calculated for a unit volume in R; $\Sigma_s(\vec{r},E)$ - the scattering cross section $\Sigma_f(\vec{r},E)$ -the fission cross section $W(\vec{r},\vec{\Omega},\vec{\Omega}',E,E')$ -the probability far a neutron at point $\vec{r}$ with the energy E' before scattering and the flight direction $\vec{\Omega}'$, to have after scattering

the energy E and direction $\vec{\Omega}$;
The function W is normalized so that

$$\frac{1}{4\pi}\int_0^\infty dE \int_{|\vec{\Omega}|=1} d\vec{\Omega} W(\vec{r},\vec{\Omega},\vec{\Omega}',E,E') = 1 \qquad (1.5)$$

$\nu(\vec{r},E)$ -the overage number of secondary neutrons emitted in one fission event per one captured neutron.

$\chi(E)$ -the function describing the energy distribution of fission neutrons. X(E) is normalized so that

$$\int_0^\infty \chi(E)\,dE = 1 \qquad (1.6)$$

The system under consideration is assumed to consist of a finite number of regions (reactor zones) differing in their composition. The functions describing physical characteristics of the medium (Σ_t , Σ_s ,etc.) are step-functions $\vec{r}$. The function $\varphi(\vec{r},\vec{\Omega},E)$ is limited and continuous in all the variables everywhere except zone interfaces where its continuity in $\vec{r}$ is required along the $\vec{\Omega}$ direction.

The problem is to find a few first eigenvalues λ arranged in an increasing order and corresponding distribution eigenfunctions $\varphi(\vec{r},\vec{\Omega},E)$. In order to solve the problem let us apply the group method [1] . The neutron energy interval is supposed to be divided into a finite number of partial intervals (energy groups). Within each group the physical characteristics of medium and the functions to be found are constant and do not depend on E. Then the initial problem (1.1)-(1.4) may be represented as a multigroup set of single -velocity equations:

$$L^j\varphi^j = \lambda \frac{\chi^j}{4\pi} Q(\vec{r}) \qquad j = 1,2,\dots N \qquad (1.7)$$

$$L^j\varphi^j = \vec{\Omega}\nabla\varphi^j + \Sigma_t^j\varphi^j - \sum_{\ell=1}^{N} \frac{1}{4\pi}\int_{|\vec{\Omega}|=1} \Sigma_s^{\ell-j}(\vec{r},\vec{\Omega},\vec{\Omega}')\varphi^\ell(\vec{r},\vec{\Omega}')\,d\vec{\Omega}' \qquad (1.8)$$

$$Q(\vec{r}) = \sum_{\ell=1}^{N} \nu^{\ell}(\vec{r}) \Sigma_f^{\ell}(\vec{r}) \int_{|\vec{\Omega}|=1} \varphi^{\ell}(\vec{r},\vec{\Omega})\, d\vec{\Omega} \qquad (1.9)$$

where $\varphi^j(\vec{r},\vec{\Omega})$ are the group neutron fluxes defined by the integrals

$$\varphi^j(\vec{r},\vec{\Omega}) = \int_{E_{j-1}}^{E_j} \varphi(\vec{r},\vec{\Omega},E)\, dE \qquad (1.10)$$

In the multigroup approximation the boundary condition at the external boundary will look as:

$$\varphi^j(\vec{r},\vec{\Omega}) = 0 \qquad (\vec{\Omega},\vec{n}) < 0 \qquad (1.11)$$

Further simplification of the problem is connected with approximate representation of $\Sigma_s^j(\vec{r},\vec{\Omega},\vec{\Omega}')$ as a function of $\vec{\Omega}\,\vec{\Omega}'$

Let

$$\Sigma_s^{\ell-j}(\vec{r},\vec{\Omega},\vec{\Omega}') = \Sigma_{s0}^{\ell-j}(\vec{r}) + 3\vec{\Omega}\vec{\Omega}'\Sigma_{s1}^{\ell-j}(\vec{r}) \qquad (1.12)$$

With such assumption the set (1.7) will look as:

$$\Omega\nabla\varphi^j + \Sigma_t^j\varphi^j = \frac{1}{4}\sum_{\ell=1}^{j}\left[\Sigma_{s0}^{\ell-j}\varphi_0^{\ell}(\vec{r}_0) + 3\vec{\Omega}\Sigma_{s1}^{\ell-j}\vec{\varphi}_1^{\ell}(\vec{r})\right] + \lambda\frac{\chi^j}{4\pi}Q(\vec{r}) \qquad (1.13)$$

where $j = 1, 2, \ldots, N$

$$\varphi_0^j(\vec{r}) = \int_{|\vec{\Omega}|=1} \varphi^j(\vec{r},\vec{\Omega})\, d\vec{\Omega} \qquad (1.14)$$

$$\vec{\varphi}_1^j(\vec{r}) = \int_{|\vec{\Omega}|=1} \vec{\Omega}\,\varphi^j(\vec{r},\vec{\Omega})\, d\vec{\Omega} \qquad (1.15)$$

2. A joint equation 1,2,3 is widely used along with the equation (1.1)

$$L^*\varphi^* = \lambda\frac{\nu(E)\Sigma_f(E)}{4\pi}Q^*(\vec{r}) \qquad (1.16)$$

$$L^*\varphi^* = -\vec{\Omega}\nabla\varphi^* + \Sigma_t\varphi^* - \frac{\Sigma_s(E)}{4\pi}\int_0^\infty dE' \int_{|\vec{\Omega}|=1} d\vec{\Omega}' W(\vec{r},\vec{\Omega},\vec{\Omega}',E,E')\varphi^*(\vec{r},\vec{\Omega},E) \quad (1.17)$$

$$Q^*(\vec{r}) = \int_0^\infty dE\, \chi(E) \int_{|\vec{\Omega}|=1} \varphi^*(\vec{r},\vec{\Omega},E)\, d\vec{\Omega} \quad (1.18)$$

A boundary condition for the joint equation is

$$\varphi^*(\vec{r},\vec{\Omega},E) = 0 \qquad |\vec{\Omega},\vec{n}| > 0 \quad (1.19)$$

The function $\varphi^*(\vec{r},\vec{\Omega},E)$ is generally called as the neutron value function [3].

The multigroup analog for the system (1.16)–(1.18) with the assumption (1.12) has form of

$$-\vec{\Omega}\nabla\varphi^{*j} + \Sigma_t^j\varphi^{*j} = \frac{1}{4\pi}\sum_{\ell=j}^{N}\left[\Sigma_s^{j\to\ell}\varphi_0^{*\ell} + 3\vec{\Omega}\Sigma_{s1}^{j-\ell}\vec{\varphi}_1^{*\ell}(\vec{r})\right] + \lambda\frac{(\nu\Sigma_f)^j}{1}Q^*(\vec{r}) \quad (1.20)$$

$$Q^*(\vec{r}) = \sum_{\ell=1}^{N}\chi^\ell(E)\,\varphi_0^{*\ell}(\vec{r}) \quad (1.21)$$

with the condition at the external boundary of the system:

$$\varphi^{*j}(\vec{r},\vec{\Omega}) = 0 \qquad (\vec{\Omega},\vec{n}) > 0 \quad (1.22)$$

3. The method for finding the least eigenvalue and corresponding non-trivial solution is as follows. Let $Q^{(n)}(\vec{r})$, $n=1,2,\ldots$ be successive approximations determined from recurrent relations

$$Q^{(n)}(\vec{r}) = \int_0^\infty dE\,\nu(E)\Sigma_f(E)\int_{|\vec{\Omega}|=1}\varphi^{(n)}(\vec{r},\vec{\Omega},E)\,d\vec{\Omega}. \quad (1.23)$$

satisfying the boundary condition (1.4), and $Q^{(0)}(\vec{r})$ – some initial approximation.

Then the least eigenvalue λ is determined from the relation

$$\lambda = \lim \frac{\|Q^{(n-1)}(\vec{r})\|}{\|Q^{(n)}(\vec{r})\|} \quad (1.25)$$

and corresponding distribution of secondary neutrons is determined from

$$Q(\vec{r}) = \lim_{n\to\infty} Q^{(n)}(\vec{r})$$

The least eigenvalue of the joint problem (1.16) is calculated in the same manner. When solving the direct and the joint equations simultaneously in order to determine λ , it is strongly recommended to use the relation

$$\lambda = \lim_{n\to\infty} \frac{(Q^{(n-1)}(\vec{r}), Q^{*(n)}(\vec{r}))}{(Q^{(n)}(\vec{r}), Q^{*(n)}(\vec{r}))} \qquad (1.27)$$

where (φ, ψ) is the scalar product of the functions and ψ in the space R.

The above process with some modification may be used for finding some other values for the problem stated (see § 3).

§ 2. P_n - Approximation of the Spherical Harmonics Method.

1. The structure of the multigroup equation system (1.13) reveals that the calculation of spatial and angular neutron distribution reduces to successive solution of single-velocity equations of the following form

$$\vec{\Omega}\nabla\varphi + \Sigma\varphi = \frac{1}{4\pi}(\Sigma_{s0}\varphi_0 + 3\Sigma_{s1}\vec{\Omega}\vec{\varphi}_1 + f) \qquad (2.1)$$

where

$$\varphi_0(\vec{r}) = \int_{|\vec{\Omega}|=1} \varphi(\vec{r},\vec{\Omega})\, d\vec{\Omega} \qquad (2.2)$$

$$\vec{\varphi}_1(\vec{r}) = \int_{|\vec{\Omega}|=1} \vec{\Omega}\,\varphi(\vec{r},\vec{\Omega})\, d\vec{\Omega} \qquad (2.3)$$

$f = f(\vec{r}, \vec{\Omega})$ is the given function.

The most widely used method for solving the equation (2.1) is the method based on representation of the unknown function

$\varphi(\vec{r},\vec{\Omega})$ in the form

$$\varphi(\vec{r},\vec{\Omega}) = \frac{1}{4\pi}\left[\varphi_0(\vec{r}) + 3\vec{\Omega}\vec{\varphi}_1(\vec{r})\right] \qquad (2.4)$$

By substituting the expression (2.4) into (2.1) we obtain [1,2]:

$$\begin{aligned} \nabla\vec{\varphi}_1 + \Sigma_0\varphi_0 &= f_0 \\ \tfrac{1}{3}\nabla\varphi_0 + \Sigma_1\vec{\varphi}_1 &= f_1 \end{aligned} \qquad (2.5)$$

where

$$\Sigma_0 = \Sigma - \Sigma_{s0}\ ,\quad \Sigma_1 = \Sigma - \Sigma_{s1}$$

$$f_0 = \int_{|\vec{\Omega}|=1} f\,d\vec{\Omega}\ ,\quad f_1 = \int_{|\vec{\Omega}|=1} \vec{\Omega} f\,d\vec{\Omega} \qquad (2.6)$$

The system (2.5) must be supplemented with the boundary condition. With that aim in view we may use the approximate representation of the conditions (1.4) in the Marshak form [2]. As a result we shall have

$$\varphi_0 - 2\varphi_{1n} = 0 \qquad (2.7)$$

where φ_{1n} is the component of the vector-function $\vec{\varphi}_1$ along the outside normal. At the inner interfaces of zones there is assumed a condition of continuity for the normal component resulting from continuity of $\varphi_0(\vec{r},\vec{\Omega})$ over $\vec{r}$ along the direction $\vec{\Omega}$.

2. P_2 - approximation. In the problems of shielding calculation a marked refinement of the results is achieved by means of transition from P_1-approximation to P_2-approximation of the spherical harmonics method which describes better the behaviour of neutron fields far from the reactor core. The transition to P_2-approximation is realized especially easily in one-dimensional problems (sphere, infinite cylinder, flat layer). In this case the system of equations has the same structure as the system (2.1) [1,4].

3. In calculations of one-dimensional reactors the numerical algorithms based on the spherical harmonics method with mat-

rix factorization are widely used. The principle of these methods will be considered on an example of a spherically symmetrical transport problem (for a more detailed information see 1,5,6).

In this case the equation (2.1) has a form of

$$\mu \frac{\partial \varphi}{\partial r} + \frac{1-\mu^2}{r} \frac{\partial \varphi}{\partial \mu} + \Sigma \varphi = \frac{\Sigma_s}{4\pi} \int_0^{2\pi} d\alpha \int_{-1}^{+1} d\mu' g(\mu_0) \varphi(\vec{r}, \mu') + f \qquad (2.8)$$

$$\mu_0 = \mu\mu' + \sqrt{1-\mu^2}\sqrt{1-\mu'^2}\cos\alpha$$

The solution of the equation (2.8) will be sought for in the form of

$$\varphi(r,\mu) = \sum_{\ell=0}^{n} \frac{(2\ell+1)}{4\pi} \varphi_\ell(r) P_\ell(\mu), \quad \varphi_\ell(r) = 2\pi \int_{-1}^{1} \varphi(r,\mu) P_\ell(\mu)\, d\mu \qquad (2.9)$$

For expansion coefficients of φ_ℓ (r) we obtain

$$\ell r^{\ell-1} \frac{d}{dr}\left(\frac{\varphi_{\ell-1}}{r^{\ell-1}}\right) + (\ell+1)\frac{1}{r^{\ell+2}} \frac{d}{dr}\left(r^{\ell+2}\varphi_{\ell+1}\right) + (2\ell+1)\Sigma_\ell \varphi_\ell = (2\ell+1) f_\ell \qquad (2.10)$$

$$\ell = 0, 2, \ldots, n$$

where

$$f_\ell = 2\pi \int_{-1}^{+1} f(r,\mu) P_\ell(\mu) d\mu, \quad \Sigma_\ell = \Sigma - 2\pi \int g(\mu) P_\ell(\mu)\, d\mu \qquad (2.11)$$

In the equations (2.10) the functions with negative subscripts and with the subscripts more than n are assumed to be zeros.

The system (2.10) may be written as

$$\begin{aligned} K\vec{J} + a\vec{\varphi} &= \vec{f} \\ \mathcal{L}\vec{\varphi} + b\vec{J} &= \vec{q} \end{aligned} \qquad (2.12)$$

where the vectors $\vec{\varphi}$ ans $\vec{J}$ are

$$\vec{\varphi} = \begin{vmatrix} \varphi_0 \\ \varphi_2 \\ \vdots \\ \varphi_{n-1} \end{vmatrix}, \quad \vec{J} = \begin{vmatrix} \varphi_1 \\ \varphi_3 \\ \vdots \\ \varphi_n \end{vmatrix} \qquad (2.13)$$

a and b are the diagonal matrices

$$a = \| (1-4\ell)\Sigma_{2\ell} \|, \quad b = \| (3+4\ell)\Sigma_{2\ell+1} \| \qquad (2.14)$$

K and L are the operators

$$K=\begin{vmatrix} \frac{1}{r^2}\frac{d}{dr}r^2 & 0 & 0 & \dots \\ 2r\frac{d}{dr}\frac{1}{r} & \frac{3}{r^4}\frac{d}{dr}r^4 & 0 & \dots \\ 0 & 4r^3\frac{d}{dr}\frac{1}{r^3} & \frac{5}{r^6}\frac{d}{dr}r^6 & \dots \\ \dots & \dots & \dots & \dots \end{vmatrix}, \quad L=\begin{vmatrix} \frac{d}{dr} & \frac{2}{r^3}\frac{d}{dr}r^3 & 0 & \dots \\ 0 & 3r^2\frac{d}{dr}\frac{1}{r^2} & \frac{4}{r^5}\frac{d}{dr}r^5 & \dots \\ \dots & \dots & \dots & \dots \\ \dots & \dots & \dots & \dots \end{vmatrix} \qquad (2.15)$$

$\vec{f}$ and $\vec{g}$ are the vectors with the $\frac{n-1}{2}$ components.

The system (2.12) may be easily reduced to the difference equation of the type

$$\vec{\varphi}_{k+1} - B_k\vec{\varphi}_k + C_k\vec{\varphi}_{k-1} = -\vec{F}_k \qquad (2.16)$$

where B_k, C_k are the square matrices of the $\frac{n-1}{2}$ order, and $\vec{\varphi}_k$, $\vec{F}_k$ are the values of the vectors $\vec{\varphi}$ and $\vec{F}$ in the mesh-point K. The system (2.16) is supplemented with two conditions which may be found by approximating the initial boundary conditions with difference operators.

One of the effective methods for solving the systems (2.16) is the method of matrix factorization [1]. The final formulas which constitute the numerical scheme for solving the system (2.16) has a form of

$$\begin{aligned} \beta_{k+1} &= C_{k+1}(B_k-\beta_k)^{-1} \\ \vec{\xi}_{k+1} &= \beta_{k+1}(\vec{\xi}_k+\vec{F}_k) \\ \vec{\varphi}_k &= (B_k-\beta_k)^{-1}(\vec{\varphi}_{k+1}+\vec{\xi}_k+\vec{F}_k) \end{aligned} \qquad (2.17)$$

where β_1, $\vec{\xi}_1$, $\vec{\varphi}_N$ are determined from boundary conditions.

The above algorithm with a few modifications is extended to other one-dimensional transport problems. It is assumed as a basis for a number of programmes of one-dimensional reactor calculation in P_3-and P_5-approximations.

§ 3. The Calculation of Eigenvalues Differing from the First One.

Let us assume now that Q (r) in the right-hand part of the equation (1.1) is the known function $\vec{r}$.

Then the solution of the initial problem may be presented as follows:

$$\Psi(\vec{r},\vec{\Omega},E) = \lambda \int_{(D)} \psi(\vec{r},\vec{r}_0,\vec{\Omega},E)\, Q(\vec{r}_0)\, d\vec{r}_0 \qquad (3.1)$$

where ψ ($\vec{r},\vec{r}_0,\vec{\Omega},E$) is the solution of the equation

$$L\psi = \frac{\chi(E)}{4\pi}\,\delta(\vec{r}-\vec{r}_0) \qquad (3.2)$$

satisfying the boundary condition (1.4).

$\delta(\vec{r}-\vec{r}_0)$ is the Dirac function normalized as

$$\int_{(D)} \delta(\vec{r}-\vec{r}_0)\, dV = 1 \qquad (3.3)$$

D is the region occupied by the reactor core.

Now let us multiply the equation (3.1) by $\nu(E)\Sigma_f(E)$ and integrate over all E-energies and over the total surface of an unit spher $|\vec{\Omega}|$ =1.

Then, according to the definition (1.2) we shall have [7] :

$$Q(\vec{r}) = \lambda \int_{(D)} K(\vec{r},\vec{r}_0)\, Q(\vec{r}_0)\, d\vec{r}_0 \qquad (3.4)$$

where

$$K(\vec{r},\vec{r}_0) = \int_0^\infty \nu(E)\Sigma_f(E)\, dE \int_{(\Omega)=1} \Phi(\vec{r},\vec{r}_0,\vec{\Omega},E)\, d\vec{\Omega} \qquad (3.5)$$

For solving the equation (3.4) we divide the region D into n partial non-intersecting regions D_1, D_2, ..., D_n, then the relation (3.4) may be rewritten as:

$$Q(\vec{r}) = \lambda \sum_{j=1}^{n} \int_{D_j} K(\vec{r},\vec{r}_0)\, Q(\vec{r}_0)\, d\vec{r}_0 \qquad (3.6)$$

or, approximately, as

$$Q(\vec{r}) \cong \lambda \sum_{j=1}^{n} Q(\vec{r}_j) \int_{D_j} K(\vec{r},\vec{r}_0)\, d\vec{r}_0 \qquad (3.7)$$

where $\vec{r}_0$ is a point of the region D_j. By integrating (3.7) within the region D_j we obtain:

$$Q_i = \lambda \sum_{j=1}^{n} A_{ij} Q_j \qquad (3.8)$$

where

$$A_{ij} = \frac{1}{\Delta_j} \int_{D_i} d\vec{r} \int_{D_j} K(\vec{r},\vec{r}_0)\, d\vec{r}_0 \qquad (3.9)$$

$$Q_i = \int Q(\vec{r})\, d\vec{r}\ , \quad \Delta_i = \int_{D_i} dV \qquad (3.10)$$

Therefore, the initial problem of finding some eigenvalues and corresponding functions is reduced to the partial problem of linear algebra. For its solving we may use different methods, in particular, the exhaustion method [8].

Let us point out a method for calculating the elements of the matrix $\|A_{ij}\|$.

Let

$$\Psi_j(\vec{r},\vec{\Omega},E) = \int_{D_j} \Psi(\vec{r},\vec{r}_0,\vec{\Omega},E)\, d\vec{r}_0 \qquad (3.11)$$

The function $\Psi_j(\vec{r},\vec{\Omega},E)$ is the solution of the equation

$$L\Psi_j(\vec{r},\vec{\Omega},E) = \frac{\chi(E)}{4\pi} h_j(\vec{r}) \qquad (3.12)$$

where

$$h_i(\vec{r}) = \begin{cases} \frac{1}{\Delta_j} & \vec{r} \in D_j \\ 0 & \vec{r} \notin D_j \end{cases} \qquad j = 1, 2, \ldots n \qquad (3.13)$$

The elements of the matrix $\|A_{ij}\|$ are related to the function $\psi(\vec{r}, \vec{\Omega}, E)$ as follows:

$$A_{ij} = \int_{D_j} d\vec{r} \int_0^\infty \nu(E)\Sigma_f(E)dE \int_{|\vec{\Omega}|=1} \psi_j(\vec{r}, \vec{\Omega}, E)\, d\vec{\Omega} \qquad (3.14)$$

It is necessary to not on conclusion that the above algoritim is meant for the problem of finding a great number of eigenvalues and eigenfunctions. For finding two or three eigenvalues, we may apply the principle of the exhaustion method directly to the initial equation (1.1) solving it together with the joint equation (1.16).

§ 4. An Evaluation of Reactor Parameters by the Monte-Carlo Method

Often we have to solve the Boltzmann equation for very complex regions in order to be as close as possible to a real multiplying assembly.

It is known that there are three classes of the reactor calculation errors:

a) The errors of the kinetic equation solution resulting from idealization of the actual process of neutron transport (e.g., diffusion approximation), as well as the errors of the numerical solution an approximate equation;

b) The errors resulting from idealization of the real geometrical composition which is always a three-dimensional one;

c) and, at last, the errors caused by inaccuracy in the data on the processes of neutrons interaction with nuclei of material.

The total calculational error is a composite function of the above errors. It is very difficult to evaluate them separately in practical calculations. In addition, the fact of their being, not independent, complicates the problem. It is

especially difficult to evaluate the effect of errors in constants because it is disguised by errors of other origin.

Therefore, various methods using the results of macroscopic (integral) experiments for improving the constants require a calculational technique which has a reliable accuracy with respect to the errors of the a) and b) type.

Most reactor calculations are performed with the use of the fixed systems of group constants. It is obviously important to have a means for the control of the numerical methods with retaining one and the same system of constants.

At last, at certain stage of reactor designing there arises a need for obtaining the most precise predictions of reactor parameters.

All these arguments result in the necessity of using the Monte-Carlo methods. When choosing a sufficiently general three-dimensional composition of reactor zones the method will provide a zero errors for the б) class and an easily estimated proper statistical error.

An integral equation for the function $Q(\vec{r},\vec{\Omega},E) = \Sigma_f(\vec{r},E)\varphi(\vec{r},\vec{\Omega},E)$ which is the fission rate function for neutrons of direction and E energy, may be easily obtained from (1.1):

$$K_{eff}\,Q(\vec{r},\vec{\Omega},E) = \int Q(\vec{r}',\vec{\Omega}',E)\,\nu_f(\vec{r}',E')\,P_a(\vec{r}',E'\to\vec{r},\vec{\Omega},E)\times \quad (4.1)$$

$$\times\,\frac{\Sigma_f(\vec{r}',E)}{\Sigma_a(\vec{r}',E')}\,d\vec{r}'\,d\vec{\Omega}'\,dE', \quad K_{eff} = \frac{1}{\lambda}$$

where $\Sigma_a(\vec{r},E)$ is the macroscopic absorption cross section including fission; $P_a(\vec{r}',E'\to\vec{r},\vec{\Omega},E)$ is the probability density for a neutron born at $\vec{r}'$ as a result of nucleus fission with the E'-energy neutron to be absorbed at point $\vec{r}$ having the direction and energy of $\vec{\Omega}$ and E, respectively.

This function is normalized so that

$$\int P_a(\vec{r}', E' \to \vec{r}, \vec{\Omega}, E)\, d\vec{r}\, d\vec{\Omega}\, dE = 1$$

For the fission neutron density we have from (4.1)

$$K_{eff}\,\Theta(\vec{r}, \vec{\Omega}, E) = \int \Theta(\vec{r}', \vec{\Omega}, E')\, P_a(\vec{r}', E' \to \vec{r}, \vec{\Omega}, E) \times \tag{4.2}$$

$$\times \frac{\nu_f(\vec{r}', E')\,\Sigma_f(\vec{r}', E')}{\Sigma_a(\vec{r}', E')}\, d\vec{r}'\, d\vec{\Omega}'\, dE'$$

Let us introduce a modified fission probability

$$P_{m,f}(\vec{r}', E' \to \vec{r}, \vec{\Omega}, E) = P_a(\vec{r}', E' \to \vec{r}, \vec{\Omega}, E)\, \frac{\nu_f \Sigma_f(\vec{r}, E)}{a\,\Sigma_a(\vec{r}, E)},$$

where

$$a = \max_{\vec{r}, E} \frac{\nu_f \Sigma_f(\vec{r}, E)}{\Sigma_a(\vec{r}, E)}$$

Then

$$\frac{1}{a} K_{eff}\,\Theta(\vec{r}, \vec{\Omega}, E) = \int P_{mf}(\vec{r}', E' \to \vec{r}, \vec{\Omega}, E)\,\Theta(\vec{r}', \vec{\Omega}', E)\, d\vec{r}'\, d\vec{\Omega}'\, dE' \tag{4.3}$$

The equation (4.3) may be considered as an equation for the fictitious fission rate Θ under the assumption that one and the same number a of secondary fission neutrons is born in each fission (though actually Θ is the fission-neutron density). The kernel $P_{m,f}(\vec{r}', E' \to \vec{r}, \vec{\Omega}, E)$ controls the Markov's chain process $x_1, x_2, \ldots, x_0$ in the phase space. In this process a fission neutron born at x_i when being absorbed at point x_{i+1} would either produce the next "fission point" x_{i+1} (with the probability of $\frac{\nu_f \Sigma_f(\vec{r}, E)}{a\,\Sigma_a(\vec{r}, E)}$)

or would be observed without fission and, therefore, the chain would be broken. In practice when using the Monte Carlo method it is extremely inconvenient to deal with such degenerating chain because the number of fission points is rapidly decreased. Therefore, the methods "with preservation of the fission point number" are widely spread [9-12]. Now we describe one of these methods proposed by A.D. Frank-Kamenetsky [9].

Let $x_1^{(i)}, x_2^{(i)}, \ldots, x_N^{(i)}$ be the phase coordinates of N fission points in the i-th generation. Beginning from these fission points, and after looking through the "histories" of the corresponding fission neutrons, we shall get m_i fission points for the (i + 1)-the generation neutrons. The missing $N - m_1$ fission points of the (i + 1)-th generation are taken by means of random choice from all N points of the preceding, i-th generation.

Thus the chain of successive generations $x^{(1)}, x^{(2)}, \ldots, x^{(n)}$ is determined which is the homogeneous Markov's chain in the space of vectors $x = (x_1, x_2, \ldots, x_n)$.

As it follows from the Markov's chain theory the stationary distribution $U(x_1, x_2, \ldots, x_n)$ of N fission points is determined by the homogeneous equation

$$U(x_1, x_2, \ldots, x_N) = \int \ldots \int U(x_1', x_2', \ldots, x_N') G(x_1', x_2', \ldots, x_N' \to x_1, x_2, \ldots, x_N) dx_1' dx_2' \ldots dx_N' \tag{4.4}$$

In this case the "one-particle" distribution

$$\Theta(x) = \int U(x_1, x_2, \ldots, x_N) dx_2 \ldots dx_N \tag{4.5}$$

is not, generally speaking, a solution for the homogeneous equation (4.3). This result in some displacement in the reactor characteristics which should be analysed theoretically.

It may be shown that for the above method of increasing

the fission point number the kernel G is equal to

$$G(x_1', x_2', \ldots, x_N' \to x_1, x_2 \ldots x_N) = \prod_{\ell=1}^{N} [P_{mf}(x_\ell' - x_\ell) + \quad (4.6)$$

$$+ (1 - P_{mf}(x_\ell')) \frac{1}{N} \sum_{i=1}^{N} \delta(x_i' - x_\ell)$$

where

$$P_{mf}(x') = \int P_{mf}(x' - x)\, dx$$

It may be easily verified that

$$\int G(x_1', x_2', \ldots x_N' \to x_1, x_2, \ldots, x_N)\, dx_1\, dx_2 \ldots dx_N = 1$$

Due to the symmetry of the kernel G the solution of the equation (4.4) is symmetrical and all the "one-particle" distribution functions

$$\widetilde{\Theta}_i(x) = \int \cdots \int dx_1, \ldots, dx_{i-1} dx_{i+1} \ldots dx_N\, U(x_1, x_2, \ldots, x_N)$$

coincide; therefore $\widetilde{\Theta}(x)$ may be represented as

$$\widetilde{\Theta}(x) = \frac{1}{N} \sum_{i=1}^{N} \int \ldots \int dx_1 \ldots dx_N\, U(x_1, \ldots, x_N)\, \delta(x - x_i) \quad (4.7)$$

Then we multiply (4.4) by $\frac{1}{N} \sum_{n=1}^{N} \delta(x_n - x)$ and integrate it over all $x_1, x_2, \ldots, x_N$. Taking into account (4.6) and (4.7) we obtain the following equation for the "one-particle" distribution function $\widetilde{\Theta}(x)$

$$\int P_{mf}(x' - x)\, \widetilde{\Theta}(x')\, dx' = k_N(x)\, \widetilde{\Theta}(x) \quad (4.8)$$

where

$$k_N(x) = \frac{1}{\widetilde{\Theta}(x)} \int \ldots \int dx_1 dx_2 \ldots dx_N\, U(x_1, x_2, \ldots x_N) \frac{1}{N} \sum_{i=1}^{N} \delta(x - x_i) \frac{1}{N} \sum_{n=1}^{N} P_{mf}(x_n)$$

This equation differs from (4.3) only in the dependence of k_N on x. At sufficiently great N the function

$$\frac{1}{N} \sum_{k=1}^{N} P_{mf}(x_k) \quad (4.9)$$

differs slightly from some constant K and, therefore, $k_N \approx k$.

Practical calculations and model examples reveal [10] that displacement of K_{eff} caused by the finiteness of N, has an order of $\frac{1}{N}$. In practice it is enough to take N within the limits of some hundreds.

After tracing neutron "histories" from some number of generations D, when the source distribution has been settled, K_{eff} is estimated over each following j-th generation according to the general theory of evaluations of the linear functionals by the Monte Carlo method [13]. For example, the estimation by means of the collision density looks like

$$k_{eff}^{(j)} = \frac{1}{N} \sum_{i=1}^{N} \sum_{\kappa} \left(\frac{\nu_f \Sigma_f}{\Sigma_t} \right)_{i,j,k} \qquad (4.10)$$

where summation is performed over all the collision points of the i-th neutron in the j-th generation. Other estimations are also possible for example, the estimation by means of the path length and the optimum estimation [13].

Then the obtained values of K_{eff} are averaged over M generations

$$k_{eff} \approx \sum_{j=1}^{M} \frac{1}{M} k_{eff}^{(j)}$$

and thus the estimation for the effective multiplication coefficient over all H.H. neutron "histories" is obtained. In this case some of the first generations of neutrons are excluded from the process of averaging to avoid the effect of non-settled source distribution.

The estimation of some other reactor parameters is also reduced to the use of the general theory of the flux functionals estimations and to following averaging of these estimations over neutron generations. As an example let us consider the estimation of the mean prompt-neutron lifetime T which is of great importance for reactor kinetics.

According to the above scheme of statistical tests let us

determine the random lifetime of a neutron between two successive fission. The normalized distribution of fission sources $Q(x)$ being settled down, evidently the mean lifetime is

$$\langle \tau \rangle = \frac{\int Q(x)dx \int \tau\, M(x,x',\tau)\, dx' d\tau}{\int Q(x)dx \int M(x,x',\tau)\, dx' d\tau} \qquad (4.11)$$

where $M(x,x',\tau)$ is the density of fission prompt neutron birth at point x' at a time τ after the fission neutron arrival at point x.

Let $Q(x,t)$ be the fission neutron density at point x at a time t. Then, in the absence of external neutron sources.

$$Q(x,t) = \int_{-\infty}^{t} Q(x',t')\, M(x',t' \to x,t)\, dx'\, dt' \qquad (4.12)$$

Using the separation of variables

$$Q(x,t) = Q(x)\, e^{\alpha t}$$

we obtain

$$Q(x) = \int Q(x')\, dx' \int_{0}^{\infty} d\tau\, e^{\alpha t}\, M(x,x',\tau) \qquad (4.13)$$

Taking into account the fact that in a state near to critical $e^{\alpha\tau}$ is close to 1 in the region where M differs noticeably from zero, we obtain, after expansion $e^{\alpha\tau}$ into $\alpha\tau$ degrees and retaining the first two terms, the following expression:

$$Q(x) = \int Q(x')dx' \int_{0}^{\infty} M(x,x',\tau)d\tau + \alpha \int Q(x')dx' \int_{0}^{\infty} \tau\, M(x,x',\tau)\, d\tau \qquad (4.14)$$

The value $T(x,x') = \int_{0}^{\infty} \tau\, M(x,x',\tau)d\tau$

is proportional to the mean lifetime of a neutron between two successive fissions at x and x'. Taking into account that

$$P_{mf}(x' \to x) = \int_{0}^{\infty} M(x,x',\tau)\, d\tau$$

the equation (4.14) may be written as

$$Q(x) = \int Q(x')\, P_{mf}(x' \to x)\, dx' + \alpha \int Q(x')\, T(x' \to x)\, dx' \qquad (4.15)$$

By introducing the equation

$$Q_o^+(x) = \frac{1}{K_{eff}} \int Q_o^+(x') P_{mf}(x \to x')\, dx' \qquad (4.16)$$

which is the joint equation to the conditionally critical (4.3) multiplying the equation (4.15) by $Q_o^+(x)$ and (4.16) by $Q(x)$ $Q(x)$ integrating over x and subtracting the obtained equations we find

$$\alpha = \frac{K_{eff} - 1}{T}$$

On the other hand, it may be shown that the lifetime

$$T = \frac{\iint Q(x) Q_o^+(x') T(x \to x') dx\, dx'}{\int Q_o^+(x)\, Q(x)\, dx} \qquad (4.17)$$

coincides with the expression for the lifetime presented in the work by L.N.Usachev [3] under the assumption that $Q(x) = \ominus(x)$

The expression (4.17) differs from $\langle \tau \rangle$ in two respects. Firstly, $T(x \to x')$ in (4.17) is weighted with the weight $Q(x)$ whichis the first eigenfunction of the equation (4.14) but not with the weight $\ominus(x)$. Of course, in critical reactor $\alpha = 0$ and $Q(x) = \ominus(x)$; however, for the state very far from critical the replacement of $Q(x)$ by $\ominus(x)$ may lead to noticeable errors.

Secondly, besides $Q(x')$, $Q_0(x)$(joint integral equation solution) is also a weighting function for $T(x' \to x)$. We must be sure that the replacement of $Q_o(x)$ by the constant (then $\langle \tau \rangle$ is reduced to T) would not result in considerable errors. Since the functional T is a ratio of two linear functionals the difference of Q_o^+ from the constant does not usually produce any significant errors; nevertheless, there arises a problem of evaluation of the bilinear functionals for the homogeneous integral equation which has not been yet resolved.

§ 5. A Survey of Most Important Programmes

The methods presented above have been realized as the programmes for the computer M-20 which are widely used for reactor calculations. A brief description of their principal characteristics is given below.

a) The complex 9M is intended for calculating the space-energy distribution of fluxes and joint fluxes of neutrons in reactors in P_1- and P_3-approximations in the one-dimensional geometry. The calculations are performed on the basis of the total conservative file for the 18- and 21 group microscopic cross-sections written on the magnetic tape. The organization of all the calculations is performed with the use of a special control programme which complex a set of programmes and cross-sections, i.e. an operative file for solving a given problem.

The principal characteristics of the programme are: the number of energy groups, up to 21; the number of different elements constituting reactor composition, up to 43; the number of zones with different physical composition, up to 9; the number of mesh-points in a spatial variable, up to 86.

On the basis of the 9M complex the following operations may be carries out: the calculation of the variation of the system reactivity with the use of the perturbation theory formulas (weak and strong perturbations); the calculation of neutron fields by the method of conditional separation of variables; the calculation of neutron fields within shielding layers in P-approximation with the use of the experimental relaxation lengths in the first group; the calculation reaction rates (capture, fission) and of the conversion ratio components; the calculation of the damping decrement in a non-stationary problem and of the fast-neutron lifetime; the calculation of the refined values for critical masses in the one-velocity P-approximation for spherical systems; the calculation of the central absorbing rod efficiency;

b) The complex M-26 allows to calculate the principal fast reactor characteristics with the use of 26-group macroscopic cross-sections [14] . The main programme for calculating the space-energy distribution of a neutron flux is the one-dimensional programme M-26 in the P_1-or P_2-approximation (which allows also to use 18- and 21-group systems of constants). The principal parameters of the programme are: geometry-sphere, cylinder, flat layer, the number of zones, up to 9; the number of space mesh-points within a zone, not more than 31; the total number of space mesh-points, up to 130; the number of different elements, up to 25; the number of energy groups, 18, 21, 26.

Inelastic transitions for every element are taken into account within the limits of the first eleven groups.

The complex M-26 includes the programmes for: processing the microscopic cross-sections; calculating and processing the macroscopic cross-sections; formation and factorization; unreflected reactor calculation; calculating the corrections to the macroscopic elastic-moderation cross-sections; evaluating the absorbing rod efficiency; the calculation of the square length of moderation $\tau(a)$; calculating the reaction rates; averaging of the microscopic and macroscopic cross-sections; calculating the neutron fields within the shielding layers in P_2-approximation with the use of the experimental relaxation lengths in some first groups. The number of shielding layers is up to 30. It is possible to take into account approximately the air gaps between shielding layers and to calculate the system reactivity change according to the perturbation theory formulas.

All the above programmes are combined by the control programme that allows to arrange the programmes according to some given problem. The complex of programmes M-26 together with the file of microscopic cross-sections for 45 elements are stored on the magnetic tape. The possibilities are provided for calculating a cell and a reactor with the central absorbing rod at the surface of which the value of the logarithmic derivative as a function of the rod properties is defined.

The rates of different reactions on any isotopes at any reactor zone are evaluated from the calculated neutron flux values with the use of blocked microscopic cross-sections. When calculating the reaction rates we may use the microscopic cross-sections stored in the file B-26 or introduce additional ones. The programme for averaging the macroscopic and microscopic cross-sections allows to obtain the cross-section for a smaller number of groups (minimum number of groups is 3) on the basis of 26-group cross-sections and space-energy distribution of neutron fluxes calculated in P_1- and P_3-approximations. With the use of the reduced macroscopic cross-sections we may carry o out the calculations with the programmes 9П, P_3 and P_5 as well as with the two-dimensional reactor programmes.

c) The complex of programmes for the fast reactor calculations in P_3- and P_5-approximations allows to obtain the space-energy distribution of neutron fluxes and neutron joint fluxes in one-dimensional flat, cylindrical and spherical geometries.

The main parameters of the programme are: the number of energy groups, up to 26; the number of reactor zones, up to 9; the number of spatial mesh-points, up to 85;

The programme for calculating a spherically-symmetrical reactor in P_5-approximation.

The main parameters are: the number of energy groups, up to 26; the number of reactor zones, up to 5; the number of spatial mesh-points, up to 50.

On basis of global fluxes calculated in P_3-P_5-approximations there is provided a possibility for calculating small perturbations and the differential neutron flux functions.

d) For two-dimensional reactor calculations two programmes are used at the Institute of Physics and Power Engineering: small-group and multigroup programmes for nuclear reactor calculation in diffusion approximation [1, 15, 16].

A small-group programme has the following parameters: the geometry (x,y), (r,z) and (r, φ); the number of groups ≤ 4;

the number of zones differing in physical characteristics, ≤ 63; the number of zones differing in geometrical characteristics, ≤ 256; the number of spatial mesh-points 1000. The macroscopic cross-sections are taken from the punched cards.

A multigroup programme performs a calculation in (x,y) and (r,z) geometries with the number of groups being not more than 21. Its parameters and structure coincide with the preceding programme. In constant to the small-group programme it employs the acceleration of the external iteration convergence with the use of the extrapolation method based on Chebyshev's polynomials. The macroscopic cross-sections for this programme are calculated with the use of one of the programmes from 9M or M-26 complex. The running time depends considerably on the character of the problem and its parameters and is about 2-4 hours per one variant in the (r,z) geometry.

e) The programme for the three-dimensional reactors by the Monte-Carlo method. The library of procedures is written in the computer codes. With the use of these procedures the programmes may be constructed performing the following calculations: the calculation of K_{eff} and of the fission neutron source distribution over zones with the use of the optimum combination of estimations over the collision density and over the path length for calculating K_{eff} [13] and evaluation over the collision density for calculating the secondary neutron sources; the calculation of K_{eff} and of the secondary neutron soures distribution over zones with the use of the arithmetical average for the estimations over the path length and collision density for calculating K_{eff}; the calculation of K_{eff} and ΔK_{eff} for two reactors having similar geometrical configuration and different composition in some reactor regions [17].

The systems of 13-, 26- and 21-group constants may be used in the calculations.

The calculation is performed in the"modified, transport approximation" [14] for the reactors without hydrogen. In hydrogeneous reactors the scattering from hydrogen is modeled strictly and at scattering from the nuclei of other elements the

transport approximation is used.

The composition of a reactor which may be calculated with this programme represents a set of non-intersecting axially-parallel circular cylinders of equal height enclosed into a cylinder of the same height. Any reactor volume contained between the cylindrical surface and the surfaces of the first step of insertion may be cut into parts by the planes parallel to the cylinder bottom. Such part is called a geometrical zone.

The library of procedures contains also a "geometrical" procedure allowing to calculate the reactor representing a complex of non-intersecting spheres enclosed in a sphere of greater diameter.

The reactor parameters which may be calculated by the described programme are limited only by the size of the core memory available with a computer and by the time spent for the calculation. So the number of physical zones (reactor regions differing in composition) is not more than 64, and the number of geometrical zones is about 400.

Any isotope for which there are group constants in the library may be present in the reactor.

In the development and putting into practic of the programmes described in this report, besides the authors, the following persons took an active part: Baryba N.A., Elizarov G.I., Kuznetsova L.I., Kosolova M.N., Novinitsa A.I., Novikovskaya E.I., Ponenko V.V., Polivanskii V.P.

REFERENCES

1. Marchuk G.I., Methods for Reactor Calculations, Gosatomizdat, 1961.

2. Davison B., Neutron Transport Theory, Atomizdat, 1960.

3. Usachev L.N., An Equation for the Value of Neutrons, Reactor Kinetics and Perturbation Theory, Collection of Articles "Reactor Design and Reactor Theory", The USSR Academy of Sciences, 1955.

4. Marchuk G.I., Nikolaishvili Sh.S., Podudalina E.I., Belskaja Z.N., Kochubei N.P., Application of Spherical Harmonic Methods to some Neutron Transport Theory Problems, Pn - Approximation. In the collection of articles "Theory and Methods for Reactor Calculation", Gosatomizdat, 1967.

5. Marchuk G.I., Numerical Methods for Reactor Calculations, Atomizdat, 1958.

6. Marchuk G.I., Podudalina E.I., Tjuterev I.P., Numerical Method for the Solution of Kinetic Equations in P-approximation for Spherical Symmetrical Systems. Proceedings of the Second International Conference on Peaceful Utilization of Atomic Energy, Vol. 2, Atomizdat, 1959.

7. Placzek G. and Volkoff G. A Theory on Neutron Multiplication Canadian Journal of Research, Vol. 25, no. 4, 276, 1947, A.

8. Fadeev D.K., Fadeeva V.N., Calculational Methods of Linear Algebra, Physmatgiz, 1960.

9. Frank-Kamenetzkii A.D., Calculation of Multiplication Factor for a Nuclear Reactor by a Monte-Carlo Method. In the collection of Articles "Method Monte-Carlo in Neutron Transport Theory", Editor: Marchuk G.I., Atomizdat, 1967.

10. Liberoth J. Nucleonik, B. 11, H. 5,213 (1969).

11. Davis D. in "Methods in Computational Physics", Vol. 1, p. 69, New York, Academic Press, 1963.

12. Mikhailov G.A., Journal of Mathematics and Mathematical Physics, Vol. 6, no. 1, 71 (1966).

13. Zolotukhin V.G., "On the Application of the Monte-Carlo Method to Calculations of Flux Functionals, Their Perturbations and Effective Constants"; in the collection of articles "Physics of Nuclear Reactors", Proceedings of Institute of Physics and Nuclear Eng., Obninsk, N 1, 1968.

14. Abagjan L. P., Bazazjanz, N.O., Bondarenko I.I., Nikolaev M.N., Group Constants for Reactor Calculations, Gosatomizdat, 1964.

15. Richard S. Varga. Matrix Iterative Analysis.

16. Varga R., "Numerical Methods for Solution of Multi-Dimensional Multigroup Diffusion Equations"; in the collection of articles "Theory of Nuclear Reactors", Gosatomizdat, 1963.

17. Collection of articles, "Passage of Radiations through heterogeneous Shields", Editor: Leipunskii O.I. and Mashkevich V.P., Atomizdat, 1968.

THE METHOD OF AVERAGE GROUP CROSS-SECTION CALCULATION IN THE REGION OF UNRESOLVED RESONANCES

Nikolaev M.N., Abagyan L.P., Petrova L.V.,
Poplavskaja T.A., Korchagina J.A.

The Institute of Physics and Power Engineering
Obninsk, USSR

Translation made at Obninsk
Edited by NDS

Abstract

This report describes a method of average group cross-section calculation which takes into account resonance self-shielding in unresolved resonance regions. Parameters of quasi-random sequence of resonances, taking fluctuations of neutron widths and level spacings into account, are calculated.

1. Introduction

The object of this work has been to devise a method to obtain average group cross-sections taking into account the temperature and the resonance self-shielding in the region of unresolved resonances. In order to give this problem the average parameters (average widths Γ_γ and Γ_f, strength functions S_c and S_i, average level spacing D, as well as the width distribution and distances between levels must be known.

There exist many methods to calculate the width fluctuation and level spacing fluctuation in the region of unresolved resonances; in particular the Monte-Carlo method and the analytical method [1]. The application of Monte-Carlo method for this purpose is not economical because of the need for a large number of random selections in order to obtain a sufficiently high degree of accuracy in the very wide distribution of reduced neutron widths. The analytical method to account for the fluctuations described in reference [1] is not universal and is inconvenient when it is necessary to average the different dependences.

The present report develops a somewhat different approach to this problem. First, one selects a quasi-random sequence of resonances which satisfies given distributions of reduced neutron widths, and level spacings. Using this sequence it is then possible to obtain average group cross-sections in the region of unresolved resonances using (computer) programmes, like URAN (reference [2]), which are used in the resolved resonance region.

2. Selection of a Resonance Sequence Satisfying Given Distributions of Widths and Level Spacings.

2.1 The Substitution of Integral Distributions by Finite Sums.

Let us take $f(x)$ as a distribution function of the considered quantity. Substituting the integral distribution by a finite sum, we have

$$\int_0^{\infty} f(x)dx = \sum_{i=1}^{n} \int_{\Delta x_i} f(x)dx \qquad (1)$$

For this we divide the x axis into n intervals so that the integrals in these intervals are equal to

$$\int_{U_{i-1}}^{U_i} f(x)dx = \frac{1}{n} \quad \underline{OR} \quad \int_0^{U_i} f(x)dx = \frac{i}{n} \qquad (2)$$

From this condition we find the value of interval limits U_i. It is necessary to select the value of X_i in every interval so that the average values of $\overline{X}$ are equal to 1.

$$\overline{X} = \frac{1}{n} \sum_{i=1}^{n} X_i = 1 \qquad (3)$$

At the same time

$$\overline{X} = \int_0^{\infty} xf(x)dx \qquad (4)$$

or writing the integral in the form of a sum over the intervals we obtain

$$\overline{X} = \sum_{i=1}^{n} \int_{\Delta x_i} x\, f(x)\, dx \qquad (5)$$

From equations (3) and (5) we obtain

$$X_i = n\int_{u_{i-1}}^{u_i} x\, f(x)dx \qquad (6)$$

The fluctuations of neutron widths obey a χ^2-distribution with one channel ($\nu = 1$). The fluctuation of fission widths obey a χ^2-distribution with a different number of channels ($\nu = 1,2,3$). In the general case the χ^2-distribution has the form [3]:

$$f_\nu(x)\,dx = \frac{\nu}{2}\cdot\Gamma\left(\frac{\nu}{2}\right)^{-1}\left(\frac{\nu x}{2}\right)^{\frac{\nu}{2}-1} e^{-\frac{\nu}{2}x}dx \qquad (7)$$

Level spacing distributions assume the form of a Wigner distribution

$$f_B(x) = \frac{\pi}{2}\cdot x\cdot e^{-\frac{\pi x^2}{4}} \qquad (8)$$

or χ^2-distribution with $\nu = 10$, [1]

$$f_{10}(x) = \frac{3125}{24}x^4 e^{-5x} \qquad (9)$$

Equations for calculating U_i (2) and X_i (6) for different distributions are listed in Table 1.

As it was shown above, upon selection of x_i, conditions (2) and (3) guarantee the conservation of the zeroth and the first moments of the distribution. The other moments are described by the finite numbers X_i not exactly. The values $\overline{x^2}$ and $\overline{x\sqrt{x}}$ were calculated to check the accuracy of their description. Also the values $\overline{\sqrt{x}}$ and $\left(\overline{x/(x+a)}\right)$ have been calculated because they directly enter into the investigated functions: the combinations with $\sqrt{x}$ were necessary for the calculation of self-shielding factor of cross-section and the value $x/(x+a) \sim \frac{\Gamma_n}{(\Gamma_n+\Gamma_\gamma)}$ was necessary for the calculation of capture cross-section. Thus the following integrals were considered:

$$\overline{\sqrt{x}} = \int_0^\infty \sqrt{x}\, f(x)\, dx$$

$$\overline{x\sqrt{x}} = \int_0^\infty x\sqrt{x}\, f(x)\, dx \qquad (10)$$

$$\overline{x^2} = \int_0^\infty x^2 f(x)\, dx$$

The exact integral values (10), obtained for different distributions are listed in Table 2. A comparison with the approximate values gives us a feeling for the precision of the considered approximation of these distributions.

2.2 The Selection of the Optimum Number of Resonances

In order to obtain X_i, the neutron width distribution was divided into an optimum number of intervals n. For a more exact description of this distribution, it is necessary to break it up into more intervals. On the other hand, a more detailed subdivision of the distribution range generates an increased number of effective resonances, which proportionaly increases the computing time of the cross-section energy dependence for each spin state of every nucleus being investigated; in other words, the method becomes unsuitable for large scale calculations Also, as will be shown below, as one increases the number of intervals, it becomes more difficult to order the resonances in a given sequence.

Values of X_i were found for the $f_1(x)$ distribution for different numbers of intervals, namely, for n= 4,8,10,20 and 50 (see Table 3). The results of the calculations of $f_1(x)$ with different number of intervals (n) and their comparison with the exact values ($n \to \infty$), taken from Table 2, are shown in Table 4. The comparison of the

function

$$\frac{x}{x+a} = \int_0^\infty \frac{x}{x+a} f_1(x)\,dx = 1 - \sqrt{\frac{\pi a}{2}}\, e^{a/2}\left[1 - \Phi\left(\sqrt{\frac{a}{2}}\right)\right] \qquad (12)$$

with exact values, for $\nu = 1$, is given in Table 5.

On the basis of the results given in Tables 4 and 5, it was decided to stop at 20 resonances. Another factor which influenced this decision is the fact that the URAN Programme 2 , which will be used in the future to calculate the energy dependence of the cross-section, considers the influence of 10 levels lying on either side of each resonance being calculated. It must be noted that if 20 resonances are enough to describe the f_1-distribution, this number of resonances is certainly enough to describe the more "narrow" distributions f_m $(n>1)$ and f_β . The results of the calculations of U_i and X_i for the f_1 and f_β distribution in the case of 20 resonances ($n = 20$) are listed in Table 6. The comparison of the exact values with the approximations leads to the conclusion that 20 resonances suffice to describe the considered distributions. For the f-distribution, this can be seen in Table 4, for the f_3-distribution the deviation from the exact solution is (-0.3%) even for $\overline{x^2}$.

3. Quasi-Random Sequence of Resonances

3.1 Sequential Ordering of Resonances by Widths

After selecting a resonance sequence which satisfies the width and level spacing distributions, it is necessary to order the X_i values (Table 4) in a "most random fashion". In the case of the assumed sequential order of chosen resonances, it is particularly essential to avoid correlation between the widths of neighboring resonances. In order to satisfy this condition, it will be necessary that the assumed sequential order describes the theoretical distribution of the neighboring resonance width dependence as well as possible. The latter can be easily achieved if one assumes that the resonance widths are not correlated. In this case, the distribution of $Z = X/Y$ is:

$$F(z) = \int_0^\infty f_x[x(z)]\, f_y[y]\, \frac{dx[z,y]}{dz}\, dy \qquad (13)$$

Where f_x and f_y are distributions which are a function of x and y.

$$F(z) = \int_0^\infty f_x(yz)\, f_y(y)\, y\, dy \qquad (14)$$

For the case when x and y are widths of neighboring resonances, then

$$x = \frac{\Gamma_{n_1}}{\Gamma_n} \qquad \text{and} \qquad y = \frac{\Gamma_{n_2}}{\Gamma_n}$$

$f_x(x)$ and $f_y(y)$ are distributions of the form f_1. Then,

$$F(z) = \frac{1}{\pi\sqrt{z}\,(z+1)} \qquad (15)$$

It is easy to check that the normalization condition $\int_0^\infty F(z)\,dz = 1$ (Equation 16) is satisfied.

The F(z) distribution, just as f(x) can be subdivided into intervals. For the interval boundaries $Z_{b,k}$ and the mean values $\overline{Z}_k$ in the interval can be obtained from the following equation:

$$Z_{b,k} = tg^2\left(\frac{k\pi}{2n}\right) \tag{17}$$

Where K = number of the interval

n = total nunber of intervals

$$\overline{Z}_k = n\int_{Z_{b,k-1}}^{Z_{b,k}} z\,F(z)\,dz = \frac{2n}{\pi}\left(\sqrt{Z_{b,k}} - \sqrt{Z_{b,k-1}}\right) - 1 \tag{18}$$

The results of the calculation of $Z_{b,k}$ and Z_k for n = 10 are given in Table 7.

In the process of sequentially ordering the chosen resonances according to their widths, they were separated into two groups. All X_{2k-1} resonances were assigned to the first group and all X_{2k} resonances were assigned to the second group; where X_k is the sequence of the values according to their increasing magnitude (see Table 6).

It was assumed that in the case of a random sequence, the resonances of these groups must alternate. Furthermore, a matrix A_{ij}, whose terms were equal to

$$a_{ij} = X_i/X_j \quad \text{where } i = (2k-1) \text{ and } j = 2k \tag{19}$$

was constructed for every set of 20 resonances. At the same time, it was necessary to determine to which "K" Group, the piece-wise continuous $F(z)$ approximating function belonged. The resulting A_{ij} and the distribution of a_{ij} according to groups (B_{ij} Matrix) are given in Tables 8 and 9.

It was then necessary to choose two sequences of a_k from the A_{ij} Matrix, each of which satisfied the following two conditions:

1. That each Group "K" would contain one pair of resonances (i.e. β_{ij} matrix)
2. That each resonance is considered only once.

In this case, for each resonance, it will be determined which resonance lies to its right (the first Q_k sequence), and which to its left (the second Q_k sequence). These two sequences cannot overlap at any point, otherwise it can happen that a given resonance level lies both to the left and to the right of the given resonances.

Figure 1 gives the F(z) distribution for f_1 and the 10 group description of this function for the finally determined Q_K sequence, is shown in Table 9. From this curve it can be seen how well the chosen resonance ordering sequence describes the theoretical $F(z)$ distribution. The final sequence of the $x = \Gamma_m/\overline{\Gamma}_m$ values for the case of twenty resonances is given in Table 10.

3.2 The distribution of distances between resonances

Having determined the resonance sequence according to their widths, it is now necessary to find the most likely distribution of the distances from one resonance to another, based on the chosen inter-resonance distances (D) (see f in Table 8). This is important so as to correctly account for the fluctuations in the interfering terms. The distributions of the relationship of the resonance widths to the distances between them and to that of the preceeding levels have been described.

Defining: $$x = \frac{\Gamma_m}{\overline{\Gamma}_m} \quad ; \quad y = \frac{D}{\overline{D}} \qquad \xi = \frac{x}{y} \tag{20}$$

It is assumed that x is a function of $f_1(x)$, and that y is a function of $f_2(y)$, and that they are independent. It results then, that

$$f_\xi(\xi) = \frac{1}{2}\sqrt{\frac{\pi}{2\xi}} \int_0^\infty u^{3/2} e^{-\frac{\xi}{2}u - \frac{\pi}{4}u^2} du \qquad (21)$$

The theoretical distribution $f_\xi(\xi)$ was obtained by nummerically integrating expression (21). The differential distribution f_ξ yielded the integral

$$F_\xi = \int_0^\xi f_\xi(\xi') d\xi' \qquad (22)$$

which was subdivided into 20 groups in accordance with the chosen number of resonances. In order to obtain the earlier values of x_i and y_i, a Matrix with the following terms was constructed

$$\xi_{ij} = x_i / y_j \qquad (23)$$

Then, in the same manner in which it was done for the other distributions, 20 values of ξ_k, which describe the distrubtion well enough (see Figure 2), were chosen from the set of ξ_{ij} values. The resonances were thus distributed according to the distances between them. The values of $x = \Gamma_n / \overline{\Gamma_n}$, and the corresponding values of $y = D/\overline{D}$ for 20 resonances are listed in Table 10.

The above described method can be used to account for the fluctuation of the fission width Γ_f for known nummbers of channels, as well as for the fluctuation of the neutron width D. Since this report had primarily a methodological character, only the fluctuation of Γ_n and D have been investigated, i.e. the results obtained here are pertinent to non-fissionable nuclei.

4. The Method to Calculate Group Cross-sections

On the basis of known average parameters, such as Γ_γ, D, S_o, etc..., as well as selected values of $\varkappa$ and γ (Table 10), it has been possible to construct quasi-random sequences of resonances for every state of a given nucleus. For instance, for U-238 in the region where the d-wave does not have any contribution, this state is ($\ell = 0$, $j = 1/2$) and ($\ell = 1$, $j = 3/2$). In principle it is possible to take into account any number of states which contribute to the group values of a given element. Furthermore, using a computer programme like URAN (see reference 2) for each of the i-states it is possible to calculate transmission as a function of thickness (t), thus

$$Tt_i(t) = \int_{\Delta u_{gr}} e^{-\rho_i \sigma_{t,i} \cdot t}\, du$$

$$Tc_i(t) = \int_{\Delta u_{gr}} \sigma_{c,i}\, e^{-\rho_i \sigma_{t,i} t}\, du \qquad (24)$$

where

Δu_{gr} - the width of the considered energy group in units of lethargy

σ_t, σ_c - the total and capture cross-sections as a function of energy

ρ_i - density of the considered nuclei

From this notation it follows that it is possible to perform the same calculations for mixtures of nuclei. Following the evaluation of Tt_i and Tc_i for each of the components, one determines then the transmission values for the given element. However, since the different states are correlated, it is advisable to use the following transformations.

$$Tt(t) = \int_{\Delta u_{gr}} du\, e^{-\sum_i \rho_i \sigma_{t,i} t} = \prod_i Tt_i(t)\,;$$

$$Tc(t) = \int du \left(\sum_i \sigma_{c,i}\right) e^{-\sum_i \rho_i \sigma_{t,i} t} = \sum_i \left[\left(\prod_{i \neq j} Tt_i(t)\right) Tc_j(t)\right] \qquad (25)$$

Similarly, just as for $\overline{T_c}(t)$, it is possible to calculate transmissions $\overline{T_s}(t)$ and $\overline{T_f}(t)$ for scattering and fission.

The transmission values for each considered element were calculated for various temperatures. From these, it is possible to obtain average group characteristics such as $\left\langle \frac{1}{\sigma_t} \right\rangle$ and $\left\langle \frac{\sigma_c}{\sigma_f} \right\rangle$ by integration of the transmissions over the thicknesses (Ref-1).

Finally, depending on the given problem it is also possible to calculate resonance self-shielding factors for cross-sections at different temperatures and dilutions (Reference 2), or sub-group parameters (Reference 4).

REFERENCES

1. S. Collatz. Kernenergie, II, I, 1968.

2. L.P. Abagyan, M.N. Nikolaev, L.V. Petrova.

   USSR Nuclear Data Centre Bulletin,
   Vol. 4, 392 (1967).

3. P. Creebler, B.A. Hutchins. "Physics of fast and intermediate reactors". Vienna, 18/59, 1961.

4. M.N. Nikolaev, Z.F. Chochlov,

   USSR Nuclear Data Centre Bulletin,
   Vol. 4, 420 (1967)

Table 1

Equations **for Calculation U_i and X_i**

Distribution type

The type of distribution	
$f_1(x)$	$\Phi\left(\sqrt{\frac{u_i}{2}}\right) = \frac{i}{n}$; $x_i = 1 + \frac{2n}{\sqrt{\pi}}\left(\sqrt{\frac{u_{i-1}}{2}}e^{-\frac{u_{i-1}}{2}} - \sqrt{\frac{u_i}{2}}e^{-\frac{u_i}{2}}\right)$;
$f_2(x)$	$u_i = \ln\left(\frac{n}{n-i}\right)$; $x_i = n\left[(u_{i-1}+1)e^{-u_{i-1}} - (u_i+1)e^{-u_i}\right]$;
$f_3(x)$	$\Phi\left(\sqrt{\frac{3}{2}u_i}\right) - \frac{2}{\pi}\sqrt{\frac{3u_i}{2}}e^{-\frac{3u_i}{2}} = \frac{i}{n}$; $x_i = \frac{n}{4}\left[\Phi\left(\sqrt{\frac{3}{2}u_i}\right) - \Phi\left(\sqrt{\frac{3}{2}u_{i-1}}\right)\right] - \frac{n}{6\sqrt{2\pi}}\left[\sqrt{u_i}e^{-\frac{3u_i}{2}}(u_i+3\sqrt{3}) - \sqrt{u_{i-1}}e^{-\frac{3u_{i-1}}{2}}(u_{i-1}+3\sqrt{3})\right]$;
$f_4(x)$	$(2u_i+1)e^{-2u_i} = 1 - \frac{i}{n}$; $x_i = n\left[(2u_{i-1}^2+2u_{i-1}+1)e^{-2u_{i-1}} - (2u_i^2+2u_i+1)e^{-2u_i}\right]$;
$f_5(x)$	$u_i = \frac{2}{\sqrt{\pi}}\sqrt{\ln\frac{n}{n-i}}$; $x_i = n\left[\Phi\left(\frac{\sqrt{\pi}}{2}u_i\right) - \Phi\left(\frac{\sqrt{\pi}}{2}u_{i-1}\right) - \left(u_i e^{-\frac{\pi u_i^2}{4}} - u_{i-1}e^{-\frac{\pi u_{i-1}^2}{4}}\right)\right]$

where $\Phi(x) = \frac{2}{\sqrt{\pi}}\int_0^x e^{-y^2}dy$ - is the probability integral

TABLE 2

Exact values of Different Moments.

	$f_1(x)$	$f_2(x)$	$f_3(x)$	$f_4(x)$	$f_8(x)$
$\overline{\sqrt{x}}$	$\sqrt{\frac{2}{\pi}}$	$\frac{\sqrt{\pi}}{2}$	$2\sqrt{\frac{2\pi}{3}}$	$\frac{3}{2}\sqrt{\frac{\pi}{2}}$	
$\overline{x\sqrt{x}}$	$2\sqrt{\frac{2}{\pi}}$	$\frac{3}{4}\sqrt{\pi}$	$\frac{4}{3}\sqrt{\frac{2}{3\pi}}$	$\frac{15}{32}\sqrt{2\pi}$	
$\overline{x^2}$	3	2	$\frac{5}{3}$	$\frac{3}{2}$	$\frac{4}{\pi}$

TABLE 3

Values of X_i for the f_1 - Distribution.

n / i	4	n / i	8	n / i	10	n / i	20	n / i	50				
1	0.0332	1	0.008I7	1	0.00522	1	0.00I34	1	0.0002	2I	0.290	4I	I.72
2	0.252I	2	0.05573	2	0.03598	2	0.009I5	2	0.00I69	22	0.328	42	I.88
3	0.8203	3	0.I78I	3	0.I044	3	0.02502	3	0.00383	23	0.354	43	2.I2
4	2.8944	4	0.338	4	0.2II6	4	0.04922	4	0.00907	24	0.394	44	2.25
		5	0.6I0	5	0.356I	5	0.082I7	5	0.0II6I	25	0.425	45	2.55
		6	I.03	6	0.5743	6	0.I24I	6	0.0I98	26	0.487	46	2.88
		7	I.77	7	0.8794	7	0.I763	7	0.0273	27	0.526	47	3.29
		8	4.0I	8	I.335	8	0.2392	8	0.0330	28	0.566	48	3.85
				9	2.I05	9	0.3I5I	9	0.0483	29	0.628	49	4.74
				I0	4.393	I0	0.407I	I0	0.053I	30	0.673	50	7.I7
						II	0.5II2	II	0.0760	3I	0.746		
						I2	0.6376	I2	0.0866	32	0.802		
						I3	0.788I	I3	0.0990	33	0.870		
						I4	0.9704	I4	0.II99	34	0.944		
						I5	I.I94	I5	0.I379	35	I.034		
						I6	I.476	I6	0.I44I	36	I.I2		
						I7	I.846	I7	0.I949	37	I.23		
						I8	2.368	I8	0.2I02	38	I.32		
						I9	3.203	I9	0.2575	39	I.44		

TABLE 4

Comparison of Approximate Values **of Moments with the** Exact Values **for** the f_1 Distribution

Number of intervals	4	8	I0	20	50	
$\overline{\sqrt{x}}$	0.8228	0.8073	0.8039	0.800I	0.7989	0.7979
deviation(%)	3.I2	I.I8	0.75	0.28	0.I3	-
$\overline{x\sqrt{x}}$	I.449	I.524	I.542	I.570	I.584	I.596
deviation(%)	-9.2I	-4.5I	-3.38	-I.63	-0.75	-
$\overline{x^2}$	2.279	2.599	2.680	2.83I	2.92I	3
deviation (%)	-24.0	-I3.4	-I0.7	-5.6	-2.6	-

TABLE 5

Comparison of Approximate Values of $\overline{\frac{x}{x+a}} \Big/ \frac{\bar{x}}{\bar{x}+a}$ **with the** exact values **for** the f_1 Distribution

a \ n	4	8	I0	20	50	∞
0.000I	0.999	0.998	0.998	0.996	0.99I	0.988
0.00I	0.992	0.984	0.980	0.976	0.964	0.958
0.003	0.978	0.958	0.952	0.948	0.938	0.937
0.0I	0.939	0.907	0.90I	0.900	0.894	0.893
0.026	0.880	0.852	0.849	0.845	0.844	0.844
0.05I	0.828	0.807	0.804	0.80I	0.800	0.800
0.I	0.776	0.762	0.759	0.758	0.755	0.755
0.2	0.73I	0.7I8	0.7I5	0.7I3	0.7I2	0.7I2
0.3	0.7I3	0.70I	0.698	0.696	0.694	0.694
0.5	0.702	0.688	0.685	0.683	0.682	0.682
I.0	0.7I3	0.698	0.694	0.690	0.690	0.690
2.0	0.758	0.738	0.734	0.729	0.726	0.726
3.0	0.794	0.773	0.768	0.763	0.76I	0.76I
5.0	0.843	0.822	0.8I8	0.8I2	0.809	0.806
I0.0	0.903	0.886	0.882	0.876	0.873	0.868
30.0	0.96I	0.953	0.95I	0.947	0.945	0.930
I00.	0.988	0.985	0.984	0.982	0.982	0.980

TABLE 6

Values of U_1 and X_1 for n=20 of the f_1 and f_β Distribution

f_1						f_β					
i	u_i	x_i	i	u_i	x_i	i	u_i	x_i	i	u_i	x_i
I	0.0039	0.00I34	II	0.5706	0.5II2	I	0.2555	0.I694	II	I.008	0.9732
2	0.0I58	0.00915	I2	0.7083	0.6376	2	0.3663	0.3I42	I2	I.080	I.0436
3	0.0358	0.02502	I3	0.8734	0.788I	3	0.4549	0.4II0	I3	I.I56	I.II9
4	0.0642	0.04922	I4	I.074	0.970I	4	0.5330	0.4952	I4	I.238	I.I97
5	0.I0I5	0.082I7	I5	I.323	I.I94	5	0.6052	0.5692	I5	I.329	I.282
6	0.I485	0.I24I	I6	I.642	I.476	6	0.6739	0.6404	I6	I.432	I.378
7	0.2059	0.I763	I7	2.072	I.846	7	0.7406	0.7070	I7	I.554	I.492
8	0.2750	0.2392	I8	2.706	2.368	8	0.8065	0.7728	I8	I.7I2	I.628
9	0.3573	0.3I5I	I9	3.84I	3.203	9	0.8725	0.8400	I9	I.953	I.822
I0	0.4549	0.407I	20	∞	5.577	I0	0.9394	0.9060	20	∞	2.240

TABLE 7

Values of $Z_{gr,\kappa}$ and Z_κ for k=20

κ	I	2	3	4	5	6	7	8	9	I0
$Z_{гр,к}$	0.0253	0.I056	0.2596	0.5279	I.000	I.894	3.852	9.472	39.86	∞
Z_κ	0.0083	0.060I	0.I752	0.38I8	0.7408	I.396	2.733	6.095	I9.60	–

TABLE 8

The Matrix A_{ij} for 20 Resonances

	I	2	3	4	5	6	7	8	9	I0
$2k-1$ / $2k$	I	3	5	7	9	II	I3	I5	I7	I9
2	6.83	0.366	0.III	0.05I9	0.0290	0.0I79	0.0II6	0.00766	0.00496	0.00286
4	36.7	I.97	0.599	0.279	0.I56	0.0963	0.0625	0.04I2	0.0267	0.0I54
6	92.6	4.96	I.5I	0.704	0.394	0.243	0.I57	0.I04	0.0672	0.0387
8	I79	9.56	2.9I	I.36	0.759	0.468	0.304	0.200	0.I30	0.0747
I0	304	I6.3	4.95	2.3I	I.29	0.796	0.5I7	0.34I	0.22I	0.I27
I2	476	25.5	7.76	3.62	2.02	I.25	0.809	0.534	0.345	0.I99
I4	724	38.8	II.8	5.50	3.08	I.90	I.23	0.8I3	0.526	0.303
I6	IIOI	59.0	I8.0	8.37	4.68	2.89	I.87	I.24	0.799	0.46I
I8	I766	94.6	28.8	I3.4	7.5I	4.63	3.00	I.98	I.28	0.739
20	4I62	223	67.9	3I.6	I7.7	I0.9	7.08	4.67	3.02	I.74

TABLE 9

The Matrix B_{ij} for 20 Resonances

2_{k-1} / 2_k	I	3	5	7	9	II	I3	I5	I7	I9
2	8	4	3	2	(2)	[I]	I	I	I	I
4	9	7	[5]	4	3	2	2	2	2	(I)
6	I0	8	6	(5)	4	3	3	[2]	2	2
8	I0	9	7	6	5	4	[4]	(3)	3	2
I0	I0	9	8	7	6	5	(4)	4	[3]	3
I2	I0	[9]	(8)	7	7	6	5	5	4	3
I4	I0	(9)	9	8	[7]	7	6	5	4	4
I6	I0	I0	9	[8]	8	(7)	6	6	5	4
I8	[I0]	I0	9	9	8	8	7	7	(6)	5
20	(I0)	I0	I0	9	9	9	8	8	7	[6]

□, ○ -selected resonance sequences

TABLE 10

Values of $x = \frac{\Gamma_n}{\bar{\Gamma}_n}$ and $y = \frac{D}{\bar{D}}$ for 20 Resonances

i	x	y		i	x	y
I	x_I = 0.00I34	y_8 = 0.7728		II	x_{II} = 0.5II2	y_{I9} = I.822
2	x_{20} = 5.577	y_{I7} = I.492		I2	x_{I6} = I.476	y_I = 0.I694
3	x_{I9} = 3.203	y_{I5} = I.282		I3	x_7 = 0.I763	y_{I2} = I.0436
4	x_4 = 0.04922	y_{I4} = I.I97		I4	x_6 = 0.I24I	y_2 = 0.3I42
5	x_5 = 0.082I7	y_7 = 0.7070		I5	x_{I5} = I.I94	y_9 = 0.8400
6	x_{I2} = 0.6376	y_{I6} = I.378		I6	x_8 = 0.2392	y_5 = 0.5692
7	x_3 = 0.02502	y_4 = 0.4952		I7	x_{I3} = 0.788I	y_{II} = 0.9732
8	x_{I4} = 0.9704	y_{I8} = I.628		I8	x_{I0} = 0.407I	y_6 = 0.6404
9	x_9 = 0.3I5I	y_{I3} = I.II9		I9	x_{I7} = I.846	y_3 = 0.4II0
I0	x_2 = 0.009I5	y_{I0} = 0.9060		20	x_{I8} = 2.368	y_{20} = 2.240

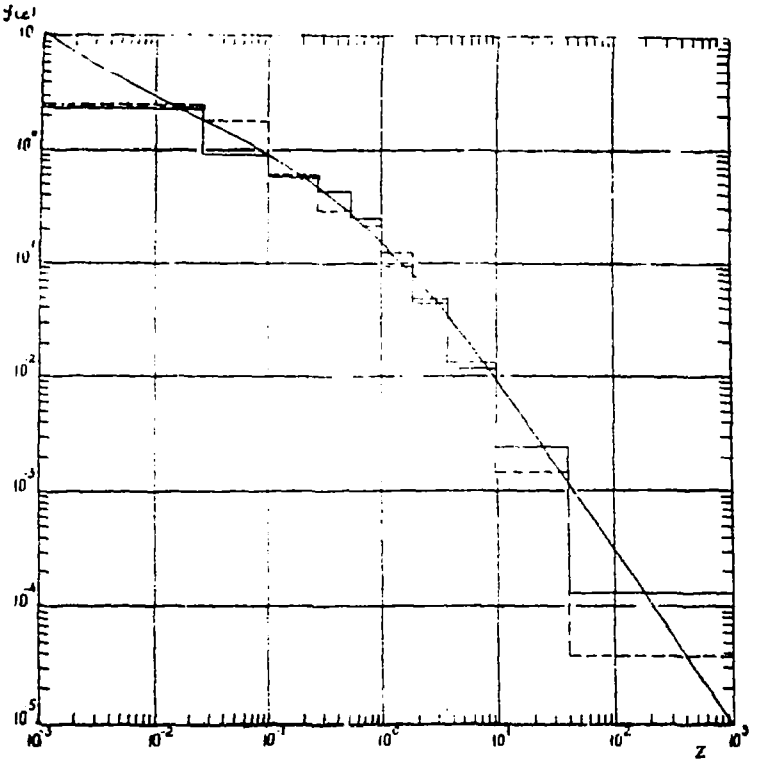

fig 1

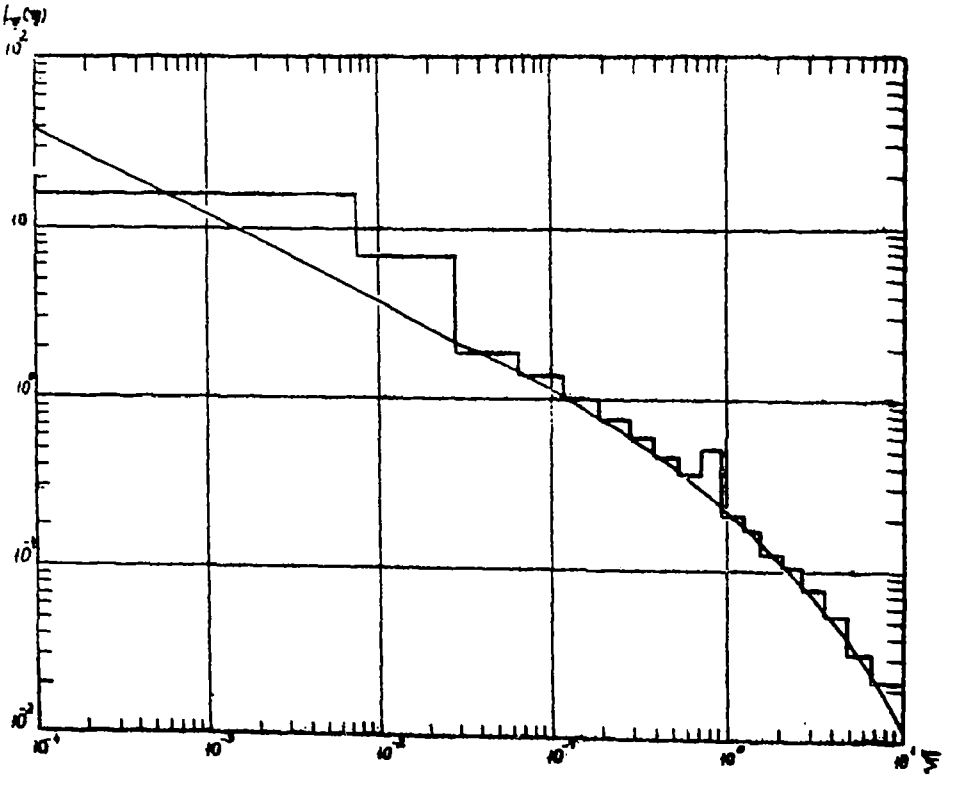

fig.2

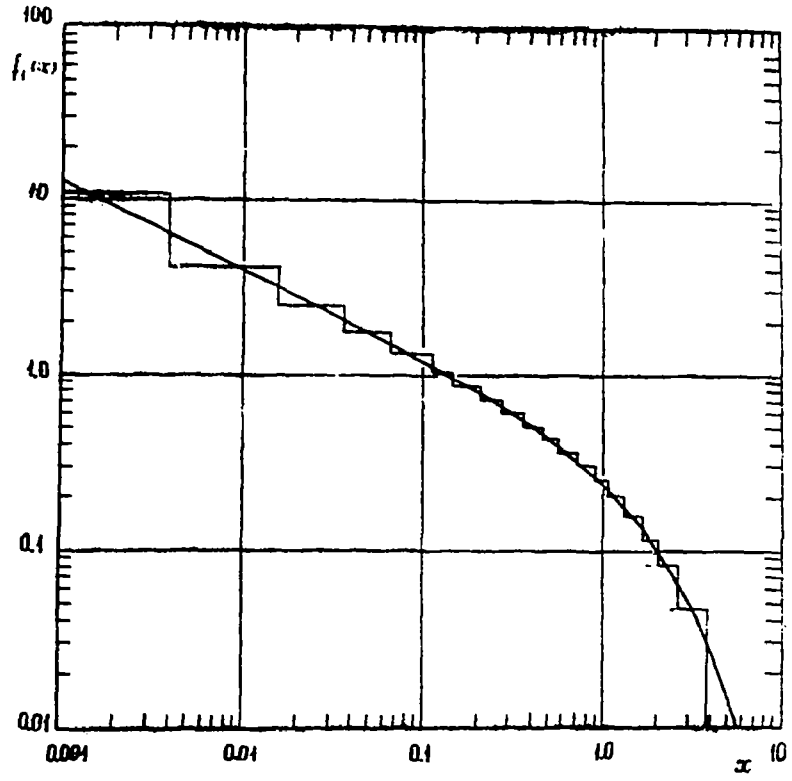
100
10
1.0
0.1
0.01
0.001
0.01
0.1
1.0
10
x

fig 3

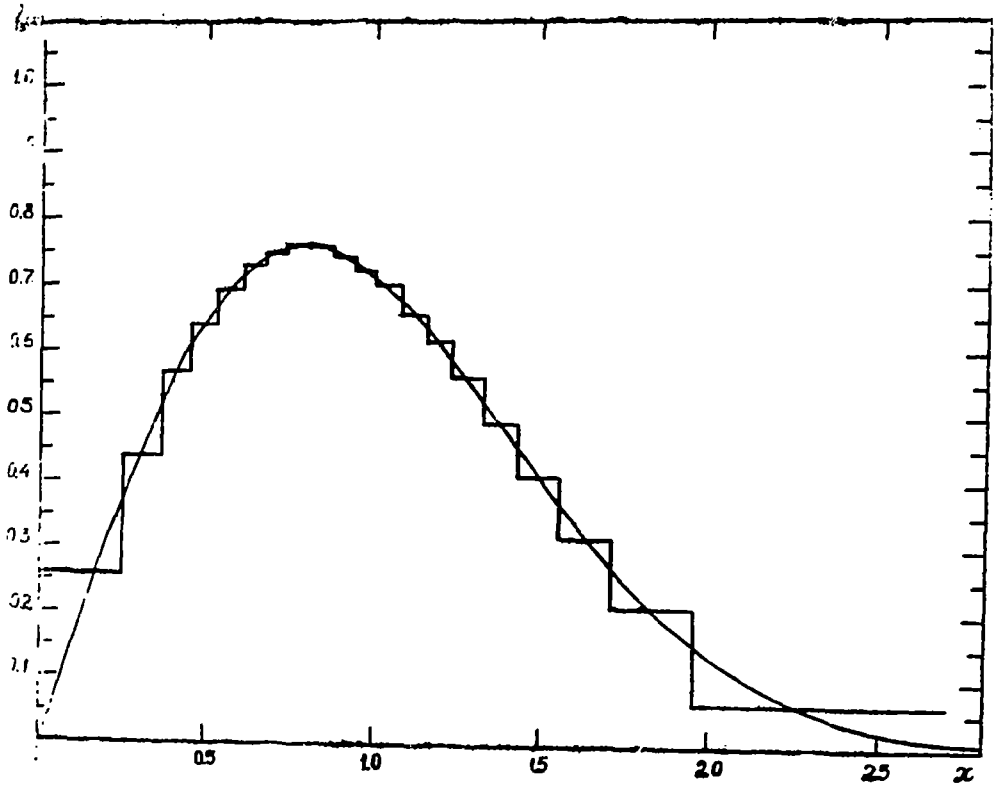
0.8
0.7
0.6
0.5
0.4
0.3
0.2
0.5
1.0
1.5
2.0
2.5
x

fig. 4

TEMPERATURE DEPENDENCE OF THE CROSS-SECTION STRUCTURE OF ^{238}U IN THE REGION OF UNRESOLVED RESONANCES

A.A. Vankov, Yu.V. Grigoriev, M.N. Nikolaev, V.V. Filippov
(Institute of Physics and Power Engineering, Obninsk, USSR)

B. Boehmer, S. Collatz
(Central Institute of Nuclear Research, Rossendorf
German Democratic Republic)
and

L.B. Pickelner
(Joint Institute for Nuclear Research, Dubna, USSR)

Institute of Physics and Power Engineering
Obninsk, USSR

Translation made by IAEA

1. Introduction

In fast power reactors using ceramic fuel and sodium coolant, the Doppler effect or the temperature coefficient of reactivity is the basic factor which compensates for any increase in reactivity during accidental ejection of sodium from the core. For this reason, a fairly accurate knowledge of these competing factors is essential if we are to make reliable assessments of nuclear safety in power stations using fast reactors. The most difficult problem is to calculate the Doppler effect as our information about the average resonance parameters which determine the Doppler effect in the unresolved resonance region (very important in the case of fast reactors) is not very reliable. Hence there arose the problem of carrying out sufficiently direct measurements of the parameters which govern the Doppler effect on the main isotopes undergoing fission - over the whole energy range where this effect occurs. The present work aims at a solution of this problem. As the first object of study we chose ^{238}U, which accounts for 20% of the total Doppler effect in fast power reactors.

2. Method

In the resonance region, capture and scattering cross-sections and the diffusion coefficient of the medium, averaged over the neutron spectrum, can be represented as shown below in expressions (1) and (2), with the approximation of constant collision density and isotropic scattering (which is justified in the case under consideration):

$$\overline{\Sigma}_c = \frac{\langle \Sigma_c / \Sigma_t \rangle}{\langle 1 / \Sigma_t \rangle} \tag{1a}$$

$$\overline{\Sigma}_s = \frac{\langle \Sigma_s / \Sigma_t \rangle}{\langle 1 / \Sigma_t \rangle} \tag{1b}$$

$$\overline{D} = \frac{\langle 1/\Sigma_t^2 \rangle}{3\langle 1/\Sigma_t \rangle} \qquad (1c)$$

Here the angular brackets denote averaging over an energy range containing many resonances but narrow enough for the energy dependence of the mean resonance parameters or collision density to have little effect on the results of averaging. A bar above the symbols indicates that they are effective parameters of the medium with which the resonance-averaged neutron flux can be calculated.

Doppler broadening of the resonances changes the results of averaging, i.e. it changes the effective parameters and hence the multiplying properties of the medium.

Let us assume that ^{238}U is the only resonance absorber in the medium over the energy range considered. Then,

$$\langle \Sigma_c/\Sigma_t \rangle = \left\langle \frac{\sigma_c^8}{\sigma_t^8+\sigma_0} \right\rangle + \sum_{n\neq 8} \frac{\rho_n \langle \sigma_c^n \rangle}{\langle \Sigma_t \rangle} \qquad (2)$$

Here the superscript 8 denotes that the quantity relates to ^{238}U, ρ_n is the density of nuclei of the n kind and

$$\sigma_0 = \frac{1}{\rho_8} \sum_{n\neq 8} \rho_n \langle \sigma_c^n \rangle \qquad (3)$$

is the "cross-section of dilution" of ^{238}U by other components of the medium. The temperature dependence of $\langle \Sigma_c/\Sigma_t \rangle$ is given, under the conditions considered here, by the first term on the right-hand side of expression (2). In the same way, we can also represent other average qualities on the right-hand sides of the equations in (1). Thus, to determine the temperature dependence of the effective macroscopic parameters in (1) which are governed by the Doppler effect on ^{238}U, we need to know the average values of

(4)

as a function of the mean energy of the averaging interval - generally speaking for any values of σ_o .

The quantities in expression (4) can be written as integrals of the transmission functions T(t) and $T_x(t)$ for a beam of neutrons (distributed over the energy range Δ E, the averaging interval) passing through filters of the material under study with thickness t, measured in "good" geometry by means of a detector with constant energy sensitivity (T(t)) or a detector which registers x-type reactions in a thin sample of the material located beyond the filter ($T_x(t)$):

$$\left\langle \frac{1}{(\sigma_t^g + \sigma_o)^n} \right\rangle = \frac{1}{(n-1)!} \int_0^\infty t^{n-1} T(t) e^{-N\sigma_o t} dt \tag{5a}$$

$$\left\langle \frac{\sigma_x^g}{\sigma_t^g + \sigma_o} \right\rangle = \langle \sigma_x^g \rangle \int_0^\infty T_x(t)\, e^{-N\sigma_o t} dt \tag{5b}$$

where

$$T(t) = \frac{1}{\Delta E} \int_{\Delta E} e^{-N\sigma_t^g(E)t} dE \tag{6a}$$

$$T_x(t) = \frac{\int_{\Delta E} \sigma_x^g(E)\, e^{-N\sigma_t^g(E)t} dE}{\int_{\Delta E} \sigma_x^g(E)\, dE} \tag{6b}$$

The purpose of the present study is to measure the functions T(t) and $T_x(t)$ and their temperature dependence, mainly for ^{238}U. So far the temperature dependence of T(t) has been measured at energies up to 120 keV (i.e. over the whole energy range where the Doppler effect on ^{238}U is significant) and a preliminary analysis of the results has been performed. Tentative measurements of $T_c(t)$ have also been carried out.

3. Experimental lay-out

The experimental lay-out is shown in Fig. 1. A beam of neutrons from the core of the IBR pulsed fast reactor was passed through an evacuated neutron tube to fall on a detector installed at a path length of 1000 m. A vacuum furnace

containing a set of metallic uranium samples 1-128 mm in thickness and 195 mm in diameter was placed at a distance of 75 m from the reactor in a gap in the neutron tube. Before reaching the furnace, the neutron beam was narrowed to a diameter of 50-180 mm by a collimator. The transmission functions were measured at room temperature as were the variations in these functions with rising temperature up to $770 \pm 30^{\circ}C$. The variations were determined by alternate measurements of the count rate from hot and cold samples of equal thickness (the latter installed outside the furnace, since heating and especially cooling of the samples inside the furnace required a lot of time). A liquid scintillation detector [3] with a scintillator surface area of 800 cm^2 was used for these measurements. The efficiency of the detector was almost independent of energy and amounted to about 30% at 10 keV.

We also performed preliminary rough measurements of the "capture" transmission functions $T_c(t)$, using a liquid scintillation detector [4] in which the ratio between the gamma-ray and scattered-neutron detection efficiencies was about 150. The detector was placed at a path length of 240 m. The results thus obtained are not, however, sufficiently reliable owing to the high background level and the difficulty of calculating it. In future, we intend to use improved detectors for measuring the $T_c(t)$ functions. For the basic measurements the IBR was operated in two régimes - in pulsed reactor and in microtron conditions. In the first case, the average power of the reactor was n = 3 kW, neutron burst frequency was f = 5 c/s and burst width at half-height τ = 60 μsec. In the second case, the reactor worked as a booster multiplying the neutrons generated in the target of an electron microtron accelerator. Here n = 0.6 kW, f = 50 c/s and τ = 3 μsec. The resolution, with allowance for the time-channel width of the analyser, was 68 nsec/m in pulsed reactor operation and 3.5 nsec in microtron operation.

For time analysis of the pulses from the detector 2048- and 4096-channel analysers were used, and the information thus obtained was transmitted to a Minsk-2 computer for preliminary processing.

4. Background and other corrections

The intrinsic background of the detector was highly stable and could easily be taken into account. Let us denote by N(t) the count rate of the detector in some time-channel, minus the intrinsic background, when the beam passes

through a filter of thickness t. Let $\alpha(t)$ be the proportion of background pulses due to the operation of the reactor in relation to the total count rate of the detector. We then have, for the channel under consideration,

$$T(t) = \frac{N(t)\,[1-\alpha(t)]}{N(0)\,[1-\alpha(0)]} = \frac{N(t)}{N(0)}\left[1-\frac{\alpha(t)-\alpha(0)}{1-\alpha(0)}\right] \qquad (7)$$

The values of $\alpha(t)$ were determined by means of resonance filters (manganese, iron, sodium, aluminium and uranium-238 filters) up to an energy of 7 keV in the case of pulsed reactor operations and up to 35 keV in microtron operations for thicknesses of $t \leqslant 64$ mm. It was found that the background accounted for 10-20% of the total count rate and, within an error of about 2%, did not depend on filter thickness in the above-mentioned thickness and energy ranges. It was assumed that the background would continue to be independent of thickness at $t \leqslant 64$ mm for higher energies as well, but the validity of this assumption diminishes with increasing energy and the accuracy is only $\pm$ 4% at E ~ 100 keV. This very slight dependence of the background on thickness is due to the weak energy dependence of transmission for thicknesses up to 64 mm: average transmission for energies in the 1-100 keV range differs from the maximum by only 15%. Since the background itself accounts for 15% of the total number of pulses, the difference between background attenuation and neutron attenuation in the filters should not exceed 20%.

The background was not measured with thicker filters. However, for t = 128 mm the quantities measured were not the transmission functions themselves but their ratios:

$$\frac{T(t_1)}{T(t_2)} = \frac{N(t_1)}{N(t_2)}\left[1-\frac{\alpha(t_1)-\alpha(t_2)}{1-\alpha(t_1)}\right] \qquad (8)$$

Here t_1-t_2 was not more than 64 mm. Therefore, the term in square brackets in expression (8) could also be taken as equal to unity, with the same accuracy.

Apart from the background correction - which, as has been pointed out, effects only the error and not the quantity being determined, T(t) - corrections for counting losses were made in the count rate. When transmission functions for relatively small thicknesses (t = 32; 64 mm) were being measured in pulsed reactor

conditions in the high-energy range, these corrections were sometimes very considerable and highly approximate owing to the time dependence of the dead time of the recording system, which resulted from overloading of the detector. To eliminate overloading we had to reduce the intensity by collimating the beam and attenuating it with a lead filter. There was no detector overloading during microtron operation.

The change in transmission with heating of the filter is due not only to the Doppler effect but also to the reduction in filter thickness which accompanies thermal expansion: $t \rightarrow t\,(1 - 2\alpha\Delta\vartheta)$ where α is the linear coefficient of thermal expansion and $\Delta\vartheta$ is the temperature increment. Thus, a hot sample represents a somewhat thinner filter than a cold sample. The experimental results were not corrected for filters of different thicknesses, a fact which should be taken into consideration when these data are used.

5. Results of measurement

Tables 1 and 2 show measured transmission functions for thicknesses up to 256 mm and the temperature-induced variations in these functions. The results are given for fairly wide neutron groups so as to reduce the effect of statistical fluctuations in neutron widths and level spacings.

The effect of these fluctuations can be seen in Figs 2 and 3, which show the temperature variation of the transmission function versus neutron energy for thicknesses of 20, 32, 64 and 128 mm (with a more detailed energy break-down than in Table 2). It is interesting to note that all characteristics of the temperature variation of $T(t)$ falling outside the limits of error correlate with the characteristics of the energy dependence of $T(t)$ for large t (i.e. a large Doppler effect corresponds to the minima in the total cross-section).

Fig. 4 shows the energy dependence of the temperature variation of "capture" transmission: $T_c(8\text{ mm},\ 20^\circ C)/T_c(8\text{mm},\ 770^\circ C)$.

The temperature effect in all the transmission curves changes sign as energy increases. In the case of the normal transmission functions this is wholly due to the effect of thermal expansion, which is opposite in sign to the Doppler effect on $T(t)$. However, the effect of Doppler broadening on $T_c(t)$ can also change its sign.

The transmission functions thus obtained, after correction for thermal expansion of the filters, can be used directly for calculating $\langle 1/(\sigma_t^8 + \sigma_o)^n \rangle$ by formulas similar to (5a):

$$\left\langle \frac{1}{(\sigma_t + \sigma_o)^n} \right\rangle = \frac{1}{(n-1)!} \int_0^\infty t^{n-1} e^{-N\sigma_o t} \left[T_\vartheta^e(t) + 2\alpha\Delta\vartheta \frac{\partial T_\vartheta^e}{\partial \vartheta} \right] dt \qquad (9)$$

Here, $T_\vartheta^e(t) = K_{\Delta\vartheta}(t) T_{\vartheta_o}(t)$

where $K_{\Delta\vartheta}$ is the experimentally measured ratio of the transmissions obtained when the temperature of the sample is changed from room temperature (ϑ_o) to temperature ϑ; and $T_{\vartheta o}(t)$ is transmission at room temperature. It must be borne in mind here that for large thicknesses the transmissions $T_{\vartheta_o}(t)$ have to be calculated as products of a whole series of experimentally measured transmission ratios; the accuracy is accordingly reduced owing to statistical errors and the accumulation of possible systematic errors associated with inaccurate background correction (in the case of thin samples $\frac{\alpha(t) - \alpha(o)}{1 - \alpha(o)}$ may differ appreciably from zero). Therefore, the accuracy of the quantities in expression (5a) will diminish rapidly with increasing n owing to the greater significance of the values of $T(t)$ for large t, which involve correspondingly large errors. However, when $n = 1$ and 2 the accuracy with which the integrals are calculated should be fairly high (1-3%, according to evaluations).

To enable the data to be used in this manner, we are now subjecting the transmission functions to mathematical processing with a view to representing them as the sum of two or three exponents. The parameters required for this presentation have not yet been fully determined.

6. Determination of average resonance parameters for ^{238}U

As has been pointed out, the information we now have on the cross-section structure of ^{238}U is not adequate for direct determination of the necessary average characteristics by the formulas in expression (5), since we have not yet measured the functions $T_c(t)$. We can, however, try to use the whole set of data obtained thus far to determine the average resonance parameters for ^{238}U and to calculate, with their help, the quantities of interest. In any case determination of the average resonance parameters naturally has an independent value of its own.

We shall denote the whole set of 102 experimental quantities given in Tables 1 and 2 by x_i and select by the method of least squares that group of average resonance parameters which best describes this set. The group of resonance parameters to be determined consists of:

- the average reduced neutron width for s-waves - $\overline{\Gamma^0_{n0}}$;
- tne average reduced neutron width for p-waves - $\overline{\Gamma^0_{n1}}$;
- the average spacing between the s-levels of the compound nucleus - $\overline{D_0}$;
- the potential scattering cross-section normalized for zero neutron energy - σ_{po}; and
- the average radiation width - $\overline{\Gamma\gamma}$.

For the energy dependences of the widths and potential scattering the following equalities were assumed:

$$\overline{\Gamma_{n0}} = \overline{\Gamma^0_{n0}}\sqrt{E}\,;\quad \overline{\Gamma_{nl}} = \overline{\Gamma^0_{nl}}\sqrt{E}\cdot v_l\,;\quad \sigma_p = 4\pi\lambda^2 \sin^2(kR')$$

$$v_1 = \frac{(kR)^2}{1+(kR)^2}\,;\qquad \sigma_p(l,J) = 4\pi\lambda^2 g(J)\cdot \sin^2\delta_l$$

R' being determined from the condition $\sigma_p(E=0) = \sigma_{po}$

The spin dependence of $\overline{D}$ was taken equal to

$$\overline{D}_J = \frac{D}{2J+1}\, e^{\frac{J+1/2}{2\sigma^2}}$$

where $\sigma^2 = 1{\cdot}12{\cdot}10^{-2}{\cdot}A^{5/3}$. The spin dependence of the p-resonance widths was determined from the condition of the spin dependence of the strength functions:

$$\left(\frac{\overline{\Gamma^0_{n1}}}{\overline{D}}\right)_{J=1/2} = \left(\frac{\overline{\Gamma^0_{n1}}}{\overline{D}}\right)_{J=3/2}$$

Fluctuations of radiation width were ignored; fluctuations in neutron widths were described by the Porter-Thomas method by χ^2-distribution with one degree of freedom, and the distribution of level spacings by an χ^2-distribution with ten degrees of freedom. Let us now denote all the parameters of interest by a vector $\vec{a}$ with components a_j. The values of these parameters are then determined from the minimization condition of the functional

$$S = \sum_{i=1}^{m} \frac{[x_i(\vec{a}) - x_i^{exp}]^2}{\sigma_i^2} \qquad (9)$$

where $\chi_i(\vec{a})$ and χ_i^{exp} are values of $\{\chi\}$ calculated by means of the set of average resonance parameters and experimentally determined values of $\{\chi\}$, respectively; and σ_i represents the errors in χ_i (see Tables 1 and 2).

The transmission values in terms of which the values of $\{\chi\}$ are expressed were calculated by means of an algorithm described in Ref. [5]. The average value of the transmission function in (6a) can be calculated by integrating $\exp(-N\sigma_t t)$ over energy in the region between resonances and over the width of each level (neglecting the contribution of other resonances). In the algorithm used here, it was possible to reduce the quadruple integration needed for this procedure to a calculation of two double integrals, given the properties of the χ^2-distribution with ten degrees of freedom. The cross-sections were calculated by means of the single-level Breit-Wigner formula; and the resonances were additively superimposed on each other. Since the cross-sections were calculated only between resonances, none of the combinations of widths and resonance spacing could give rise to negative cross-sections.

In calculating the observed temperature variations of the transmission functions, we also took account of the effect of thermal expansion of the samples. For this purpose the coefficient of linear expansion was taken as $23 \times 10^{-6}/^{\circ}C$.

The MIREPA programme for minimization of the quadratic functional in (9) was written in the ALGOL-60 language. In order to find the minimum, we need to solve the system of normal equations obtained from the condition that the derivatives of S for parameters $a_j (j = 1, 2 \ldots . n)$ are equal to zero. This system of non-linear equations was solved in the MIREPA programme by a linearization method which consisted in expanding the non-linear functions in a Taylor series around the chosen test vector $\vec{a}_0$. Once the vector $\vec{a}_1$ has been found (in a first approximation) by solving the resultant linear problem, we repeat the expansion of the functions, this time around the vector $\vec{a}_1$. If the zero approximation is correctly chosen, this iteration process converges rapidly.

Since it proved an extremely cumbersome operation to calculate the coefficients of the system of normal equations in our case, we confined ourselves as a rule to only one or two iterations and subsequently refined the solutions by determining the approximate minimum of the functional S

along the vector $\delta\vec{a}_1$: if $S(\vec{a}_1) < S(\vec{a}_o)$, we calculated $S(\vec{a}_1 + \delta\vec{a}_1)$ where $\delta\vec{a}_1 = \vec{a}_1 - \vec{a}_o$ and determined the point $\vec{a}_2$ corresponding to the minimum of a parabola passing through the three points found. In cases where $S(\vec{a}_1) > S(\vec{a}_o)$, the third point was calculated for $\vec{a} = \vec{a}_1 + \frac{1}{2}\delta\vec{a}$.

The dispersion of the parameters is determined by the diagonal elements of a matrix reciprocal to the matrix of the system of normal equations. The dispersion values calculated in this way do not allow for the fact that the values of χ^{exp} are obtained by averaging over the final number of levels and therefore differ from the general average values. Possible systematic errors in the experimental results are not taken into account either. To allow for the effect of these factors, we multiplied the diagonal elements by $S_{min}/(m-n)$, where S_{min} is some minimum value, m the number of points and n the number of parameters. When there are no random errors and no random deviations of χ_i^{exp}, from the general averages due to the finite number of resonances in the energy groups, $S_{min}/(m-n) \simeq 1$. In our case $S_{min}/(m-n)$ was of the order of 3. As will be seen later, this high value of $S_{min}/(m-n)$ is due to systematic errors in calculation or experiment.

The results of the calculations are given in the first column of Table 3. The fifth column gives the figures recommended by Schmidt on the basis of his analysis of data on the parameters of the resolved levels of ^{238}U [6]. One is struck by the good agreement between the values of the s-wave strength function and the potential scattering cross-section, which naturally emerge most reliably from total cross-section data. Substantial discrepancies are found between the values for the remaining parameters - particularly large in the case of the p-wave strength function. Here, however, we must bear in mind that the errors given in Table 3 - especially the large errors, as in $\overline{\Gamma}_\gamma$ - may by nature depart substantially from the Gaussian; in particular, the probability of deviation from the average by a quantity greater than the error itself can appreciably exceed the probability that would follow from a Gaussian distribution (0.682). Therefore, to find the accuracy with which these parameters have been determined, we need to perform a whole series of calculations, keeping one or more of the parameters constant. The preliminary results of these calculations (one iteration) are given in columns 2, 3 and 4 of Table 3. It will be seen that a deviation of $\overline{D}$ and $\overline{\Gamma}_\gamma$ from the most probable values, even by two to three times the

root-mean-square error, leads to a comparatively small increase in $S_{min}/(m-n)$; moreover the s-wave strength function and the potential scattering cross-section, are affected very little when these parameters are kept constant at the levels mentioned, though the effect of this procedure on the p-wave strength function can be very considerable.

Let us now examine the problem of $S_{min}/(m-n)$ and consider why it differs from unity. Analysis shows that deviations of the average values in the energy groups of a finite width from the general averages cannot result in values of $S_{min}/(m-n)$ substantially higher than 1.5. Therefore, the reasons why the sum of the standard deviations exceeds the expected level must be sought in systematic deviations between the calculated and experimental values of χ_i. Such deviations have in fact been found. Thus, the experimentally determined transmission values for a filter thickness of 1 mm have been found to be systematically lower than the calculated values by factors of 1-5 (3 on average) times the error. For t = 2 mm, the deviations drop to 1.5 times the root-mean-square error, but remain systematic as before. This means that the average cross-sections determined from the slope of the initial segments of the transmission curves appear systematically higher than those calculated from average resonance parameters, evaluated on the basis of the whole set of data.

Systematic deviations also occur in the values obtained for the temperature variation of the transmission functions (see Fig. 2).

The systematic deviations mentioned above may be due to experimental errors as well as to imperfections in the calculation model. For example, the high value of the average cross-sections may be due to hydration of the surface of the cold uranium samples: absence of hydration was not verified. Nor do we know for sure how neglecting inter-resonance interference in the calculating model affects the results of calculation.

The study of these and other possible reasons for the above-mentioned systematic deviations is now just beginning. Therefore, the experimental results presented in this paper should be regarded as preliminary.

Table 1

Experimental transmission values for ^{238}U (corrected for dead time, intrinsic background of the detector and reactor background)
Thicknesses are given in millimetres

E_{gr}(keV)	T(1)	T(2)	T(4)	T(8)	T(16)	T(32)	T(64)	T(128)	T(160)/T(128)	T(192)/T(160)	T(224)/T(192)
0.46-1.45	0.900±0.004	0.860±0.006	0.784±0.016	0.636±0.010	0.412±0.011	0.208±0.014	0.0505±0.0060	0.0048±0.0016	0.491±0.050	0.565±0.060	0.583±0.060
0.145-3.30	0.908±0.005	0.848±0.009	0.766±0.013	0.594±0.010	0.386±0.009	0.209±0.012	0.0511±0.0050	0.0120±0.0020	0.631±0.060	0.687±0.060	0.768±0.060
3.30-6,85	0.912±0.007	0.872±0.006	0.773±0.011	0.594±0.008	0.372±0.009	0.165±0.011	0.0346±0.0035	0.0045±0.0009	0.458±0.050	0.561±0.050	0.616±0.050
6.85-13.50	0.916±0.005	0.867±0.008	0.774±0.018	0.609±0.010	0.375±0.009	0.165±0.011	0.0345±0.0035	0.0034±0.0008	0.377±0.050	0.473±0.050	0.515±0.050
13.5-21.8	0.925±0.008	0.870±0.006	0.786±0.025	0.613±0.007	0.387±0.022	0.158±0.014	0.0328±0.0048	0.0024±0.0009	0.349±0.040	0.433±0.040	0.489±0.040
21.8-49.0	0.928±0.006	0.881±0.010	0.780±0.008	0.637±0.008	0.408±0.010	0.165±0.010	0.0352±0.0030	0.0023±0.0008	0.330±0.030	0.385±0.040	0.440±0.040
49.0-120	0.936±0.009	0.883±0.009	0.809±0.010	0.667±0.010	0.422±0.020	0.182±0.015	0.0370±0.0030	0.0023±0.0008	0.314±0.030	0.345±0.030	0.365±0.040

Table 2

Experimental values of temperature-induced transmission variations ($T_{20°C}/T_{770°C}$) for ^{238}U, uncorrected for thermal expansion of filters

E_{gr} (keV)	8 mm	16 mm	32 mm	64 mm	128 mm
0.46 - 1.45	1.004 ± 0.010	1.020 ± 0.009	1.022 ± 0.007	1.101 ± 0.008	1.541 ± 0.032
1.45 - 3.30	1.011 ± 0.004	1.030 ± 0.009	1.050 ± 0.013	1.156 ± 0.008	1.550 ± 0.032
3.30 - 6.85	0.999 ± 0.004	1.021 ± 0.009	1.038 ± 0.012	1.140 ± 0.010	1.978 ± 0.150
6.85 - 13.50	0.988 ± 0.005	1.007 ± 0.009	1.009 ± 0.007	1.115 ± 0.008	1.665 ± 0.094
13.5 - 21.8	0.989 ± 0.008	1.000 ± 0.011	1.030 ± 0.008	1.130 ± 0.009	1.840 ± 0.173
21.8 - 49.0	0.985 ± 0.006	0.978 ± 0.009	0.982 ± 0.010	1.052 ± 0.010	1.367 ± 0.072
49.0 -120.0	0.976 ± 0.004	0.990 ± 0.008	0.957 ± 0.013	0.964 ± 0.012	1.117 ± 0.045

Table 3

Average resonance parameters of ^{238}U

Parameter	Results of processing of transmission data				Recommended in compilation [6]
	All parameters varied	$\overline{\Gamma_\gamma}$ kept constant	$\overline{\Gamma_\gamma}$ and $\overline{D}$ kept constant	$\overline{\Gamma_\gamma}$ and $\overline{D}$ kept constant	
$\overline{\Gamma_{n0}^0}/D \cdot 10^4$	0.90 ± 0.07	0.91 ± 0.06	0.86 ± 0.04	0.89 ± 0.004	0.90 ± 0.10
$\overline{\Gamma_{n1}^0}/D \cdot 10^4$	1.28 ± 0.33	1.31 ± 0.13	2.19 ± 0.07	1.87 ± 0.03	2.5 ± 0.5
D ($\ell=0$)	25.1 ± 1.4	24.6 ± 0.9	20.8(kept const.)	20.8(kept const.)	20.8 ± 1.1
S_0	10.71 ± 0.17	10.70 ± 0.17	10.25 ± 0.15	10.30 ± 0.13	10.6 ± 0.2
$\overline{\Gamma_\gamma}$	17.2 ± 4.6	19.1*(kept const.)	19.1*(kept const.)	24.8(kept const.)	24.8 ± 5.6
$S_{min}/(m-n)$	2.96	3.01	3.52	3.40	4.78

*/ From data in Ref. [7].

REFERENCES

[1] ABAGYAN, L.P., BAZAZYANTS, N.O., BONDARENKO, I.I., NIKOLAEV, M.N., Gruppovye konstanty dlja rasčeta jadernyh reaktorov (Group constants for nuclear reactor calculations), Atomizdat, Moscow (1964).

[2] ABAGYAN, L.P., MIKHAILUS, F.F., NIKOLAEV, M.N., ORLOV, V.V., Rasprostranenie rezonansnyh nejtronov v gomogennyh sredah. Teorija i specialnye funkcii (Propagation of resonance neutrons in homogeneous media. Theory and special functions) Byulleten' informacionnogo centra po jadernym dannym (Bulletin of the Nuclear Data Information Centre), No. 5, Appendix 1, Atomizdat, Moscow (1968).

[3] VIZI, I. et al., Nuclear electronics, 1, IAEA, Vienna (1962), 27-36.

[4] PICKELNER, L.B., et al., Pribory i Tekn. Eksp., 2 (1963) 48-50.

[5] COLATZ, S., Kernenergie, 2 (1968) 1.

[6] SCHMIDT, J., KFK 120, 1 (1966).

[7] GLASS, N.W. et al., Proc. Second Conf. Neutron Cross-Sections and Technology, Washington, Vol. 1 (1968) 573.

FIGURE CAPTIONS

Fig. 1. Experimental lay-out for studying the Doppler effect in ^{238}U.

Fig. 2. Doppler effect as a function of transmission ratios $T_{20°C}/T_{800°C}$ in ^{238}U samples 20 mm and 32 mm thick.

Fig. 3. Doppler effect as a function of transmission ratios $T_{20°C}/T_{800°C}$ in ^{238}U samples 64 mm and 128 mm thick.

Fig. 4. Doppler effect as a function of ratios $N_{20°C}/N_{770°C}$, where $N_{20°C}$ and $N_{800°C}$ are the gamma detector counts from a 0.25 mm sample of $^{238}U_{20°C}$ at different temperatures of the 8 mm ^{238}U filter, corrected for the intrinsic background of the detector and the reactor background.

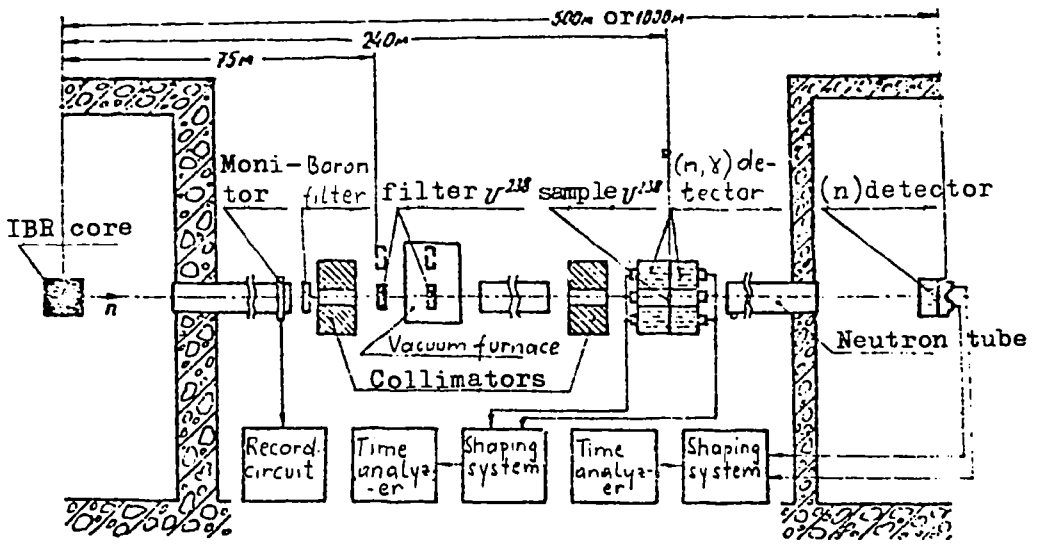

Figure 1

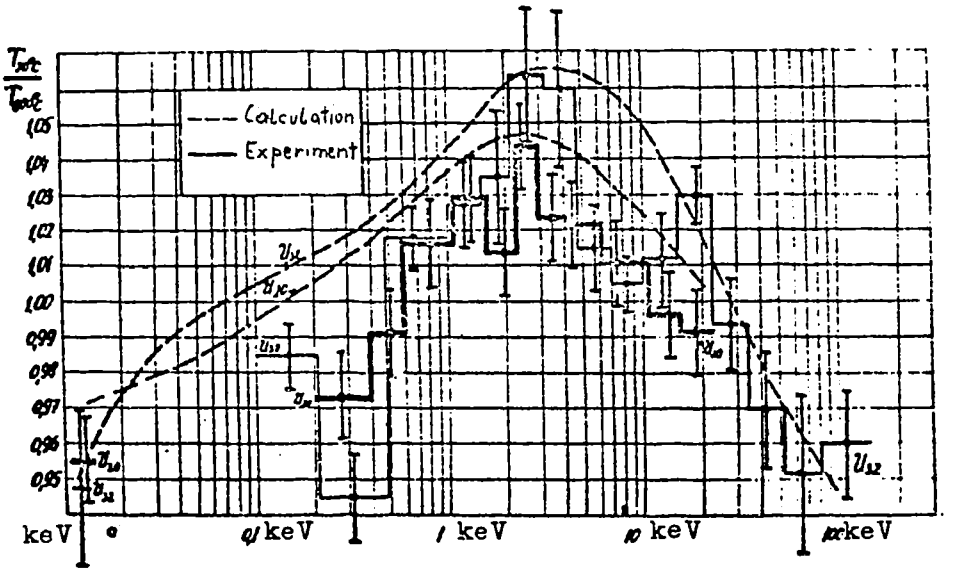

Figure 2

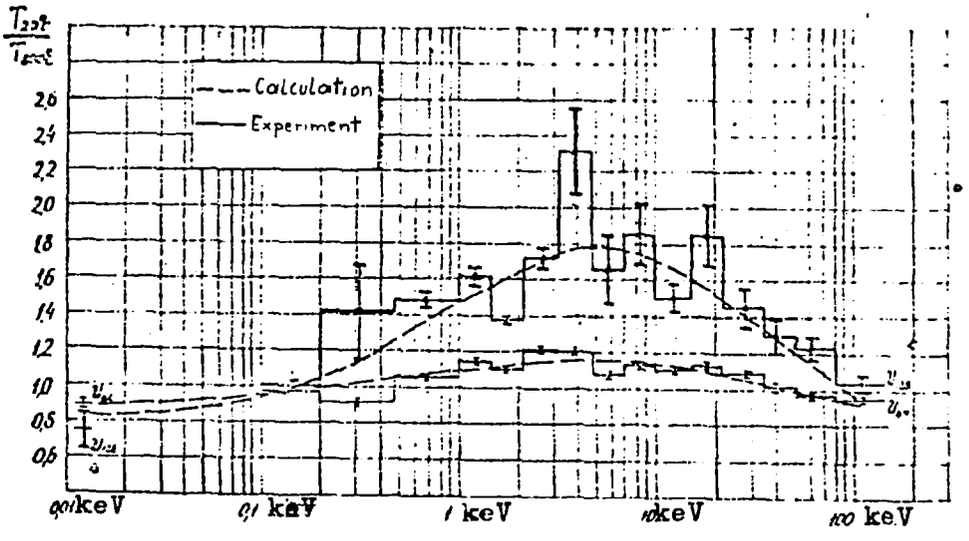

Figure 3

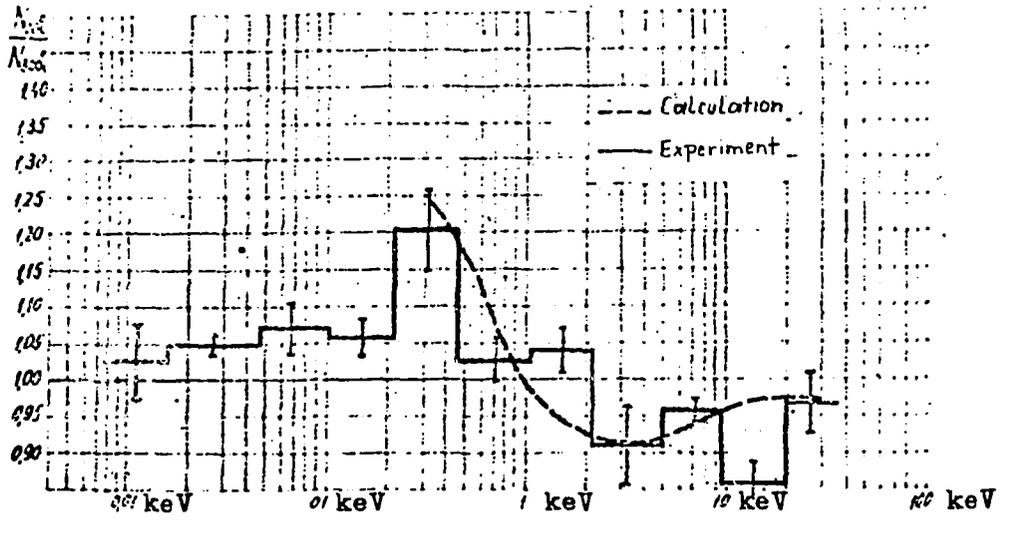

Figure 4

MEASUREMENT OF THE STRUCTURE OF TOTAL NEUTRON CROSS-SECTIONS

V.V. Filippov and M.N. Nikolaev
Institute of Physics and Power Engineering
Obninsk, USSR

Translation made by IAEA

Presented at the

BRITISH-SOVIET SEMINAR ON NUCLEAR CONSTANTS
FOR REACTOR CALCULATIONS
Dubna, 18-22 June, 1968

MEASUREMENT OF THE STRUCTURE OF TOTAL NEUTRON CROSS-SECTIONS

V.V. Filippov and M.N. Nikolaev
Institute of Physics and Power Engineering
Obninsk, USSR

Introduction

The accuracy of the group cross-sections used for reactor calculations depends, in the resonance energy region, on the accuracy with which resonance self-shielding effects are taken into account. The data on cross-section structure required for this purpose are known, in the comparatively low energy region, from high-resolution experiments. Where higher energies are concerned, existing spectrometers do not enable us to resolve the details of the energy dependence of the cross-sections. On the other hand, computational evaluations of cross-section fluctuations in the region of unresolved resonances are not reliable either because specific effects not found in the region of resolved resonances appear here, viz. inter-resonance interference, a contribution of neutrons with high orbital momenta and so on.

For this reason experiments aimed at determining the average characteristics of cross-section structure have a special interest - experiments from which we can determine the effects of resonance self-shielding without having recourse to high energy resolution. The Institute of Physics and Power Engineering has accordingly proposed a new method [1, 2] for determining the characteristics of the cross-section structure by analysis of transmission functions measured to significant attenuations.

In the present paper we consider the results obtained with this method when it was used for an analysis of the total neutron cross-section structure of a number of elements in the energy region from a few tens of keV to several MeV. The conditions in which the experiment was carried out and the methods used in processing the results are also described.

Method

The experimental method used for determining the structure of the total neutron cross section for energies from E to E + ΔE consists in measuring the transmission function T(t), for transmission of neutrons distributed over the energy range of interest through samples of the substance under study, as a function of the thickness t of the samples. If the conditions of "good geometry" are observed, the deviation of the measured relationship from exponential gives a measure of the cross-section structure.

Let us assume that the total neutron cross-section σ_{tot} (E) undergoes substantial changes in the range from E to E + ΔE, which depends on the energy distribution f(E) of the neutrons over this range which is used in measuring the transmission function T(t) with the help of a detector of efficiency ε(E). Then the transmission

$$T(t) = \frac{\int_{E}^{E+\Delta E} f(E)\,\varepsilon(E)\,e^{-\sigma_{tot}(E)\,t}\,dE}{\int_{E}^{E+\Delta E} f(E)\,\varepsilon(E)\,dE} \tag{1.1}$$

differs from the values given by the simple exponential law

$$T_o(t) = e^{-\langle\sigma_{tot}\rangle t} \tag{1.2}$$

calculated from the average total cross-section

$$\langle\sigma_{tot}\rangle = \frac{\int_{E}^{E+\Delta E} f(E)\,\varepsilon(E)\,\sigma_{tot}(E)\,dE}{\int_{E}^{E+\Delta E} f(E)\,\varepsilon(E)\,dE} \tag{1.3}$$

and coincides with it only at sufficiently small thicknesses, when the expansion of the exponent in expression (1.1) requires only one term:

$$T(t) = \frac{\int_{E}^{E+\Delta E} f(E)\,\varepsilon(E)\left\{1 - \sigma_{tot}(E)\,t + \dots\right\} dE}{\int_{E}^{E+\Delta E} f(E)\,\varepsilon(E)\,dE} =$$

$$= 1 - \langle\sigma_{tot}\rangle t + \dots \cong e^{-\langle\sigma_{tot}\rangle t}$$

(1.4)

In the general case, however, the values of T(t) should be higher than values given by relation (1.2) because of the effect of resonance self-shielding in the total cross-section. The physical significance of this effect lies in the fact that, when the beam passes through the sample, neutrons with energies corresponding to the total cross-section maxima are extracted from the beam more rapidly than those of other energies. As a result, the neutron spectrum acquires, as the beam passes through the sample, a structure the maxima and minima of which are the inverse of the resonances of the total cross-section, and the total cross-section values obtained after averaging over such a spectrum tend to be low. To take a specific example, let us consider an analytical expression for the average cross-section obtained when the neutron beam has already passed through thickness t of the substance under study:

$$\langle\sigma_{tot}\rangle_t = -\frac{1}{T(t)}\frac{dT(t)}{dt} = \frac{\int_{E}^{E+\Delta E} f(E)\,e^{-\sigma_{tot}(E)t}\,\varepsilon(E)\,\sigma_{tot}(E)\,dE}{\int_{E}^{E+\Delta E} f(E)\,e^{-\sigma_{tot}(E)t}\,\varepsilon(E)\,dE}$$

(1.5)

Comparing this expression with relation (1.3), we conclude that in fact the whole difference lies in the averaging function and that this difference is such that regions with high total cross-section values are suppressed when we average by formula (1.5); moreover, the higher the value of t, the greater is the suppression.

Let us now introduce a function $\frac{dP(\sigma)}{d\sigma}$, which is the probability density of finding, in the given energy range ΔE, a value of the total cross-section equal to σ. Knowing this function we can calculate the average value over ΔE of any function of the total cross-section. Instead of the usual form of averaging over energy,

$$\langle f(\sigma) \rangle_{\Delta E} = \frac{1}{\Delta E} \int_{\Delta E} f[\sigma(E)]\, dE \tag{1.6a}$$

(where $f(\sigma)$ is any function of the total cross-section), we have only to integrate over the cross-section

$$\langle f(\sigma) \rangle_{\Delta E} = \int_{\sigma_{min}}^{\sigma_{max}} \frac{dP(\sigma)}{d\sigma} f(\sigma)\, d\sigma \tag{1.6b}$$

where integration is performed over all values assumed by the function $\sigma(E)$ in the range ΔE.

Obviously the function $\frac{dP(\sigma)}{d\sigma}$ is given for some range of cross-section values:

$$\sigma_{min}^{(\Delta E)} \leq \sigma \leq \sigma_{max}^{(\Delta E)}$$

(where $\sigma_{min}^{(\Delta E)}$ and $\sigma_{max}^{(\Delta E)}$ are the minimum and maximum values of the total cross-section in the range ΔE). Let this function also be normalized to unity:

$$\int_{\sigma_{min}^{(\Delta E)}}^{\sigma_{max}^{(\Delta E)}} \frac{dP(\sigma)}{d\sigma}\, d\sigma = 1 \tag{1.7}$$

We then find the relationship between changes in the cross-section over the range ΔE and the function $\frac{dP(\sigma)}{d\sigma}$. For this purpose we integrate, in the range ΔE, with respect to the cross-section and no longer with respect to energy as in expression (1.6a), regarding energy now as a function of the cross-section $E = E(\sigma)$ (the inverse of the function $\sigma = \sigma(E)$):

$$\langle f(\sigma)\rangle_{\Delta E} = \frac{1}{\Delta E}\int_{\Delta E} f\,[\sigma(E)]\,dE = \frac{1}{\Delta E}\int_{\sigma_{min}}^{\sigma_{max}} f(\sigma)\left|\frac{dE(\sigma)}{d\sigma}\right| d\sigma \tag{1.6c}$$

The integrand contains the absolute value of the derivative, since in the descending sectors of the curve $\sigma(E)$, where $\frac{dE}{d\sigma} > 0$, integration for the cross-section should ordinarily be performed from larger to smaller cross-sections. To avoid this inconvenience and to be able to integrate with respect to the variable σ consistently in one direction, it is advisable to use the absolute value of the derivative. Comparing the resulting expression with relation (1.6b), we see that

$$\frac{dP(\sigma)}{d\sigma} = \frac{1}{\Delta E}\left|\frac{dE(\sigma)}{d\sigma}\right| \tag{1.8a}$$

If the function $\sigma(E)$ is non-monotonic in the range ΔE, the function $E(\sigma)$ will obviously not be single-valued (i.e. identical cross-section values will recur at several energy values). Hence the derivative $\frac{dE(\sigma)}{d\sigma}$ will not be single-valued either. In this case we must take into account all branches of the function $\frac{dE(\sigma)}{d\sigma}$ in expression (1.6b). A more rigorous formula will accordingly be

$$\frac{dP(\sigma)}{d\sigma} = \frac{1}{\Delta E}\sum_{i=1}^{N}\left|\frac{dE(\sigma)}{d\sigma}\right|_i \tag{1.8b}$$

where N is the number of branches of the function $E(\sigma)$.

Let us consider what possibilities of determining the distribution function of the total cross-section $\frac{dP(\sigma)}{d\sigma}$ are available to us once we know the transmission function $T(t)$ for a given energy range ΔE. We first try to determine the analytical form of $\frac{dP(\sigma)}{d\sigma}$. The analytical expression for transmission (1.1) can be rewritten in accordance with relation (1.6b):

$$T(t) = \int_{\Delta\sigma} \frac{dP(\sigma)}{d\sigma}\, e^{-\sigma t}\, d\sigma \tag{1.9}$$

Here the measured total cross-section distribution generally differs from the true distribution because of the influence of the transmission averaging function $f(E)\varepsilon(E)$, but we can neglect this difference provided the neutron spectrum is close to rectangular and the detector efficiency has a smooth energy characteristic. Expression (1.9) is an integral equation from which we can normally determine $\frac{dP(\sigma)}{d\sigma}$ provided the transmission function $T(t)$ is known. In fact we shall consider $T(t)$ as a Laplace transform of the function $\frac{dP(\sigma)}{d\sigma}$. Then, representing the transmission function $T(t)$ in an analytical form for which there also exists an analytical form of the inverse transformation we can find the unknown function $\frac{dP(\sigma)}{d\sigma}$. For this, however, it is essential that the form of the inverse transformation should have characteristics typical of the function $\frac{dP(\sigma)}{d\sigma}$.

This cannot be done, in the general case, for a function as complex as $\frac{dP(\sigma)}{d\sigma}$. But even if it were possible to choose the appropriate analytical form, the accuracy with which the function $\frac{dP(\sigma)}{d\sigma}$ can be established from the integral equation in expression (1.9) - the left side of which is inaccurate owing to experimental errors - would still be insufficient to justify the attempt to determine $\frac{dP(\sigma)}{d\sigma}$ in full detail.

We may, nevertheless, try to determine $\frac{dP(\sigma)}{d\sigma}$ in some approximate form which would adequately reflect its most essential characteristics. One possibility is to represent it as a table of moments M_k:

$$M_k = \int_{\Delta\sigma} \sigma^k \frac{dP(\sigma)}{d\sigma} d\sigma \; ; \qquad k = \pm 1, \pm 2, \ldots \tag{1.10}$$

Let us perform a Taylor-series expansion of some function $f(\sigma)$, whose average value in the range ΔE is to be determined, around the value $\sigma = \bar{\sigma}$ and insert this expansion in expression (1.6a). We then have

$$\langle f(\sigma) \rangle = f(\bar{\sigma}) + \sum_{k=1}^{\infty} \frac{1}{k!} \frac{d^k f(\bar{\sigma})}{d\sigma^k} \int_{\Delta\sigma} \frac{dP(\sigma)}{d\sigma} (\sigma - \bar{\sigma})^k d\sigma =$$

$$= f(\bar{\sigma}) + \sum_{k=2}^{\infty} \frac{1}{k!} \frac{d^k f(\sigma)}{d\sigma^k} \cdot C_k \tag{1.11}$$

where C_k are the central moments of the $\frac{dP(\sigma)}{d\sigma}$ distribution related to the moments M_k by

$$C_k = \int_{\Delta\sigma} \frac{dP(\sigma)}{d\sigma} (\sigma - \bar{\sigma})^k d\sigma$$

(1.12)

Thus, if the moments of the $\frac{dP(\sigma)}{d\sigma}$ distribution function are known, the average values of the different functions of the total cross-section can easily be calculated provided the series in expression (1.11) converges rapidly enough. To determine the positive moments M_k $(k>0)$, we represent the transmission function T(t) in the form

$$T(t) = \int_{\Delta\sigma} \frac{dP(\sigma)}{d\sigma} e^{-\sigma t} d\sigma = e^{-\langle\sigma\rangle t}\left[1 + \sum_{k=2}^{\infty} \frac{(-1)^k}{k!} t^k C_k\right]$$

(1.13)

Using this form to approximate the experimental curve by the method of least squares, we can determine the moments sought. The maximum number of moments which can reasonably be determined for the specific transmission function given above can be found with the help of the Gaussian criterion.

Equation (1.13) also allows a graphic determination of the moments M_k. The average cross-section $\langle\sigma\rangle = M_1$ is determined from the slope of the initial sector of the curve $\ln T(t)$. The second central moment C_2 can be found from the slope of the initial sector of the relation $e^{\langle\sigma\rangle t} \ln T(t) = f(t^2)$. The curvature of this relation for small t determines C_3, and so on. As we see, positive moments of the distribution function are determined by differentiation of the transmission curve. Therefore, to determine them we need a very accurate measurement of the transmission function, in particular its initial sector. In this region $T \cong 1$ and $\ln T \cong 1-T$. The values of these small differences contain fairly sizable errors and for this reason the positive moments are determined from the transmission functions with comparatively low accuracy. We need, therefore, to find an approximate representation of the distribution function for the cross-section $\frac{dP(\sigma)}{d\sigma}$ in the form of a set of weighted delta functions:

$$\frac{dP(\sigma)}{d\sigma} \cong \sum_{i=1}^{n} a_i \delta(\sigma - \sigma_i)$$

(1.14)

Physically, a representation of this kind is equivalent to changing from a continuously distributed cross-section to a cross-section given in the form of a histogram.

Inserting relation (1.14) in the expression for the transmission function, we obtain

$$T(t) = \sum_{i=1}^{n} a_i \int_{\Delta\sigma} \delta(\sigma - \sigma_i)\, e^{-\sigma t}\, d\sigma = \sum_{i=1}^{n} a_i\, e^{-\sigma_i t}$$

(1.15)

Thus, to find the parameters (a_i, σ_i and n) of such a representation of the distribution function, we must approximate the transmission curve by a sum of exponents. For each number of exponents n this approximation can be performed by the method of least squares, which will give the parameters a_i and σ_i for the representation in (1.14) together with all their matrices of errors. The minimum necessary number of exponents n should be taken to describe the experimental points accurately to within the limits of error. To determine this number we may, for instance, make use of the Gaussian criterion [4].

The average value of the arbitrary total cross-section function $f(\sigma)$ is now determined as

$$\langle f(\sigma) \rangle = \sum_{i=1}^{2n} x_{2i-1}\, f(x_{2i})$$

(1.16)

(where the even parameters x_{2i} are the cross-sections and the odd parameters x_{2i-1} are their contributions to the distribution in (1.4)), and the dispersion of this quantity is expressed in terms of the elements of the error matrix ϱ_{ij}:

$$D\left(\langle f(\sigma) \rangle\right) = \sum_{i,j} \frac{\partial f}{\partial x_i} \frac{\partial f}{\partial x_j}\, \varrho_{ij}$$

(1.17)

The advantage of representing cross-section structure data in this manner lies in the fact that two or three exponents are generally sufficient to describe the experimental transmission functions, i.e. the number of unknown parameters is comparatively small. Given two exponents, for example, we need seek only three independent parameters, a_1, σ_1 and σ_2, since a_2 is found from the condition $a_1 + a_2 = 1$. The proposed representation is such that the total cross-section structure data can be used directly in reactor calculations by the method of sub-groups [5]; this makes it possible to allow for the influence of cross-section structure on neutron propagation in media without making any assumption regarding constant collision density in the neighbourhood of the resonance. In this method, neutrons having energies within a given energy group ΔE are divided into several sub-groups, each of which is assigned its own total cross-section value - this value now being constant. For example, one sub-group includes the resonance neutrons and another the inter-resonance neutrons. The values of cross-sections in the sub-groups and the relative contributions of these sub-groups can be determined, for example, from the measured transmission function for the whole group ΔE and its approximation by formula (1.15). Then a_i represents the "weights" of the sub-groups and σ_i the sub-group cross-sections. It is interesting to note that the method of sub-groups was actually conceived as a result of interpretation of the data obtained in transmission function analysis.

In the present work, all information on cross-section structure is represented in accordance with formula (1.15).

Experiment

To determine the characteristics of the total cross-section distribution function of a number of elements for fast and intermediate neutrons, the Institute of Physics and Power Engineering has for a number of years (since 1960) been measuring transmission as a function of sample thickness in conditions of "good geometry". The experiments have been carried out on the Institute's Van de Graaf generators. Neutrons were obtained from the $T(p,n)^3He$ and $D(d,n)^3He$ reactions. After passing through the sample under study without scattering and through a collimator in the shield (Figs 1 and 2) the neutrons impinge on the detector. Batteries of proportional boron counters of the SNMO-5 type placed in the water-containing moderator block constituted the detector. Below we consider the operating characteristics of the neutron source and detector and the basic steps of the measurement procedure.

Source

To obtain neutrons with energies below 4 MeV the $T(p,n)^3He$ reaction was used. A few measurements were performed at higher energies with neutrons from the $D(d,n)^3He$ reaction. Hydrogen ions were accelerated by Van de Graaf generators designed for 5 million and 2.5 million volts, respectively. Neutron energies were determined from the emission angle and from the proton energy. Using the $T(p,n)^3He$ reaction with a large accelerator at 0° to the proton beam we were able to obtain mono-energetic neutrons with energies up to 4 MeV. Lower neutron energies were obtained with a different apparatus which used neutrons emitted at an angle $\varphi = 100^\circ$ on bombardment of tritium by protons from the smaller Van de Graaf generator.

It must be noted here that strictly mono-energetic neutrons need not be used for transmission function measurements the purpose of which is to determine average characteristics of cross-section structure. Indeed, a certain spread of neutron energies in the beam is essential if this structure is to be revealed through transmission. It is necessary only that the form of the energy spectrum used in the experiment should be as simple as possible; and it is desirable in particular that the neutrons should be grouped around some average energy.

Ordinarily, solid tritium targets were used; each of these consisted of a molybdenum disk 14.2 mm (or 45 mm) in diameter, to which a thin layer of titanium (or zirconium) containing tritium was applied. The ratio of the number of titanium nuclei to the number of tritium nuclei was usually of the order of 1-2. When working with neutrons emitted from the target at an angle of 10° to the proton beam, we used a holder providing water-cooling of the target: a layer of distilled water 2 mm in thickness flowed over the back side of the target at a rate of 1 litre/h. Such cooling proved sufficient to compensate for the thermal effect of the proton current for powers up to 200 W (current up to 50 μA and proton energy $E_p \leqslant 4$ MeV) without any appreciable change in the target characteristics, i.e. the yield and average energy of the neutrons. Moreover, the apparatus comprising target holder and cooling system was light enough to cause practically no distortion of the neutron spectrum formed in the reaction. The experiment was also facilitated by the fact that the neutron yield was generally at a maximum in the direction in which the measurements were performed (i.e. at an angle of 0° to the proton beam). However, when working at an angle of 100° to the proton beam (to obtain neutrons with $E_n < 300$ keV) we found that the neutron yield

in the required direction was 3-5 times lower than in the forward direction, and a less effective method of cooling - by air jet with a water spray - had to be used in order to reduce the contribution of neutrons scattered by the holder into the detector. With this method of cooling we were able to extract powers of up to 500 W (current ~ 25 μA at E_p ~ 2 MeV) from the target.

Our deuterium targets - similar to the tritium targets in design and nuclear density - were usually cooled with water as fairly wide spectra (ΔE ~ 1-2 MeV) were generated and the contribution of neutrons scattered in the holder was accordingly less significant. Nevertheless, the deuteron current was usually kept at only 5-8 μA so as to minimize the time change of spectrum characteristics. The large cross-section of the $D(d,n)^3He$ reaction enabled us to obtain adequate neutron intensities even at these low values of deuteron current.

Detector

To register fast and intermediate neutrons in these experiments we used batteries of proportional counters of the SNMO-5 type, connected in parallel and located in the paraffin moderator (see Figs 1 and 2). To prevent counting of scattered radiation, the detectors were surrounded on all sides by a reliable shield which made the experimental setups very bulky. As it was desirable to move the detector as little as possible, we conducted the experiments with two units - one for neutrons emitted in the forward direction and the other for neutrons emitted at an angle of 100°. Let us now consider the design and operating characteristics of the two units.

The experimental setup for neutrons with $E \lesssim 300$ keV (see Fig. 1) consisted of a cylindrical tank containing water (Ø 2 m x 2 m), mounted on a carriage which could be moved towards the target in a direction perpendicular to the proton beam and pushed aside after completion of a series of measurements. With the experimental setup in its operating position, the distance between target and detector was 2 m. The detector was placed in the tank in such a way as to be shielded in front by 1 m of water; the water shield in the back was slightly thinner but nowhere less than 50 cm. The neutron beam entered the detector after passing through a collimator, the diameter of which was normally 45 mm but could be narrowed by means of special plexiglass or steel inserts. The detector proper and the collimator leading into it were surrounded by a layer of boron carbide and water.

The extension of the collimator aperture in the shield was a continuous channel passing through the detector and the back shield. During transmission function measurements a thick (T ~ 0.01) organic glass neutron scatterer was placed in this channel at the centre of the detector. Twenty-three counters, chosen in advance on the basis of their characteristics, were located in the paraffin moderator of the detector by means of two cylindrical rings 8 and 12 cm in radius around the axial aperture (ø 5 cm).

The efficiency of the detector, measured with neutrons from a standard plutonium source ($\bar{E}_n$ = 1 MeV), was 10%. The energy dependence of the detector efficiency, measured in a fission chamber with a layer of uranium-235, was low enough to have no effect on the measurement results. Under typical measuring conditions (target thickness 2.5 mg/cm^2, current 20 μA and proton energy E_p ~ 2 MeV) the count rate of neutrons in the free beam was ~ 1 x 10^3 pulses/sec, and the minimum count rate at which the measurements could still be carried out was ~ 0.1 pulses/sec - about twice the detector's intrinsic background.

The experimental setup for neutrons with E 300 keV (see Fig. 2) had a slightly smaller water shield (50 cm in front and not less than 30 cm on the sides). The detector and collimator tube (30 mm in diameter) were surrounded, as in the other unit, by a layer of a boron-containing absorber. Seven SNMO-5 counters were placed in the moderator (paraffin) perpendicular to the collimator. With a titanium-tritium target 0.7 mg/cm^2 in thickness, and with E_p ~ 2 MeV and current ~ 20 μA, the neutron count rate in the free beam after its passage through the collimator was about 150 pulses/sec. Transmission values were measured to T = 0.005.

Background

Since the count rate in the open beam was quite high, the maximum beam attenuation that could be measured was determined by the background level.

As a result of the measures adopted in our experiments (bulky shielding, boron layer surrounding the collimator tube and detector, small transverse dimensions of samples and so on), the background level during measurements in the high energy range was never more than 10^{-4} x the count rate in the open beam. At lower energies the background represented as much as 0.1% of the open beam count.

Analysis of the geometry of the experiment showed that the contribution of multiple scattering was always negligibly small, i.e. the conditions of "good geometry" were satisfied.

Subtraction of the background at high attenuations sharply increases the error in the corrected transmission values; it would require extremely reliable determination of the background and its error. Therefore, no background corrections were introduced into the measured transmission curves; the correct value of the background as a constant component of the decreasing transmission function was determined by mathematical analysis of the measured transmission curve.

Resolution function

The energy resolution in these experiments was generally determined by the thickness of the target under study. Other factors [6], such as the angular spread of neutron energies (1-2 keV/degree), instability of proton energy (0.5-1%) and especially thermal motion of the target nuclei in the fairly thick targets, made a negligibly small contribution, as can be seen from the table below.

Table

Factors affecting resolution	Energy E<300 keV (target 0.6 mg/cm^2, 0° to proton beam)	Energy E>300 keV (100° to beam, target 2.6 mg/cm^2)
Target thickness	40-30 keV	300-150 keV
Angular spread	~ 3 keV	~ 2 keV
Instability of accelerator	~ 3 keV	~ 10 keV
Doppler effect	~ 1 keV	~ 1 keV

When deuterium targets were used, the resolution was determined to an even greater extent by the target thickness, the figure here being of the order of 1 MeV. Since the distribution of tritium through the titanium layer in the targets could be considered uniform and the cross-section of the $T(p,n)^3He$ reaction in the energy range determined by the target thickness usually varied little (except in the 300-600 keV range for E>300 keV and in the E<50 keV range for the experiments conducted

at an angle of 100°), the assumption of a rectangular resolution function was generally a good approximation. The neutron energy was determined from the kinematics of the nuclear reaction used, from the energy of the bombarding hydrogen ions and from the angle of neutron emission. The proton energies were calibrated in advance with reference to the threshold for the $T(p,n)^3He$ reaction. For not-too-thick targets (of the order of a few tens of keV) the energy scale of the neutrons was further verified by measuring the position of known resonances in the total cross-sections of magnesium (E_n = 85 keV, $\Gamma \simeq$ 8 keV), beryllium (E_n = 620 keV, $\Gamma \simeq$ 25 keV) and carbon (E_n = 2080 keV, $\Gamma_n \simeq$ 7 keV). The shape of the measured cross-section in the region of these resonances was also used for an experimental determination of the energy resolution from the maximum of the measured cross-section [6], and for evaluating the form of the resolution function from the shape of the peak observed. The energy resolution measurements confirmed the calculated values and the shape of the peaks showed that there were no "tails" in the resolution function.

Monitors

The constancy of the beam was monitored by several methods. The monitors were usually one or more boron counters in paraffin, arranged in such a way as not to distort the beam of neutrons in the direction in which these were used. Sometimes a fission chamber with a layer of uranium-235 placed very close to the target was used. Monitoring the constancy of the neutron beam emerging from the $D(d,n)^3He$ reaction was somewhat complicated by the fact that not only the target itself but all parts of the ion tube on which the beam of accelerated deuterons was incident acted as a neutron source - especially the magnet of the analyser located in the same room as the target. However, the collimated detector "sees" the target preferentially, and it was therefore possible to use a fission chamber placed beside the target as a monitor. An ion current integrator which registered the ion current passing through the target was also used for purposes of monitoring. This integrator, based on the Ellmor-Sands circuit was likewise used for measuring the threshold energy of the $T(p,n)^3He$ reaction.

Samples

Chemically pure substances were generally used for measuring the transmission function, the amount of impurity not exceeding 0.3-0.5% as a rule. Elements like Be, Mg, Al, Si, Ti, V, Fe, Ni, Cu, Zn, Ga,

Zr, Nb, Cd, Pb, Th and U were in the form of regular cylinders. Chromium and tungsten were in powder form densely packed in cylindrical steel containers with walls 0.03 cm thick and sealed. Sulphur was melted and poured into tubes, the ends of which remained open. The diameter of the samples was 35–50 mm. The thicknesses (i.e. the height of the cylinders) were so chosen that, by combining a set of samples before the collimator, the greatest possible number of thicknesses could be obtained between the maximum and minimum thickness used. For this purpose we increased the thickness of the samples successively by a factor of two - 0.4, 0.8, 1.6, 3.2, 6.4, 12.8 cm and so on. The maximum thickness of the samples was generally quite large (as much as 1 m) so that extremely small transmission values could be obtained - so small that the detector count was in the end due almost wholly to background. The density of the samples was measured by weighing in water, with an error of the order of 0.5–1%.

Special manipulators were used for remote handling of the samples in front of the collimator during the operation of the accelerator (Figs 1 and 2). The movement of the samples and their position were monitored with the help of signal lamps on the control panel.

Measurement procedure

The experiment consisted in measuring the neutron count rate of the detector as a function of the thickness of the sample placed between the target and the detector, for each of the neutron energy ranges used. Three to five measurements were carried out for each sample thickness (including zero thickness) in order to verify the stability of the pulses. For this same purpose the count rate measurement in the free beam was repeated periodically (every 5–7 thicknesses). The resulting root-mean-square error of transmission was somewhat higher than the statistical accuracy - 0.5–1% at the initial points of the transmission function ($T \sim 0.9$–0.7) and 3–5% at the last points ($T \sim 0.01$). The transmission function was measured at 15–40 points, depending on its complexity

Before measurement, the samples suspended in front of the collimator were carefully adjusted to ensure complete closing of the aperture. Control measurements were performed periodically, at different magnitudes of the current passing through the target, to make sure that there were no counting losses. For most elements, three to five measurements of the transmission function were performed in each energy range. The results of these measurements were averaged. Altogether about 1500 transmission functions were measured.

Treatment of transmission curves

The treatment of the experimental data consisted in determining by the method of least squares the parameters a_i and σ_i having the analytical form:

$$T(t) = \sum_{i=1}^{n} a_i e^{-\sigma_i t} + \left(1 - \sum_{i=1}^{n} a_i\right) \tag{18}$$

which describes the experimental points of T(t) (18). In our case, the problem to be solved by the method of least squares was as follows:

(a) We wished to find those values of the parameters a_i and σ_i which would give the minimum value of the functional

$$F_n = \sum_{i=1}^{n} \sum_{j=1}^{m} \omega_j \left(a_i e^{-\sigma_i t_j} - T_j\right)^2 \tag{19}$$

where m is the number of experimental points,

n the number of exponents in expression (18),

$T_j = T(t_j)$=the experimental value of transmission at point t_j, and

$\omega_j = \frac{1}{\Delta T_j^2}$ the statistical weight of the point, equal to the reciprocal of the square of its error;

(b) Secondly, we wished to find the matrix of errors for these parameters. Differentiating the expression for functional F_n with respect to a_i and σ_i and equating to zero the derivatives

$$\frac{\partial F_n}{\partial a_i} = \frac{\partial F_n}{\partial \sigma_i} = 0 \tag{20}$$

we obtain a system of 2 n transcendental equations in relation to the unknown parameters a_i and σ_i:

$$\begin{aligned} &\sum_{i=1}^{n} \sum_{j=1}^{m} \omega_j e^{-\sigma_i t_j} \left(a_i e^{-\sigma_i t_j} - T_j\right) = 0 \\ &\sum_{i=1}^{n} \sum_{j=1}^{m} \omega_j a_i t_j e^{-\sigma_i t_j} \left(a_i e^{-\sigma_i t_j} - T_j\right) = 0 \end{aligned} \tag{21}$$

which was solved by the method of successive approximations by linearizing the equations.

This treatment gave us the parameters a_i and σ_i, the dispersions of these quantities and the matrix of the correlation coefficients P_{pq}. Calculations were performed successively for an ever-increasing number of exponents in expansion (18). The algorithm for minimization of the functional did not enable the unknown parameters to be determined when their number was not justified by the accuracy of the experimental data (in this case the process of successive approximations did not converge). This was precisely the criterion for choosing the number of exponents in the superposition. The processing was done on an M-20 computer with the help of the NMK-1 programme prepared by M.Z. Tarasko.

The data obtained were used for calculating the following characteristics of the cross-section structure in the corresponding energy ranges:

average cross-section

$$\langle \sigma \rangle = \sum_{i=1}^{n} a_i \sigma_i \tag{22}$$

dispersion of the cross-section

$$D = \langle \sigma^2 \rangle - \langle \sigma \rangle^2 = \sum_{i=1}^{n} a_i \sigma_i^2 - \left(\sum_{i=1}^{n} a_i \sigma_i \right)^2 \tag{23}$$

and the quantities

$$\langle \sigma \rangle \left\langle \frac{1}{\sigma} \right\rangle = \sum_{i=1}^{n} a_i \sigma_i \sum_{i=1}^{n} \frac{a_i}{\sigma_i} \tag{24}$$

and

$$\frac{\left\langle \frac{1}{\sigma} \right\rangle}{\langle \sigma \rangle \left\langle \frac{1}{\sigma^2} \right\rangle} = \frac{1}{\sum_{i=1}^{n} a_i \sigma_i} \frac{\sum_{i=1}^{n} \frac{a_i}{\sigma_i}}{\sum_{i=1}^{n} \frac{a_i}{\sigma_i^2}} \tag{25}$$

These describe the effects of resonance self-shielding of the cross-sections in the medium [3]. Expression (25) is essentially the resonance self-shielding coefficient of the transport cross-section. Expression (24) is the reciprocal of the self-shielding factor of the scattering cross-section when the capture cross-section is small.

The above-mentioned characteristics and their dispersions were calculated on the M-20 computer with the supplementary ALGOL programme RAMO.

The final results of processing of the total cross-section structure data are given in the tables in the Appendix.

Results

Below we consider total cross-section data for 27 elements from beryllium to uranium. The element tables given in the Appendix contain the most comprehensive information. The first column gives neutron energy and its scatter, and the second the parameters a_i, the even parameters being the cross-sections and the odd their contribution to the distribution. The errors in the parameters are noted alongside. The third column gives the correlation matrix of the parameters found. The last column gives, for each energy range, the average cross-section $\langle\sigma\rangle$ (first line), dispersion of the cross-section $\langle\sigma^2\rangle - \langle\sigma\rangle^2$ (second line) and the coefficients $K = \langle\sigma\rangle\langle\frac{1}{\sigma}\rangle$ and $f = \langle\frac{1}{\sigma}\rangle/(\langle\sigma\rangle\langle\frac{1}{\sigma^2}\rangle)$ needed for calculating the mean range of neutrons and the transport cross-sections. For the sake of clarity the parameters of cross-section structure and its average characteristics are illustrated - for many elements - by means of graphs. Numerical values are shown in the graphs by rectangles, the horizontal dimension giving the energy interval to which the value relates and the vertical dimension the error in the value.

Beryllium $_4$Be

The transmission functions for $_4$Be, the cross section of which is well known, were measured largely for purposes of control. Below the energy of the first level of the ^{9}Be + n system at E_n = 620 keV, the contribution of one cross-section component predominates in the distribution (see Appendix). The second cross-section component shows up very weakly as its contribution is small, so that the values for the contribution and for the cross section itself are not very reliable. At high energies the two cross-section components describing the cross-section structure are closer to equality, and the values of the average distribution characteristics (Appendix, fourth column) show the cross-section structure appearing outside the range of error.

It has been reported [8] that peculiarities in the behaviour of the cross-section of $_4$Be appear at E ~ 200 keV. The experiment in question was performed with a resolution of 10-20 keV. The authors interpreted their result as an S-resonance with parameters E_o = 208 keV and J = 1. We measured the

total cross-section of $_4$Be in the range 160 keV<E< 250 keV with a resolution of 8–10 keV, using different sample thicknesses ranging from 0.06 x 10^{24} to 0.36 x 10^{24} atoms/cm^2. The results are shown in Fig. 3 together with the atlas data from Ref. [7]. They show a monotonic cross-section pattern in the range of interest.

The possibility of peculiarities in the behaviour of the beryllium cross-section was further checked by analysing the dispersion values of the cross-section measured over energy intervals of ~35 keV. In the energy range under consideration, the dispersions through all intervals were found to be ~0.03 barn^2, a figure which is in good agreement with the value of 0.023 barn^2 obtained on the assumption of monotonic variation of the cross-section according to the law $\sigma(E) = \sigma_{const} - aE$ (a = 0.0065 barn/keV), and an order of magnitude lower than the value of 0.26 barn^2 obtained by numerical calculations based on the assumptions in Ref. [8]. However, this value may be regarded only as the lower boundary in view of the inaccuracies in the calculation and the influence of resolution.

Magnesium

In the 0.6 < E < 3 MeV energy range studied, the total cross-section of magnesium exhibits a clearly defined structure. The distribution of the total cross-section (see Appendix, second column) is well described by two cross-section components whose magnitudes and contributions are determined with reasonable accuracy. The average values found are in fair agreement with those given in the atlas [7] (see Fig. 4). In the energy range considered the dispersion of the cross-section first tends to diminish (up to $E_n \sim 1.5$MeV) and then remains more or less constant, as can be seen from Fig. 5.

Aluminium

The total cross-section structure of aluminium has been studied in considerable detail. It is clearly exhibited over the whole energy range up to $E_n \sim 2.5$ MeV. We note from the characteristics of the cross-section distribution given in the second column of the Appendix that first of all there are cases where the structure is described by three cross-section components. At E<200 keV the intervals ΔE were comparable with the level spacings, so that the cross-section structure here varies considerably from interval to interval. At these

energies the transmission functions were combined in pairs and treated again in order to obtain better averaging. The final results are given in Fig. 6. The sub-groups describing the structure are clearly separated. Agreement with existing total cross-section data (Fig. 7) is good. The dispersion (Fig. 8), as was to be expected, diminishes uniformly with energy.

The dotted line in Fig. 6 represents the sub-groups calculated in Ref. [9] from the data on cross-section structure given in Ref. [3]. The agreement between the calculated and the measured structure, as can be seen from Fig. 6, is on the whole very good except at the lowest and the highest energies. At low energies preference should clearly be given to the calculated data since, as we have noted, the experimental values were obtained by averaging two transmission functions, a procedure which could lead to loss of the cross-section structure. There is also the possibility that an insufficient number of points was used in measuring the transmission function and that the neutron spectrum was assymetric; these factors must be taken into account.

At high energies ($E > 1.5$ MeV) the cross-section structure is too weakly defined in the calculations, so that the dispersion of the total cross-section (Fig. 8) exceeds the calculated values by a factor of two. In this range the experimental data are more reliable.

Silicon

The distribution functions of the total neutron cross-section for silicon are well described by two cross-section components (Fig. 9), which make roughly equal contributions, and the measured values of the average cross-sections $\langle\sigma_t\rangle$ agree with the atlas data [7]. The anomalous energy dependence of the dispersion of the total cross-section for silicon is interesting in the energy range studied: the dispersion increases with energy (see Fig. 10), attaining a value of about 2 barns^2 in the 1.5-2 MeV range, although the average cross-section diminishes at the transition from 0.5-1.0 MeV to 1.5-2.0 MeV.

Phosphorus

The total cross-section of phosphorus was measured in the neutron energy range 0.9 MeV $< E_n <$ 2 MeV with a titanium-tritium target 0.30 m/cm^2 thick giving a resolution of $\Delta E \sim 40$ keV at $E_n \simeq 300$ keV and $\Delta E \sim 20$ keV at $E_n \simeq 2.5$ MeV. The sample of red phosphorus 0.281 atom/barn thick was placed

in a steel container with a 0.2 mm wall. Agreement with the data of other authors [7] (see Fig. 11) was satisfactory, and the position of the peaks at E ~ 950 keV and E ~ 1150 keV shows fair agreement, though the cross-section values obtained are, on the whole, slightly higher than the results obtained at high and low energies from the atlas [7]. The cross-section structure for phosphorus was not measured.

An interesting peculiarity of the energy dependence of the measured total cross-section, as can be seen in Fig. 11, is an apparent intermediate structure with widths of the order of 100 keV - much greater than the level spacing of the compound nucleus.

Sulphur

As the total cross-section for sulphur is fairly well known [7], we can compare the observed energy behaviour of the cross-section distribution characteristics with the expected behaviour. The average cross-sections (Fig. 12) agree well with available data and show a broad maximum at E ≃ 3 MeV which cannot be described by the optical model and is most likely due to fluctuations in the level density of the compound nucleus of ^{33}S. Thus, the "smoothing out" of the fluctuations in the cross-section distribution was not sufficiently complete in this case, although, as with beryllium and silicon, the experimental transmission functions were combined in pairs before treatment for adjacent energy intervals. This evidently explains the sharp dispersion peak at ~3 MeV (Fig. 13).

Corresponding anomalies are also found in the behaviour of the larger of the cross-section components σ_δ and its fraction a_δ.

Potassium

The total cross-section for potassium was measured in the energy range 0.4 MeV < E <3.9 MeV with a resolution of ~100 keV. The results given in Fig. 14 were obtained from measurements of the transmission functions, which showed no substantial deviations from the exponential law. From this we may conclude that within the limits of the resolution function the cross-section shows little fluctuation. Agreement with existing data is quite good over the whole range studied.

It is interesting to note that the cross-section values given in the atlas [7] for the interval 0.9 MeV < E < 1.7 MeV, evidently obtained with a rather high resolution, display at first sight a fairly detailed structure. The dispersion of the cross-section calculated by us from these values for the interval in question was ~0.15 barn^2. However, the error in this calculated quantity, determined from the accuracies ($\Delta\sigma \simeq 0.15$ barn) given in the atlas [7], was 0.18 barn^2. Thus, these data do not contradict our conclusion that there were no appreciable changes in the total cross-section of potassium over the energy interval considered.

Titanium

The results obtained for titanium $_{22}$Ti provide a good illustration of the proposed approach to the description of cross-section structure. The values of the cross-section components ("sub-groups") describing the distribution of the cross-section (Fig. 15) were determined with good accuracy and vary smoothly with energy. The average total cross-sections are in good agreement with known values. The dispersion of the cross-section (Fig. 17) decreases smoothly on the whole with energy. The downward jump at $E_n \sim 0.3$MeV corresponds to a similar characteristic found in the shape of the average cross-sections.

Since this element had not been studied sufficiently, we also carried out separate measurements of the cross-section with an energy resolution of ~20 keV in the range 0.3 MeV < E_n < 2.5 MeV, with an energy step of ~10 keV (Fig. 16).

Vanadium

A fairly good determination of the total cross-section structure for vanadium was made. The parameters of this structure - the magnitudes of the cross-sections (Fig. 18) and their relative contributions - were found with good accuracy and vary smoothly with energy. The average cross-sections agree well with the values given in the atlas [7]. The dispersion (Fig. 10), decreasing smoothly with rising energy, reaches a constant level of ~0.3 barn^2 at E_n ~ 1.5 MeV. The values of the average cross-sections and dispersions show quite good agreement with the results of calculations [9] performed for small energies (up to ~100 keV). Further, our dispersion data at E_n ~ 0.7 MeV do not agree with values obtained numerically from the results given in Ref. [7]. This is apparently due to a flattening in the trend of

the cross-section structure given in Ref. [7] as a result of inadequate resolution. Another possible explanation is that the structure was not measured in sufficient detail.

Measurements of the total cross-section of vanadium were also made in the range 1.1 MeV < E < 2.1 MeV with an energy resolution of 20 keV and an energy step of 5 keV. Three metallic samples 0.106 x 10^{24}, 0.170 x 10^{24} and 0.212 x 10^{24} atoms/cm^2 in thickness were used. In the processing of the measurements, the results for the different thicknesses were averaged and combined in pairs for the various energy intervals. The final data, together with the results of other authors [7], are given in Fig. 20. At low energies the agreement is good but at E_n ~ 2 MeV our results are about 0.5 barn higher than the atlas data [7].

Chromium $_{24}$Cr

The characteristics of the distribution function of the total cross-section for chromium (Figs 21 and 22) were determined fairly precisely, though the peculiarity of the structure at E_n ~ 2 MeV was not fully understood. The impression is that up to this energy the structure increases and then decreases. The dispersion results (Fig. 23) also lead to the same conclusion. The average cross-sections obtained in these measurements of the structure agree with the atlas data [7] for E_n > 2.5 MeV and also with the data (Fig. 24) for lower energies which we obtained in another experiment with a resolution of 20 keV using a sample 0.228 x 10^{24} atoms/cm^2 thick. We should point out that the dispersion values calculated from these data for the 0.6–1.0 MeV and 0.8–1.2 MeV intervals were lower than the measured values approximately by a factor of two. Here, as in the case of vanadium, the advantage of direct determination of the total cross-section structure is apparent.

Iron $_{26}$Fe

Examining the characteristics of the total cross-section distribution for iron (Figs 25 and 26), we note that below E_n ~ 0.5 MeV three sub-groups are needed to describe the cross-section structure. The more pronounced structure of the iron cross-section (compared with other elements) is due to a whole series of properties, viz. magic nucleus, low level density at high strength function values, predominance of one even-even isotope $^{56}_{26}$Fe in

the natural mixture, etc. The resonance structure of the cross-sections for iron cannot well be averaged (see Fig. 27) even over intervals of the order of 200 keV obtained by combining 3-5 experimental transmission functions measured for ~ 40 keV intervals.

Figures 25 and 26 also give calculated values for the characteristics of the cross-section distribution (the dotted line for three cross-section components and the dotted line with crosses for two cross-section components). It will be seen that agreement with the experimental representation of the structure (white squares denoting three cross-section components, half-shaded squares two cross-section components) is not bad as regards the magnitude and relative distribution of the contributions. As it happens the upper boundary of the region in which the experimentally determined structure is represented by thres cross-section components is ~ 1.7 MeV and in the case of the calculated structure ~1.4 MeV. However, the numerical characteristics of the structure, as can be seen from the dispersion graph (Fig. 28), is not affected.

Figure 26 deserves separate comment in the interests of clarity. In all the results considered in the present work we have given the contribution a_δ of the larger of the cross-section components. In Fig. 26 this is what we do for $E_n < 0.7$ MeV. At lower energies, however, where the cross-section structure is described by three cross-section components, we give not only the contribution of the largest of the cross-section components (which is always smaller) but also the values of the average cross-section.

The solid line in Fig. 27 shows calculated results for the cross-section of $_{26}Fe$ obtained by averaging the atlas data [7] over intervals of ΔE = 100 keV; and the dotted line represents the values of the group constants [3]. We must draw attention to the appreciable discrepancies between calculated and experimental dispersion values (Fig. 28) at the lowest (~ 100 keV) and highest (E_n < 4 MeV) energies. As in the case of aluminium, at lower energies the calculated values (which are considerably higher than the experimental ones) appear to be more accurate, while at higher energies, where the calculated dispersion is lower than the experimental, the latter should be used.

Nickel $_{28}Ni$

The total cross-section for nickel shows (Fig. 29), over the whole energy range investigated, a clearly defined structure decreasing smoothly with energy. It compares satisfactorily with the calculations in Ref. [9] based on average cross-sections (Fig. 30, dotted line); but the structure (Fig. 29) at E_n < 0.7 MeV shows up rather less clearly than would be expected from the calculations - the smaller the values of the larger cross-section,

the greater is its contribution. It is therefore not surprising that there should be a divergence between calculated [9] and experimental dispersion values for these energies (Fig. 31). The values given by the experimental representation of the cross-section structure seem to be confirmed by the fact that the experimental dispersion value of 4.8 ± 0.4 barns^2 in the interval 120 keV $< E_n <$ 260 keV agrees well with the value of 4.3 barns^2 calculated from the accurately measured cross-section behaviour [7] at these energies.

Copper $_{29}$Cu

The total cross-section structure for copper (Figs. 32 and 33) decreases smoothly with energy. The calculations in Ref. [9] describe, on the whole satisfactorily, the experimental values of both the parameters and the average characteristics of the structure - average cross-section and dispersion of the cross-section. The calculations actually give a somewhat larger cross-section structure at high energies but this difference is not perceptible in the dispersion values (possibly owing to insufficient accuracy of the experimental dispersion values). For the reciprocal moments ($\langle \frac{1}{\sigma} \rangle$, $\langle \frac{1}{\sigma^2} \rangle$, etc.) this difference should be smaller, since the values of the smaller cross-sections show better agreement between calculation and experiment.

Zinc $_{30}$Zn

The total cross-section structure for zinc was studied in a comparatively narrow range: 20 keV $< E_n <$ 300 keV. At these energies the average cross-section (see Appendix) diminishes gradually with energy; the dispersion assumes fairly high values, but was determined with poor accuracy.

The data relating to this element are of a preliminary nature; the measurements are to be repeated later on and extended to higher energies.

Gallium

The total cross-section of gallium in the energy range 5 keV $< E_n <$ 500 keV is not well known (Fig. 34), and there was accordingly every reason to attempt simultaneous measurements of the average cross-sections and the structure. In the upper part of Fig. 34 we have plotted average cross-section values measured with a resolution of ~ 30 keV and in the lower part the dispersions obtained for the same intervals from analysis of the transmission

functions. Then, in order to obtain better averaging and a more compact representation of the cross-section structure, we combined the transmission functions into groups of three - after which the transmissions seemed to be smooth functions of energy - and processed the results anew.

The final data on the cross-section structure of gallium are presented in Fig. 35 and in the Appendix. The structure found is small; the relative contribution of the second cross-section is approximately 0.05, and the value of this cross-section itself - as known at present - contains a fairly large error. Even so the dispersion of the cross-section (Fig. 36) has been determined with satisfactory accuracy. The points show dispersion values calculated for the corresponding intervals from the data provided in Ref. [7].

Zirconium $_{40}Zr$

The total cross-section structure of Zr (Appendix) showed up in measurements up to $E_n \sim 0.6$ MeV; at higher energies it was not possible to find deviations of the transmission functions from the exponential law with any degree of reliability. The average cross-sections (Fig. 37), measured with a resolution of 30 keV at $E_n \sim 30$ keV and with a resolution of ~ 100-200 keV at high energies, show good agreement with the corresponding data in Ref. [7] and with calculations based on the optical model [10].

Niobium $_{41}Nb$

The total cross-section structure of niobium (Figs. 38 and 39) appeared at energies below $E \sim 0.5$ MeV. The average cross-sections (Appendix) are in good agreement with the available values, which are shown in Fig. 40 together with our results for the intervals used in the experiment ($\Delta E \sim 30$ keV at $E < 500$ keV and $\Delta E \sim 200$ keV at high energies), and with calculations based on the optical model [10].

Molybdenum $_{42}Mo$

The total cross-section of molybdenum $_{42}Mo$ exhibited at $E_n < 350$ keV a fully defined structure (Figs 41 and 42) decreasing with energy, as can be seen from the gradually increasing predominance of the contribution from one of the cross-sections that describe the structures (Fig. 42) and from the diminishing dispersion (Fig. 43). The average cross-section (Fig. 44) is in good agreement with the atlas data [7].

The results indicate that in the system of constants in Ref. [3] the cross-section structure of molybdenum and the self-shielding of the average group cross-sections due to it at high energies have not been sufficiently evaluated. The authors of Ref. [3] assume that for $E_n > 10$ keV resonance self-shielding is not important.

Cadmium $_{48}$Cd

Measurements of the transmission functions for $_{48}$Cd over the range 10 keV < E_n < 300 keV and our analysis of these measurements did not reveal the structure of the cross-section (Appendix); the fraction attributable to the greater contribution is equal to unity within the limits of error, and the dispersion of the cross-section, also within the limits of error, is equal to zero. Fig. 45 gives the values obtained for the average cross-sections together with the available atlas data.

Tungsten $_{74}$W

The cross-section structure of tungsten over the range 20 keV < E_n < 100 keV is such that the smaller of the cross-section components can be determined satisfactorily. In the determination of the larger cross-section component there is a considerable error and it makes, moreover, a small contribution, as one would expect in regions with strong resonances. It is therefore not surprising that the dispersions of the cross-section (Appendix) should be determined in these preliminary measurements with poor accuracy. The average cross-section values obtained in the present work are about 20% higher than those in the atlas [7], but the reasons for this discrepancy are not clear.

Rhenium $_{75}$Re, Osmium $_{76}$Os and Iridium $_{77}$Ir

The total cross-sections of these elements were measured in the 20 keV-7 MeV range. The thicknesses of the samples of osmium, rhenium and iridium used in the measurements were 0.0588×10^{24}, 0.0545×10^{24} and 0.0332×10^{24} atoms/cm^2, respectively. The osmium and rhenium were in powder form and the iridium in the form of a metallic disc 5 cm in diameter. Measurements below 400 keV were performed at an angle of 100° to the proton beam and the energy resolution for neutrons obtained from the T(p,n)He^3 reaction was 40-20 keV; up to 3 MeV the measurements were performed at an angle of 0°, also with neutrons from the T(p,n)He^3 reaction ($\Delta E \sim 100$ keV); and those at higher energies used neutrons from the D(d,n)He^3 reaction ($\Delta E \sim 0.5$ MeV). The measured cross-sections (see Figs 46, 47 and 48) were, as one would expect for such heavy nuclei, smooth functions of energy - a point which is clearly illustrated by the nearly perfect coincidence of the measured total cross-section for iridium $_{77}$Ir with the known [7] cross-section of platinum $_{77}$Pt in the energy range around 0.15 MeV. We note, moreover, a systematic divergence of the results for $_{76}$Os and $_{77}$Ir from those recommended in the atlas [7]. This divergence may be attributed to the fact that the total cross-section values for $_{76}$Os and $_{77}$Ir recommended by the compilers of the atlas [7] are based mainly on the results of the Newson team at Duke University.

After publication of the atlas [7], Newson and his colleagues reported that their earlier results had been on the low side because of scattering into the detector. They have not yet published their new results, but they have reported [11] that the values became higher after the geometry had been improved.

Lead $_{82}$Pb

The cross-section structure of $_{82}$Pb shows up below $E_n \lesssim 1.2$ MeV (Fig. 49), while at high energies one of the contributions predominates in the distribution (see Appendix). The average cross-sections are, on the whole, in agreement with the atlas data [7].

Thorium $_{90}$Th

Thorium has been studied comparatively little and the results (see Appendix) should be regarded as preliminary. None the less, the total cross-section structure can be followed up to energies $E_n \sim 100$ keV. As in the case of osmium and iridium, as well as uranium (see below) the average cross-sections found by us above ~ 150 keV systematically exceed the values recommended in the atlas [7].

Uranium $_{92}$U

The total cross-section of uranium shows a well-defined structure up to $E \sim 150$ keV (Figs 50 and 51). The sub-groups characterizing the distribution of the cross-section can be distinguished quite clearly. The dispersion of the total cross-section (Fig. 52) decreases with increasing neutron energy and reaches an approximately constant value of 1.5-3 barns^2 at $E \sim 150$ keV. The average cross-sections (Fig. 53, rectangles) are in good agreement with the atlas data [7] at low energies but are considerably higher at $E_n \sim 200$-300 keV. As in the case of $_{76}$Os, $_{77}$Ir and $_{90}$Th, the discrepancy seems to be due mainly to the data of the Duke team (crosses in Fig. 53) which, as has been noted above, are low owing to poor geometry.

REFERENCES

[1] NIKOLAEV, M.N., FILIPPOV, V.V., BONDARENKO, I.I., Atomn. Energ., 11 (1961) 445.

[2] ABAGYAN, L.P. et al., Proceedings of the Third International Conference on the Peaceful Uses of Atomic Energy, Geneva, 1964, Vol. 2, Paper P-357.

[3] ABAGYAN, L.P., BAZAZYANTS, N.O., BONDARENKO, I.I., NIKOLAEV, M.N., Gruppovye Konstanty dlja rasčeta jadernyh reaktorov, Atomizdat, Moscow (1964) [Group Constants for Nuclear Reactor Calculations, Consultants Bureau, New York (1964)].

[4] KLEPIKOV, N.P., SOKOLOV, S.N., Analiz eksperimental'nyh dannyh metodom maksimuma pravopodobija (Analysis of experimental data by the method of likelihood maximum), Preprint R-235, Joint Institute of Nuclear Research (1962).

[5] NIKOLAEV, M.N., FILIPPOV, V.V., Atomn. Energ., 15 (1963) 493.

[6] Fast Neutron Physics (MARION, J.B. and FOWLER, J.L., Eds) 1 and 2, InterScience Publishers, New York and London (1963).

[7] Atlas of Neutron Cross-Sections, BNL-325, 2nd Ed., Suppl. 2,
vol. I, Z from 1 to 20, May 1964,
vol. IIA, Z from 21 to 40, February 1966,
vol. IIB, Z from 41 to 60, May 1966,
vol. IIC, Z from 61 to 87, August 1966,
vol. III, Z from 88 to 98, February 1965.

[8] PERRIN et al., Compt. Rend., 255, 277 (1962).

[9] KHOKHLOV, V.F., NIKOLAEV, M.N., Podgruppovaja sistema konstant (Subgroup system of constants) (Paper presented at the present Seminar).

[10] AVERIANOV, I.I., PURTSULADZE, Z.Z., Jadernaja Fizika, 6 (1967) 293.

[11] DIVADEENAM, NEWSON, Bull. Amer. Phys. Soc., 12 1 (1967) 106.

B E R Y L L I U M

0.07	±	0.03	0.002	±	0.009	I.000	0.985 – 0.959	0.902	5.22	±	0.04
			I	±	4		I.000 – 0.991	0.872	0.04	±	0.06
			0.998	±	0.010		I.000 –	0.899	I.006	±	0.016
			5.23	±	0.07			I.000	0.96	±	0.20
0.12	±	0.02	0.004	±	0.005	I.000	0.928 – 0.999	0.934	5.11	±	0.03
			I.08	±	I.3		I.000 – 0.988	0.889	0.07	±	0.05
			0.996	±	0.006		I.000 –	0.928	I.01	±	0.01
			5.13	±	0.05			I.000	0.933	±	0.11
0.15	±	0.03	0.0002	±	0.0045	I.000	0.984 – 0.999	0.967	4.80	±	0.02
			I	±	2		I.000 – 0.991	0.863	0.003	±	0.029
			I.000	±	0.005		I.000 –	0.900	I.001	±	0.011
			4.80	±	0.04			I.000	I.00	±	0.14
0.22	±	0.02	0.1	±	0.6	I.000 –	0.986 – I.000 –	0.992	4.89	±	0.25
			7	±	15		I.000	0.986	0.960	0.4	±	2.1
			0.9	±	0.6			I.000	0.992	I.01	±	0.04
			4.3	±	0.5				I.000	0.98	±	0.05
0.26	±	0.03	0.001	±	0.010	I.000	0.956 – 0.991	0.939	4.20	±	0.05
			I	±	13		I.000 – 0.986	0.877	0.01	±	0.06
			0.999	±	0.013		I.000 –	0.924	I.00	±	0.06
			4.21	±	0.07			I.000	I.0	±	0.7
0.45	±	0.15	0.42	±	0.45	I.000 –	0.990 – I.000 –	0.983	4.44	±	0.12
			5.4	±	I.4		I.000	0.990	0.968	0.7	±	0.7
			0.5	±	0.4			I.000	0.993	I.03	±	0.02
			3.7	±	0.4				I.000	0.94	±	0.03
0.97	±	0.28	0.017	±	0.012	I.000	0.975 – 0.999	0.951	3.69	±	0.02
			I.16	±	0.39		I.000 – 0.976	0.894	0.11	±	0.05
			0.98	±	0.01		I.000	0.950	I.030	±	0.004
			3.73	±	0.05			I.000	0.90	±	0.02
I.12	±	0.13	0.007	±	0.005	I.000	0.961 – I.000	0.761	3.53	±	0.05
			0.8	±	0.3		I.000 – 0.967	0.683	0.055	±	0.025
			0.993	±	0.005		I.000 –	0.758	I.021	±	0.004
			3.55	±	0.06			I.000	0.90	±	0.03
I.95	±	0.25	0.94	±	0.19	I.000 –	0.990 – I.000-	0.994	I.82	±	0.02
			I.87	±	0.12		I.000	0.990	0.970	0.04	±	0.04
			0.06	±	0.19			I.000	0.994	I.018	±	0.008
			I.I	±	0.80				I.000	0.955	±	0.019
2.47	±	0.25	0.988	±	0.014	I.000 –	0.923 – I.000 –	0.979	2.094	±	0.016
			2.II	±	0.03		I.000	0.927	0.867	0.025	±	0.014
			0.011	±	0.014			I.000	0.974	I.019	±	0.007
			0.6	±	0.5				I.000	0.92	±	0.06

3.34	±	0.50	0.10	±	0.02	1.000	- 0.849	- 1.000	- 0.892	2.44	± 0.16
			7	±	2		1.000	0.950	0.648	3	± 2
			0.903	±	0.024			1.000	0.891	1.19	± 0.08
			1.899	±	0.026				1.000	0.79	± 0.05
4.15	±	0.85	0.24	±	0.10	1.000	- 0.984	- 1.000	- 0.986	2.33	± 0.04
			3.5	±	0.6		1.000	0.984	0.949	0.43	± 0.20
			0.76	±	0.10			1.000	0.986	1.06	± 0.02
			1.96	±	0.06				1.000	0.902	± 0.016
4.85	±	0.75	0.27	±	0.09	1.000	- 0.988	- 1.000	- 0.986	2.10	± 0.02
			3.03	±	0.33		1.000	0.988	0.954	0.33	± 0.08
			0.73	±	0.09			1.000	0.986	1.061	± 0.007
			1.75	±	0.05				1.000	0.901	± 0.007
5.55	±	0.60	0.16	±	0.03	1.000	- 0.946	- 1.000	- 0.956	2.32	± 0.06
			4.9	±	0.8		1.000	0.946	0.856	1.2	± 0.5
			0.84	±	0.03			1.000	0.955	1.13	± 0.03
			1.85	±	0.02				1.000	0.83	± 0.02

M A G N E S I U M

0.60	±	0.30	0.78	±	0.05	1.000	0.967	- 1.000	0.958	5.53	± 0.13
			4.26	±	0.09		1.000	- 0.967	0.876	5.6	± 1.9
			0.22	±	0.05			1.000	- 0.958	1.14	± 0.02
			9.9	±	1.4				1.000	0.822	± 0.020
0.98	±	0.25	0.67	±	0.07	1.000	0.980	- 1.000	0.972	3.81	± 0.04
			2.85	±	0.10		1.000	- 0.980	0.912	1.9	± 0.3
			0.33	±	0.07			1.000	- 0.971	1.114	± 0.010
			5.8	±	0.5				1.000	0.830	± 0.010
1.02	±	0.25	0.23	±	0.08	1.000	- 0.982	- 1.000	- 0.958	3.33	± 0.05
			5.4	±	0.8		1.000	0.982	0.947	1.4	± 0.4
			0.77	±	0.08			1.000	0.988	1.093	± 0.013
			2.69	±	0.09				1.000	0.864	± 0.011
1.33	±	0.25	0.83	±	0.12	1.000	- 0.994	- 1.000	- 0.997	3.04	± 0.02
			3.28	±	0.16		1.000	0.994	0.984	0.29	± 0.08
			0.16	±	0.12			1.000	0.997	1.048	± 0.004
			1.8	±	0.4				1.000	0.894	± 0.017
1.90	±	0.20	0.6	±	0.4	1.000	0.998	- 1.000	0.995	2.82	± 0.06
			2.4	±	0.3		1.000	- 0.998	0.986	0.3	± 0.2
			0.4	±	0.4			1.000	- 0.995	1.038	± 0.016
			3.5	±	0.9				1.000	0.932	± 0.016
2.10	±	0.15	0.94	±	0.08	1.000	- 0.988	- 1.000	- 0.997	2.58	± 0.03
			2.66	±	0.12		1.000	0.988	0.975	0.12	± 0.05
			0.06	±	0.08			1.000	0.997	1.039	± 0.011
			1.2	±	0.8				1.000	0.89	± 0.07

2.40 ± 0.16	0.77 ± 0.15	1.000	-0.993	-1.000	-0.998	2.50 ± 0.03
	2.79 ± 0.20		1.000	0.993	0.984	0.28 ± 0.09
	0.22 ± 0.15			1.000	0.998	1.067 ± 0.005
	1.5 ± 0.3				1.000	0.861 ± 0.016
2.67 ± 0.15	0.7 ± 0.6	1.000	-0.994	-1.000	-0.998	2.49 ± 0.09
	2.8 ± 0.7		1.000	0.994	0.985	0.3 ± 0.3
	0.2 ± 0.6			1.000	0.998	1.064 ± 0.019
	1.6 ± 1.0				1.000	0.87 ± 0.05
2.82 ± 0.15	0.098 ± 0.006	1.000	-0.359	-1.000	-0.485	2.45 ± 0.04
	4.9 ± 0.5		1.000	0.367	-0.308	0.66 ± 0.20
	0.902 ± 0.006			1.000	0.469	1.062 ± 0.015
	2.181 ± 0.009				1.000	0.914 ± 0.018
3.02 ± 0.15	0.89 ± 0.15	1.000	0.993	-1.000	0.987	2.32 ± 0.05
	2.13 ± 0.09		1.000	-0.993	0.967	0.3 ± 0.3
	0.11 ± 0.15			1.000	-0.987	1.034 ± 0.018
	3.8 ± 1.9				1.000	0.946 ± 0.018
3.15 ± 0.15	0.4 ± 0.3	1.000	0.997	-1.000	0.995	2.22 ± 0.03
	1.6 ± 0.3		1.000	-0.997	0.986	0.29 ± 0.11
	0.6 ± 0.3			1.000	-0.995	1.070 ± 0.008
	2.6 ± 0.4				1.000	0.872 ± 0.018

A L U M I N I U M

0.036 ± 0.018	0.428 ± 0.016	1.000	-0.870	-0.990	-0.914			4.21 ± 0.12
	8.3 ± 0.4		1.000	0.877	0.734			12 ± 1
	0.572 ± 0.014			1.000	0.858			2.30 ± 0.06
	1.15 ± 0.04				1.000			0.298 ± 0.010
0.069 ± 0.018	0.267 ± 0.003	1.000	-0.343	-0.352	-0.384	-0.476	-0.208	4.35 ± 0.12
	10.9 ± 0.5		1.000	0.108	-0.242	0.052	0.307	16 ± 2
	0.632 ± 0.004			1.000	0.025	-0.463	-0.348	1.98 ± 0.06
	2.14 ± 0.03				1.000	0.605	-0.486	0.32 ± 0.02
	0.101 ± 0.004					1.000	-0.067	
	0.74 ± 0.06						1.000	
0.100 ± 0.020	0.24 ± 0.07	1.000	-0.914	0.138	-0.921	-0.806	-0.740	7.6 ± 0.6
	20 ± 6		1.000	0.049	0.757	0.631	0.573	50 ± 23
	0.59 ± 0.06			1.000	-0.494	-0.698	-0.755	1.98 ± 0.16
	4.3 ± 0.8				1.000	0.962	0.915	0.33 ± 0.03
	0.17 ± 0.09					1.000	0.985	
	1.5 ± 0.4						1.000	

0.198 ± 0.020	0.35	±	0.08	I.000	- 0.965	- 0.937	- 0.866	- 0.869	- 0.818	8.40	±	0.20
	12	±	1		I.000	0.937	0.898	0.783	0.731	22	±	4
	0.97	±	0.05			I.000	0.802	0.618	0.542	1.93	±	0.12
	3.7	±	0.8				I.000	0.962	0.926	0.22	±	0.06
	0.08	±	0.03					I.000	0.990			
	0.9	±	0.4						I.000			
0.160 ± 0.019	0.38	±	0.11	I.000	- 0.969	- 0.996	- 0.976	- 0.837	- 0.700	6.82	±	0.17
	11	±	2		I.000	0.976	0.906	0.740	0.664	10	±	3
	0.59	±	0.10			I.000	0.953	0.781	0.696	1.34	±	0.09
	4.5	±	0.5				I.000	0.927	0.863	0.45	±	0.09
	0.03	±	0.02					I.000	0.980			
	1.0	±	0.4						I.000			
0.180 ± 0.019	0.48	±	0.09	I.000	0.977	- I.000	0.961			5.01	±	0.17
	3.06	±	0.18		I.000	- 0.977	0.902			3.6	±	1.2
	0.52	±	0.09			I.000	- 0.961			1.17	±	0.03
	6.8	±	0.8				I.000			0.74	±	0.03
0.200 ± 0.020	0.16	±	0.04	I.000	0.982	- 0.999	0.962			5.06	±	0.06
	2.37	±	0.25		I.000	- 0.983	0.912			1.4	±	0.2
	0.84	±	0.05			I.000	- 0.961			1.10	±	0.01
	5.57	±	0.19				I.000			0.778	±	0.014
0.220 ± 0.018	0.58	±	0.07	I.000	0.984	- 0.999	0.964			4.70	±	0.12
	2.94	±	0.014		I.000	- 0.984	0.919			4.3	±	1.2
	0.42	±	0.07			I.000	- 0.964			1.21	±	0.03
	7.2	±	0.8				I.000			0.72	±	0.02
0.260 ± 0.017	0.38	±	0.03	I.000	- 0.933	- 0.999	- 0.966			3.40	±	0.08
	5.97	±	0.45		I.000	0.935	0.859			4.1	±	0.7
	0.62	±	0.03			I.000	0.963			1.38	±	0.03
	1.82	±	0.05				I.000			0.597	±	0.014
0.281 ± 0.017	0.257	±	0.024	I.000	0.974	- I.000	0.934			4.26	±	0.07
	1.65	±	0.09		I.000	- 0.977	0.862			2.36	±	0.17
	0.743	±	0.025			I.000	- 0.932			1.26	±	0.01
	5.17	±	0.17				I.000			0.574	±	0.012
0.298 ± 0.017	0.068	±	0.027	I.000	0.982	- I.000	0.960			4.18	±	0.04
	1.7	±	0.3		I.000	- 0.984	0.907			0.46	±	0.11
	0.932	±	0.027			I.000	- 0.959			1.05	±	0.01
	4.4	±	0.1				I.000			0.834	±	0.020
0.336 ± 0.016	0.629	±	0.044	I.000	0.971	- I.000	0.946			3.92	±	0.11
	2.42	±	0.07		I.000	- 0.972	0.878			3.81	±	0.89
	0.371	±	0.044			I.000	- 0.945			1.24	±	0.03
	6.5	±	0.6				I.000			0.596	±	0.019

0.350 ± 0.016	0.51	±	0.04	1.000	0.970 – 1.000	0.930	3.91	±	0.10
	1.95	±	0.08		1.000 – 0.973	0.858	4.0	±	0.7
	0.49	±	0.04		1.000 – 0.929		1.34	±	0.03
	5.9	±	0.4		1.000		0.595	±	0.015
0.386 ± 0.015	0.11	±	0.03	1.000	0.984 – 1.000	0.945	4.04	±	0.04
	1.63	±	0.19		1.000 – 0.985	0.894	0.73	±	0.12
	0.89	±	0.03		1.000 – 0.944		1.10	±	1.01
	4.33	±	0.10		1.000		0.759	±	0.017
0.446 ± 0.015	0.61	±	0.39	1.000	0.995 – 1.000	0.991	4.00	±	0.14
	3.02	±	0.60		1.000 – 0.995	0.976	1.5	±	1.2
	0.39	±	0.39		1.000 – 0.991		1.09	±	0.02
	5.6	±	2.0		1.000		0.85	±	0.03
0.510 ± 0170	0.144	±	0.016	1.000	0.972 – 1.000	0.924	3.79	±	0.03
	1.50	±	0.07		1.000 – 0.973	0.854	0.88	±	0.09
	0.856	±	0.016		1.000 – 0.924		1.140	±	0.007
	4.17	±	0.07		1.000		0.703	±	0.008
0.71 ± 0.15	0.090	±	0.011	1.000	0.974 – 1.000	0.918	3.80	±	0.02
	1.46	±	0.07		1.000 – 0.974	0.851	0.54	±	0.05
	0.910	±	0.011		1.000 – 0.918		1.091	±	0.004
	4.02	±	0.05		1.000		0.771	±	0.006
0.90 ± 0.14	0.031	±	0.006	1.000	0.958 – 1.000	0.819	3.21	±	0.02
	1.11	±	0.08		1.000– 0.960	0.713	0.14	±	0.02
	0.969	±	0.006		1.000 – 0.818		1.038	±	0.002
	3.28	±	0.02		1.000		0.875	±	0.007
1.05 ± 0.13	0.070	±	0.017	1.000	0.982 – 1.000	0.934	3.27	±	0.02
	1.36	±	0.11		1.000 – 0.982	0.885	0.28	±	0.05
	0.930	±	0.017		1.000 – 0.934		1.060	±	0.004
	3.42	±	0.05		1.000		0.841	±	0.007
1.22 ± 0.12	0.027	±	0.007	1.000	0.977 – 1.000	0.884	3.21	±	0.01
	1.20	±	0.12		1.000 – 0.978	0.831	0.11	±	0.02
	0.973	±	0.007		1.000 – 0.884		1.030	±	0.002
	3.27	±	0.02		1.000		0.910	±	0.005
1.39 ± 0.13	0.123	±	0.023	1.000 – 0.869	1.000 – 0.945		3.59	±	0.13
	8.0	±	1.7	1.000	0.869	0.744	2.7	±	1.5
	0.877	±	0.023		1.000	0.946	1.11	±	0.06
	2.98	±	0.03			1.000	0.85	±	0.03
1.57 ± 0.11	0.94	±	0.03	1.000 – 0.962	1.000 – 0.989		3.24	±	0.02
	3.34	±	0.06	1.000	0.962	0.924	0.15	±	0.04
	0.06	±	0.03		1.000	0.989	1.020	±	0.004
	1.7	±	0.2			1.000	0.934	±	0.006
1.75 ± 0.10	0.94	±	0.03	1.000 – 0.963	1.000 – 0.991		3.09	±	0.02
	3.19	±	0.06	1.000	0.963	0.930	0.16	±	0.04
	0.06	±	0.03		1.000	0.991	1.030	±	0.004
	1.6	±	0.2			1.000	0.921	±	0.005

2.03 ± 0.10	0.972	±	0.009	I.000	- 0.928	- I.000	- 0.987	3.34	±	0.02
	3.80	±	0.03		I.000	0.928	0.881	0.12	±	0.02
	0.028	±	0.009			I.000	0.987	I.030	±	0.002
	I.29	±	0.15				I.000	0.913	±	0.005
2.17 ± 0.09	0.022	±	0.010	I.000	0.987	- I.000	0.946	3.34	±	0.02
	I.5	±	0.2		I.000	- 0.987	0.901	0.08	±	0.02
	0.978	±	0.010			I.000	- 0.946	I.020	±	0.002
	3.38	±	0.03				I.000	0.952	±	0.004
2.32 ± 0.09	0.07	±	0.03	I.000	0.990	- I.000	0.968	3.16	±	0.02
	I.70	±	0.16		I.000	- 0.990	0.934	0.16	±	0.04
	0.93	±	0.03			I.000	- 0.968	I.030	±	0.004
	3.27	±	0.05				I.000	0.926	±	0.005

S I L I C O N

0.60 ± 0.25	0.18	±	0.15	I.000	0.994	- 0.999	0.990	3.18	±	0.07
	I.5	±	0.7		I.000	- 0.995	0.972	0.62	±	0.16
	0.82	±	0.16			I.000	- 0.988	I.II	±	0.03
	3.6	±	0.3				I.000	0.76	±	0.10
0.80 ± 0.25	0.31	±	0.19	I.000	0.995	- 0.999	0.990	3.60	±	0.07
	2.2	±	0.5		I.000	- 0.995	0.975	0.9	±	0.3
	0.69	±	0.19			I.000	- 0.990	I.10	±	0.01
	4.3	±	0.5				I.000	0.81	±	0.03
I.10 ± 0.25	0.47	±	0.21	I.000	0.992	- 0.999	0.986	3.62	±	0.13
	2.2	±	0.4		I.000	- 0.992	0.963	I.7	±	0.8
	0.52	±	0.22			I.000	- 0.985	I.15	±	0.03
	4.9	±	I.0				I.000	0.76	±	0.03
I.40 ± 0.25	0.84	±	0.10	I.000	0.981	- 0.999	0.967	2.90	±	0.14
	2.32	±	0.13		I.000	- 0.983	0.921	I.8	±	1.3
	0.16	±	0.10			I.000	- 0.966	I.13	±	0.04
	6	±	2				I.000	0.83	±	0.03
I.70 ± 0.25	0.26	±	0.10	I.000	- 0.974	- I.000	- 0.987	2.96	±	0.08
	5.2	±	I.I		I.000	0.976	0.937	I.8	±	0.7
	0.74	±	0.10			I.000	0.985	I.16	±	0.02
	2.16	±	0.14				I.000	0.79	±	0.02

S U L P H U R

0.82	±	0.22	0.54	±	0.04	I.000	0.987 - I.000	0.982	2.74	±	0.02
			I.77	±	0.05		I.000 - 0.988	0.945	I.09	±	0.I2
			0.46	±	0.04		I.000 - 0.98I		I.I60	±	0.007
			3.86	±	0.I8		I.000		0.762	±	0.006
I.00	±	0.23	0.483	±	0.0I4	I.000	0.580 - I.000	0.527	2.49I	±	0.0I2
			I.88	±	0.02		I.000 - 0.590	- 0.3I5	0.35	±	0.03
			0.5I7	±	0.0I4		I.000 - 0.5I8		I.06I	±	0.005
			3.06	±	0.04		I.000		0.890	±	0.008
I.20	±	0.23	0.8I2	±	0.0I7	I.000 - 0.538	- I.000	- 0.63I	2.452	±	0.0I3
			2.66	±	0.03		I.000	0.558 - 0.242	0.I98	±	0.025
			0.I86	±	0.0I7		I.000	0.607	I.048	±	0.007
			I.52	±	0.06		I.000		0.895	±	0.0I5
I.52	±	0.2I	0.20	±	0.04	I.000	0.709 - 0.999	0.659	2.42	±	0.03
			I.42	±	0.I4		I.000 - 0.730	0.02I8	0.25	±	0.07
			0.80	±	0.04		I.000 - 0.642		I.066	±	0.0I8
			2.67	±	0.08		I.000		0.86	±	0.04
2.I7	±	0.38	0.60	±	0.23	I.000 - 0.992	- I.000	- 0.995	2.84	±	0.04
			3.35	±	0.38		I.000	0.992 0.976	0.40	±	0.I5
			0.40	±	0.23		I.000	0.995	I.059	±	0.0I0
			2.05	±	0.27		I.000		0.890	±	0.0II
2.69	±	0.I6	0.42	±	0.08	I.000 - 0.976	- I.000	- 0.987	3.36	±	0.05
			4.7	±	0.4		I.000	0.976 0.537	I.27	±	0.30
			0.58	±	0.08		I.000	0.987	I.III	±	0.0I4
			2.43	±	0.09		I.000		0.826	±	0.0I3
2.85	±	0.I6	0.58	±	0.I3	I.000 - 0.985	- I.000	- 0.992	3.40	±	0.04
			4.I6	±	0.30		I.000	0.985 0.950	0.76	±	0.20
			0.42	±	0.I3		I.000	0.992	I.077	±	0.0II
			2.39	±	0.I8		I.000		0.86I	±	0.0II
3.03	±	0.I6	0.92	±	0.04	I.000 - 0.975	- I.000	- 0.99I	3.083	±	0.025
			3.24	±	0.08		I.000	0.976 0.945	0.26	±	0.06
			0.08	±	0.04		I.000	0.990	I.064	±	0.005
			I.32	±	0.26		I.000		0.834	±	0.020
3.20	±	0.I6	0.I9	±	0.II	I.000	0.994 - I.000	0.99I	2.957	±	0.025
			I.8I	±	0.25		I.000 - 0.994	0.974	0.32	±	0.08
			0.80	±	0.II		I.000 - 0.99I		I.054	±	0.006
			3.23	±	0.I6		I.000		0.885	±	0.009
3.37	±	0.I6	0.69	±	0.I5	I.000 - 0.993	- I.000	- 0.995	2.80I	±	0.020
			3.20	±	0.2I		I.000	0.993 0.979	0.94	±	0.09
			0.3I	±	0.I5		I.000	0.995	I.056	±	0.006
			I.93	±	0.20		I.000		0.89I	±	0.007

3.55 ± 0.16	0.94	±	0.05	I.000	- 0.986	- I.000	- 0.994	2.559	±	0.020
	2.63	±	0.07		I.000	0.987	0.967	0.13	±	0.03
	0.06	±	0.05			I.000	0.993	I.046	±	0.011
	I.08	±	0.48				I.000	0.87	±	0.06

T I T A N I U M

0.090 ± 0.050	0.38	±	0.03	I.000	0.958	- I.000	0.843	4.72	±	0.24
	I.61	±	0.07		I.000	- 0.962	0.773	6.0	±	I.4
	0.62	±	0.03			I.000	- 0.841	I.56	±	0.06
	6.6	±	0.6				I.000	0.433	±	0.020
0.140 ± 0.060	0.46	±	0.08	I.000	0.982	- I.000	0.955	2.84	±	0.11
	I.45	±	0.11		I.000	- 0.983	0.907	I.6	±	0.5
	0.54	±	0.08			I.000	- 0.954	I.28	±	0.04
	4.0	±	0.4				I.000	0.63	±	0.02
0.180 ± 0.060	0.45	±	0.05	I.000	- 0.971	- I.000	- 0.987	2.20	±	0.05
	3.4	±	0.3		I.000	0.973	0.933	I.20	±	0.20
	0.55	±	0.05			I.000	0.985	I.289	±	0.020
	I.2I	±	0.06				I.000	0.645	±	0.012
0.230 ± 0.060	0.45	±	0.01	I.000	- 0.780	- 0.997	- 0.917	2.19	±	0.02
	3.42	±	0.06		I.000	0.811	0.523	I.24	±	0.06
	0.55	±	0.01			I.000	0.885	I.3I	±	0.01
	I.18	±	0.01				I.000	0.63	±	0.01
0.280 ± 0.060	0.56	±	0.10	I.000	- 0.972	- I.000	- 0.988	2.09	±	0.09
	3.0	±	0.4		I.000	0.975	0.935	I.06	±	0.20
	0.44	±	0.09			I.000	0.983	I.38	±	0.04
	0.92	±	0.15				I.000	0.55	±	0.04
0.320 ± 0.050	0.62	±	0.03	I.000	0.965	- 0.999	0.982	2.14	±	0.02
	I.19	±	0.05		I.000	- 0.976	0.905	I.45	±	0.14
	0.38	±	0.03			I.000	- 0.975	I.33	±	0.01
	3.67	±	0.20				I.000	0.63	±	0.01
0.63 ± 0.08	0.50	±	0.08	I.000	0.982	- 0.999	0.970	3.04	±	0.09
	I.64	±	0.12		I.000	- 0.985	0.926	I.98	±	0.50
	0.49	±	0.08			I.000	- 0.968	I.27	±	0.03
	4.46	±	0.48				I.000	0.65	±	0.02
0.78 ± 0.08	0.53	±	0.05	I.000	0.978	- 0.998	0.956	3.19	±	0.09
	I.66	±	0.09		I.000	- 0.981	0.904	2.6	±	0.6
	0.47	±	0.05			I.000	- 0.956	I.32	±	0.03
	4.89	±	0.44				I.000	0.62	±	0.02

0.93 ± 0.07	0.41	±	0.10	1.000	0.987 – 1.000	0.976	3.05	± 0.10
	1.57	±	D.19		1.000 – 0.989	0.942	1.5	± 0.4
	0.59	±	0.10		1.000 – 0.974		1.24	± 0.02
	4.1	±	0.5		1.000		0.66	± 0.02
1.07 ± 0.06	0.48	±	0.09	1.000	0.989 – 1.000	0.981	2.96	± 0.06
	1.75	±	0.13		1.000 – 0.990	0.950	1.4	± 0.3
	0.52	±	0.09		1.000 – 0.980		1.189	± 0.017
	4.1	±	0.4		1.000		0.722	± 0.014
1.21 ± 0.09	0.46	±	0.09	1.000	0.990 – 0.999	0.983	2.96	± 0.05
	1.76	±	0.14		1.000 – 0.991	0.956	1.17	± 0.26
	0.54	±	0.09		1.000 – 0.983		1.17	± 0.01
	3.95	±	0.34		1.000		0.74	± 0.01
1.35 ± 0.05	0.25	±	0.12	1.000	0.992 – 1.000	0.982	3.03	± 0.07
	1.5	±	0.3		1.000 – 0.993	0.957	0.75	± 0.25
	0.73	±	0.12		1.000 – 0.981		1.139	± 0.014
	3.5	±	0.3		1.000		0.74	± 0.03
1.48 ± 0.09	0.32	±	0.09	1.000	0.992 – 1.000	0.984	3.19	± 0.04
	1.89	±	0.18		1.000 – 0.993	0.960	0.81	± 0.18
	0.68	±	0.09		1.000 – 0.984		1.112	± 0.009
	3.81	±	0.25		1.000		0.796	± 0.012
1.6 ± 0.0	3.24(3)	±	0.14	1.000	0.994 – 1.000	0.985	3.23	± 0.06
	1.9	±	0.3		1.000 – 0.994	0.964	0.6	± 0.2
	0.25	±	0.14		1.000 – 0.985		1.087	± 0.011
	3.7	±	0.3		1.000		0.828	± 0.017
1.8 ± 0.0	0.36	±	0.06	1.000 – 0.980	– 1.000 –	0.994	3.32	± 0.04
	3.59	±	0.13		1.000 – 0.980	0.957	0.43	± 0.09
	0.14	±	0.06		1.000	0.994	1.071	± 0.005
	1.70	±	0.25		1.000		0.840	± 0.014
1.96 ± 0.07	0.870	±	0.019	1.000 – 0.843	– 1.000 –	0.952	3.47	± 0.02
	3.71	±	0.04		1.000 0.846	0.664	0.39	± 0.04
	0.130	±	0.019		1.000	0.950	1.056	± 0.004
	1.86	±	0.09		1.000		0.870	± 0.008
2.10 ± 0.07	0.18	±	0.20	1.000	0.996 – 0.999	0.990	3.57	± 0.07
	2.11	±	0.69		1.000 – 0.997	0.976	0.47	± 0.22
	0.82	±	0.20		1.000 – 0.990		1.06	± 0.00
	3.89	±	0.35		1.000		0.88	± 0.02
2.24 ± 0.08	0.44	±	0.15	1.000	0.993 – 1.000	0.979	3.70	± 0.09
	2.6	±	0.2		1.000 – 0.993	0.953	1.0	± 0.4
	0.56	±	0.15		1.000 – 0.979		1.084	± 0.018
	4.6	±	0.5		1.000		0.851	± 0.018
2.36 ± 0.05	0.27	±	0.15	1.000	0.993 – 1.000	0.972	3.75	± 0.09
	2.4	±	0.3		1.000 – 0.988	0.931	0.72	± 0.25
	0.72	±	0.15		1.000 – 0.967		1.070	± 0.016
	4.3	±	0.4		1.000		0.861	± 0.020

2.46 ± 0.05	0.12	±	0.12	I.000	0.995 - I.008	0.979	3.74	± 0.09
	2.0	±	0.6		I.000 - 0.995	0.958	0.41	± 0.15
	0.88	±	0.12		I.000 - 0.979		I.051	± 0.012
	4.0	±	0.3		I.000		0.880	± 0.016
2.56 ± 0.06	0.15	±	0.11	I.000	0.994 - I.000	0.979	3.87	± 0.07
	2.2	±	0.4		I.000 - 0.995	0.956	0.49	± 0.21
	0.85	±	0.11		I.000 - 0.978		I.053	± 0.011
	4.17	±	0.25		I.000		0.880	± 0.012
2.67 ± 0.05	0.24	±	0.12	I.000	0.995 - I.000	0.981	3.88	± 0.07
	2.4	±	0.3		I.000 - 0.995	0.960	0.64	± 0.20
	0.76	±	0.12		I.000 - 0.981		I.061	± 0.011
	4.3	±	0.3		I.000		0.875	± 0.013
2.78 ± 0.06	0.272	±	0.006	I.000	0.355 - I.000	0.217	3.71	± 0.04
	2.42	±	0.03		I.000 - 0.376 - 0.670		0.61	± 0.06
	0.728	±	0.006		I.000 - 0.204		I.060	± 0.005
	4.18	±	0.06		I.000		0.879	± 0.010
2.98 ± 0.06	0.16	±	0.10	I.000	0.995 - I.000	0.984	3.66	± 0.05
	2.2	±	0.4		I.000 - 0.995	0.964	0.41	± 0.14
	0.84	±	0.10		I.000 - 0.984		I.048	± 0.008
	3.94	±	0.20		I.000		0.894	± 0.009
3.00 ± 0.06	0.25	±	0.03	I.000	0.995 - I.000	0.985	3.78	± 0.03
	2.48	±	0.17		I.000 - 0.995	0.967	0.57	± 0.11
	0.75	±	0.08		I.000 - 0.985		I.054	± 0.005
	4.22	±	0.16		I.000		0.889	± 0.006
3.11 ± 0.06	0.21	±	0.11	I.000	0.995 - I.000	0.983	3.78	± 0.06
	2.4	±	0.3		I.000 - 0.995	0.964	0.56	± 0.20
	0.78	±	0.12		I.000 - 0.983		I.056	± 0.010
	4.17	±	0.25		I.000		0.882	± 0.011
3.28 ± 0.12	0.042	±	0.048	I.000	0.994 - I.000	0.971	3.61	± 0.06
	I.4	±	0.7		I.000 - 0.995	0.945	0.21	± 0.11
	0.96	±	0.05		I.000 - 0.970		I.038	± 0.006
	3.70	±	0.14		I.000		0.89	± 0.04

V A N A D I U M

0.07 ± 0.05	0.372	±	0.025	I.000	0.898 - 0.998	0.914	7.8	± 0.2
	2.03	±	0.13		I.000 - 0.913	0.740	20	± 3
	0.63	±	0.02		I.000 - 0.910		I.87	± 0.06
	II.2	±	0.6		I.000		0.32	± 0.02
0.17 ± 0.05	0.22	±	0.02	I.000	0.937 - 0.999	0.901	6.66	± 0.11
	I.77	±	0.13		I.000 - 0.944	0.782	6.8	± 0.7
	0.78	±	0.02		I.000 - 0.899		I.48	± 0.02
	8.0	±	0.2		I.000		0.403	± 0.018

0.23 ± 0.05	0.197	±	0.025	1.000	0.954 – 0.999	0.929	5.48	±	0.09
	1.60	±	0.15		1.000 – 0.962	0.843	3.7	±	0.5
	0.80	±	0.03		1.000 – 0.926		1.36	±	0.02
	6.44	±	0.20		1.000		0.469	±	0.020
0.28 ± 0.04	0.24	±	0.05	1.000	0.970 – 1.000	0.956	4.88	±	0.08
	1.66	±	0.20		1.000 – 0.972	0.887	2.8	±	0.5
	0.76	±	0.05		1.000 – 0.954		1.263	±	0.019
	5.8	±	0.3		1.000		0.581	±	0.025
0.35 ± 0.05	0.33	±	0.05	1.000	0.974 – 1.000	0.963	4.40	±	0.07
	2.04	±	0.16		1.000 – 0.976	0.899	2.8	±	0.4
	0.66	±	0.05		1.000 – 0.961		1.243	±	0.016
	5.6	±	0.3		1.000		0.635	±	0.017
0.41 ± 0.05	0.39	±	0.11	1.000	0.975 – 1.000	0.975	3.86	±	0.09
	2.0	±	0.3		1.000 – 0.977	0.916	2.3	±	0.6
	0.61	±	0.11		1.000 – 0.974		1.229	±	0.025
	5.1	±	0.5		1.000		0.66	±	0.03
0.61 ± 0.09	0.47	±	0.09	1.000 – 0.955	– 1.000 – 0.958		3.62	±	0.14
	2.4	±	0.8		1.000 0.956	0.882	3.0	±	1.0
	0.53	±	0.09		1.000	0.967	1.24	±	0.04
	2.08	±	0.13			1.000	0.68	±	0.03
0.8 ± 0.1	0.39	±	0.10	1.000	0.952 – 1.000	0.974	3.38	±	0.06
	2.04	±	0.15		1.000 – 0.982	0.930	1.2	±	0.3
	0.61	±	0.10		1.000 – 0.974		1.135	±	0.019
	4.2	±	0.3		1.000		0.774	±	0.016
0.98 ± 0.1	0.28	±	0.12	1.000	0.987 – 1.000	0.982	3.43	±	0.05
	2.18	±	0.20		1.000 – 0.990	0.954	0.6	±	0.2
	0.72	±	0.12		1.000 – 0.984		1.074	±	0.012
	3.9	±	0.3		1.000		0.856	±	0.013
1.2 ± 0.1	0.43	±	0.17	1.000	0.992 – 1.000	0.988	3.40	±	0.04
	2.53	±	0.18		1.000 – 0.992	0.966	0.57	±	0.20
	0.57	±	0.17		1.000 – 0.988		1.055	±	0.011
	4.0	±	0.4		1.000		0.897	±	0.012
1.47 ± 0.10	0.48	±	0.12	1.000	0.990 – 1.000	0.988	3.536	±	0.025
	2.71	±	0.12		1.000 – 0.990	0.962	0.61	±	0.15
	0.52	±	0.12		1.000 – 0.988		1.052	±	0.007
	4.3	±	0.3		1.000		0.904	±	0.008
1.75 ± 0.10	0.25	±	0.25	1.000	0.994 – 1.000	0.991	3.65	±	0.03
	2.7	±	0.4		1.000 – 0.994	0.977	0.28	±	0.14
	0.35	±	0.25		1.000 – 0.991		1.026	±	0.007
	4.0	±	0.3		1.000		0.946	±	0.010
2.05 ± 0.20	0.2	±	0.2	1.000	0.994 – 1.000	0.990	3.77	±	0.06
	2.6	±	0.9		1.000 – 0.994	0.972	0.24	±	0.25
	0.8	±	0.3		1.000 – 0.990		1.023	±	0.014
	4.0	±	0.4		1.000		0.950	±	0.020

C H R O M I U M

0.594	±	0.26	0.43	±	0.03	I.000	0.959 – I.000	0.935	3.15	±	0.06
			I.5I	±	0.05		I.000 – 0.960	0.849	2.04	±	0.25
			0.57	±	0.03		I.000 – 0.935	I.308	±	0.020	
			4.39	±	0.20		I.000	0.602	±	0.012	
0.8I	±	0.23	0.48	±	0.04	I.000	0.96I – I.000	0.95I	3.03	±	0.06
			I.50	±	0.05		I.000 – 0.96I	0.866	I.88	±	0.30
			0.52	±	0.04		I.000 – 0.95I	I.27I	±	0.025	
			4.34	±	0.25		I.000	0.644	±	0.015	
I.02	±	0.22	0.45	±	0.03	I.000 – 0.942	I.000 – 0.940	3.05	±	0.06	
			4.67	±	0.30		I.000 0.942	0.824	2.I	±	0.4
			0.55	±	0.03		I.000	0.940	I.265	±	0.025
			I.79	±	0.05		I.000	0.666	±	0.015	
I.22	±	0.2I	0.56	±	0.05	I.000	0.932 – I.000	0.932	3.24	±	0.I3
			I.75	±	0.06		I.000 – 0.932	0.806	2.8	±	0.8
			0.44	±	0.05		I.000 – 0.932	I.3I	±	0.05	
			5.I	±	0.6		I.000	0.63	±	0.03	
I.35	±	0.I7	0.46	±	0.03	I.000 – 0.859	I.000 – 0.849	3.37	±	0.I0	
			5.I	±	0.4		I.000 0.859	0.983	2.7	±	0.5
			0.54	±	0.03		I.000	0.847	I.20	±	0.03
			I.85	±	0.04		I.000	0.645	±	0.020	
I.48	±	0.20	0.57	±	0.06	I.000	0.930 – I.000	0.940	3.43	±	0.I3
			I.98	±	0.07		I.000 – 0.930	0.805	2.8	±	0.9
			0.43	±	0.06		I.000 – 0.940	I.26	±	0.05	
			5.4	±	0.7		I.000	0.67	±	0.03	
I.68	±	0.25	0.38	±	0.II	I.000 – 0.947	I.000 – 0.945	3.47	±	0.20	
			6	±	I		I.000 0.947	0.849	2.6	±	I.6
			0.6I	±	0.II		I.000	0.946	I.2I	±	0.08
			2.20	±	0.I2		I.000	0.72	±	0.06	
2.00	±	0.23	0.27	±	0.05	I.000	0.988 – I.000	0.960	3.28	±	0.04
			2.06	±	0.08		I.000 – 0.988	0.926	0.57	±	0.II
			0.72	±	0.05		I.000 – 0.960	I.074	±	0.009	
			3.74	±	0.I4		I.000	0.856	±	0.0II	
2.28	±	0.20	0.20	±	0.04	I.000	0.988 – I.000	0.954	3.58	±	0.03
			2.I2	±	0.09		I.000 – 0.988	0.9I5	0.55	±	0.08
			0.80	±	0.04		I.000 – 0.954	I.066	±	0.006	
			4.0	±	0.I		I.000	0.862	±	0.007	
2.5I	±	0.24	0.I39	±	0.020	I.000	0.986 – I.000	0.939	3.64	±	0.02
			I.96	±	0.07		I.000 – 0.986	0.892	0.46	±	0.05
			0.86	±	0.02		I.000 – 0.939	I.060	±	0.004	
			3.9I	±	0.05		I.000	0.864	±	0.005	

2.72	±	0.15	0.07	±	0.02	1.000	0.983 - 1.000	0.916			3.61	±	0.03
			1.70	±	0.15		1.000 - 0.984	0.860			0.28	±	0.06
			0.93	±	0.02			1.000 - 0.916			1.044	±	0.005
			3.75	±	0.07			1.000			0.886	±	0.008
2.97	±	0.20	0.067	±	0.016	1.000	0.974 - 1.000	0.877			3.53	±	0.03
			1.54	±	0.12		1.000 - 0.975	0.799			0.28	±	0.05
			0.933	±	0.016			1.000 - 0.876			1.050	±	0.004
			3.68	±	0.06			1.000			0.866	±	0.008
3.12	±	0.16	0.063	±	0.015	1.000	0.976 - 1.000	0.880			3.52	±	0.03
			1.43	±	0.13		1.000 - 0.977	0.801			0.29	±	0.05
			0.937	±	0.016			1.000 - 0.879			1.056	±	0.005
			3.66	±	0.06			1.000			0.846	±	0.006

I R O N

0.090	±	0.060	0.24	±	0.02	1.000	0.983 - 0.791	0.672	0.546	0.931	4.35	±	0.14
			1.08	±	0.05		1.000 - 0.722	0.607	0.460	0.873	12	±	4
			0.15	±	0.06			1.000 - 0.962 - 0.944 - 0.948			1.74	±	0.05
			12	±	3			1.000	0.956	0.852	0.361	±	0.012
			0.60	±	0.04				1.000	0.798			
			3.7	±	0.3					1.000			
0.160	±	0.090	0.15	±	0.04	1.000	0.986	0.256	0.957 - 0.816	0.672	4.16	±	0.20
			0.78	±	0.14		1.000	0.158	0.913 - 0.756	0.614	11	±	4
			0.62	±	0.04			1.000	0.516 - 0.767	0.837	1.81	±	0.08
			2.8	±	0.3				1.000 - 0.949	0.825	0.32	±	0.03
			0.23	±	0.06				1.000 - 0.947				
			10	±	2				1.000				
0.220	±	0.090	0.10	±	0.06	1.000	0.992	0.512	0.966 - 0.861	0.759	3.66	±	0.13
			0.71	±	0.25		1.000	0.440	0.934 - 0.815	0.710	5.2	±	1.6
			0.61	±	0.06			1.000	0.712 - 0.877	0.925	1.56	±	0.07
			2.4	±	0.4				1.000 - 0.960	0.884	0.39	±	0.07
			0.30	±	0.10				1.000 - 0.972				
			7.1	±	1.4				1.000				
0.29	±	0.09	0.55	±	0.05	1.000	0.749 - 0.911	0.935	0.459	0.353	3.11	±	0.14
			3.2	±	0.4		1.000 - 0.952	0.869	0.926	0.859	7	±	3
			0.10	±	0.07			1.000 - 0.966 - 0.784 - 0.702			1.74	±	0.08
			10	±	5				1.000	0.676	0.597	0.388	±	0.018
			0.35	±	0.03					1.000	0.980			
			0.93	±	0.05						1.000			
0.38	±	0.05	0.23	±	0.07	1.000	0.957 - 0.992	0.976				3.72	±	0.20
			0.9	±	0.5		1.000 - 0.985	0.941				2.5	±	0.4
			0.77	±	0.10			1.000 - 0.972				1.6	±	0.3
			4.6	±	0.5			1.000				0.34	±	0.18

0.52	±	0.15	0.06	±	0.07	1.000	0.986 - 0.283		0.973 - 0.847		0.696	4.35	±	0.20
			0.7	±	0.8		1.000 - 0.381		0.931 - 0.783		0.634	10	±	3
			0.65	±	0.05			1.000 - 0.066		0.265	0.416	1.66	±	0.20
			2.5	±	0.4				1.000 - 0.939		0.805	0.36	±	0.20
			0.28	±	0.08					1.000 - 0.932				
			9.3	±	1.9						1.000			
0.70	±	0.15	0.63	±	0.03	1.000 - 0.904		1.000 - 0.952				3.26	±	0.07
			4.4	±	0.2		1.000	0.906	0.804			2.2	±	0.2
			0.37	±	0.03			1.000	0.949			1.41	±	0.03
			1.27	±	0.06				1.000			0.512	±	0.014
1.00	±	0.15	0.36	±	0.04	1.000	0.968 - 1.000		0.937			2.75	±	0.05
			1.31	±	0.05		1.000 - 0.969		0.866			1.16	±	0.18
			0.64	±	0.04			1.000 - 0.936				1.249	±	0.019
			3.56	±	0.17				1.000			0.636	±	0.013
1.30	±	0.15	0.41	±	0.05	1.000	0.985 - 1.000		0.939			2.94	±	0.06
			1.78	±	0.06		1.000 - 0.986		0.884			0.95	±	0.19
			0.59	±	0.05			1.000 - 0.939				1.143	±	0.016
			3.76	±	0.22				1.000			0.767	±	0.016
1.55	±	0.10	0.33	±	0.04	1.000	0.975 - 1.000		0.940			3.11	±	0.05
			1.67	±	0.06		1.000 - 0.976		0.875			1.01	±	0.16
			0.57	±	0.04			1.000 - 0.940				1.159	±	0.015
			3.81	±	0.16				1.000			0.732	±	0.014
1.90	±	0.15	0.884	±	0.016	1.000 - 0.841		1.000 - 0.969				2.88	±	0.03
			3.21	±	0.06		1.000	0.841	0.746			0.36	±	0.04
			0.1116	±	0.016			1.000	0.958			1.083	±	0.006
			1.34	±	0.06				1.000			0.804	±	0.009
2.15	±	0.10	0.14	±	0.04	1.000	0.990 - 1.000		0.948			3.21	±	0.04
			1.61	±	0.10		1.000 - 0.990		0.917			0.43	±	0.08
			0.85	±	0.04			1.000 - 0.948				1.077	±	0.008
			3.48	±	0.10				1.000			0.827	±	0.010
2.30	±	0.10	0.109	±	0.020	1.000	0.984 - 1.000		0.926			3.22	±	0.04
			1.55	±	0.08		1.000 - 0.984		0.881			0.34	±	0.05
			0.891	±	0.020			1.000 - 0.926				1.064	±	0.007
			3.42	±	0.08				1.000			0.846	±	0.011
2.45	±	0.10	0.20	±	0.05	1.000	0.973 - 1.000		0.957			3.347	±	0.025
			1.99	±	0.13		1.000 - 0.974		0.880			0.47	±	0.08
			0.80	±	0.05			1.000 - 0.956				1.064	±	0.006
			3.70	±	0.10				1.000			0.865	±	0.009
2.65	±	0.10	0.900	±	0.025	1.000 - 0.941		1.000 - 0.984				3.44	±	0.04
			3.63	±	0.09		1.000	0.942	0.893			0.34	±	0.08
			0.100	±	0.025			1.000	0.984			1.056	±	0.008
			1.68	±	0.12				1.000			0.862	±	0.011

2,80	±	0,10	0,0124	±	0,0002	I,000 - 0,252 - 0,428	0,013	3,20	±	0,04
			0,68	±	0,04	I,000 - 0,297 - 0,145		0,080	±	0,005
			0,9876	±	0,0002	I,000 - 0,028		I,036	±	0,004
			3,24	±	0,04	I,000		0,834	±	0,020
3,0	±	I,0	0,10	±	0,03	I,000 0,984 - I,000	0,944	3,39	±	0,05
			I,4I	±	0,I6	I,000 - 0,985	0,898	0,46	±	0,10
			0,90	±	0,03	I,000 - 0,944		I,090	±	0,008
			3,62	±	0,10	I,000		0,784	±	0,012
4,0	±	I,0	0,09	±	0,03	I,000 0,987 - I,000	0,959	3,45	±	0,04
			I,57	±	0,18	I,000 - 0,987	0,92I	0,36	±	0,09
			0,9I	±	0,03	I,000 - 0,958		I,063	±	0,004
			3,64	±	0,09	I,000		0,844	±	0,010
5,0	±	I,0	0,I28	±	0,008	I,000 0,9I3 - I,000	0,765	3,487	±	0,019
			I,57	±	0,04	I,000 - 0,9I6	0,56I	0,542	±	0,030
			0,872	±	0,008	I,000 - 0,763		I,092	±	0,003
			3,77	±	0,03	I,000		0,79I	±	0,006

N I C K E L

0,I26	±	0,076	0,350	±	0,0I8	I,000 0,939 -0,999	0,9I8	5,49	±	0,07
			2,I6	±	0,07	I,000 - 0,948	0,790	6,0	±	0,5
			0,650	±	0,0I8	I,000 - 0,9I5		I,380	±	0,0I4
			7,28	±	0,20	I,000		0,524	±	0,009
0,I90	±	0,068	0,268	±	0,0I6	I,000 0,992 - I,000	0,892	5,55	±	0,07
			I,94	±	0,07	I,000 - 0,938	0,748	4,8	±	0,4
			0,732	±	0,0I6	I,000 - 0,869		I,359	±	0,0I5
			6,88	±	0,I7	I,000		0,508	±	0,0II
0,303	±	0,06I	0,24	±	0,03	I,000 0,978 - I,000	0,963	4,68	±	0,04
			2,II	±	0,II	I,000 - 0,979	0,906	I,94	±	0,23
			0,76	±	0,03	I,000 - 0,963		I,I7	±	0,009
			5,38	±	0,I5	I,000		0,692	±	0,0I0
0,50	±	0,I7	0,I4	±	0,04	I,000 0,969 - I,000	0,865	3,6	±	0,2
			I,30	±	0,I6	I,000 - 0,970	0,765	0,9I0	±	0,3
			0,86	±	0,04	I,000 - 0,864		I,I7	±	0,03
			4,0	±	0,3	I,000		0,65	±	0,04
0,69	±	0,05	0,72	±	0,I5	I,000 0,990 - I,000	0,939	3,I4	±	0,20
			2,05	±	0,20	I,000 - 0,99I	0,907	3,	±	2
			0,27	±	0,I5	I,000 - 0,933		I,25	±	0,07
			6	±	2	I,000		0,7I	±	0,05
0,75	±	0,I5	0,I5	±	0,03	I,000 0,969 - I,000	0,899	3,03	±	0,08
			I,I4	±	0,07	I,000 - 0,970	0,830	0,52	±	0,I3
			0,85	±	0,03	I,000 - 0,899		I,I62	±	0,0I9
			3,36	±	0,I4	I,000		0,670	±	0,0I9

0.99 ± 0.05	0.74	±	0.19	I.000	- 0.969	- I.000	- 0.990	3.21	±	0.10
	3.7	±	0.4		I.000	0.970	0.932	0.8	±	0.3
	0.24	±	0.18			I.000	0.989	I.13	±	0.02
	I.6	±	0.5				I.000	0.76	±	0.05
I.03 ± 0.19	0.81	±	0.03	I.000	- 0.937	- I.000	- 0.976	2.87	±	0.06
	3.22	±	0.13		I.000	0.938	0.878	0.56	±	0.11
	0.19	±	0.03			I.000	0.975	I.130	±	0.015
	I.34	±	0.07				I.000	0.743	±	0.016
I.40 ± 0.23	0.13	±	0.04	I.000	0.985	- I.000	0.937	3.16	±	0.04
	I.56	±	0.13		I.000	- 0.985	0.866	0.40	±	0.10
	0.86	±	0.04			I.000	- 0.937	I.075	±	0.010
	3.41	±	0.11				I.000	0.830	±	0.013
I.75 ± 0.10	0.805	±	0.008	I.000	- 0.155	- I.000	- 0.261	3.06	±	0.07
	3.36	±	0.10		I.000	0.158	- 0.627	0.36	±	0.07
	0.195	±	0.008			I.000	0.256	I.059	±	0.011
	I.83	±	0.06				I.000	0.87	±	0.02
I.96 ± 0.10	0.982	±	0.017	I.000	- 0.856	- I.000	- 0.982	2.66	±	0.05
	2.69	±	0.07		I.000	0.856	0.801	0.05	±	0.04
	0.018	±	0.017			I.000	0.981	I.022	±	0.007
	0.9	±	0.3				I.000	0.924	±	0.014
2.15 ± 0.15	0.02	±	0.10	I.000	- 0.970	- I.000	- 0.983	3.04	±	0.06
	3.3	±	0.2		I.000	0.970	0.920	0.34	±	0.14
	0.18	±	0.10			I.000	0.983	I.060	±	0.015
	I.78	±	0.20				I.000	0.68	±	0.02
2.35 ± 0.10	0.29	±	0.16	I.000	0.984	- I.000	0.972	3.14	±	0.06
	2.I	±	0.2		I.000	- 0.984	0.924	0.5	±	0.2
	0.7I	±	0.16			I.000	- 0.975	I.063	±	0.016
	3.6	±	0.3				I.000	0.88	±	0.02

C O P P E R

0.032 ± 0.009	0.55	±	0.07	I.000	0.961	- I.000	0.929	7.8	±	0.4
	4.18	±	0.20		I.000	- 0.961	0.841	16	±	6
	0.45	±	0.07			I.000	- 0.929	I.32	±	0.06
	12.4	±	I.8				I.000	0.62	±	0.03
0.063 ± 0.031	0.23	±	0.12	I.000	0.978	- I.000	0.947	6.8	±	0.4
	2.6	±	0.7		I.000	- 0.980	0.892	5	±	3
	0.77	±	0.12			I.000	- 0.945	I.25	±	0.05
	8.0	±	I.I				I.000	0.59	±	0.06
0.073 ± 0.041	0.49	±	0.05	I.000	0.953	- I.000	0.914	7.3	±	0.3
	3.39	±	0.18		I.000	- 0.954	0.814	14	±	4
	0.51	±	0.06			I.000	- 0.913	I.39	±	0.05
	11.0	±	I.2				I.000	0.56	±	0.03

0.081 ± 0.027	0.42	±	0.14	I.000	0.978 – I.000	0.960	6.8	±	0.3
	3.7	±	0.5		I.000 – 0.978	0.901	7	±	3
	0.57	±	0.14		I.000 – 0.960		I.20	±	0.05
	9.0	±	I.5		I.000		0.70	±	0.04
0.110 ± 0.040	0.41	±	0.05	I.000	0.976 – I.000	0.966	6.21	±	0.07
	3.60	±	0.15		I.000 – 0.977	0.908	4.8	±	0.6
	0.58	±	0.015		I.000 – 0.966		I.17	±	0.01
	8.0	±	0.4		I.000		0.74	±	0.01
0.150 ± 0.044	0.38	±	0.04	I.000	0.980 – I.000	0.949	5.86	±	0.06
	3.2	±	0.1		I.000– 0.980	0.895	4.2	±	0.4
	0.62	±	0.04		I.000 – 0.949		I.173	±	0.009
	2.4	±	0.2		I.000		0.723	±	0.008
0.176 ± 0.041	0.28	±	0.06	I.000	0.983 – I.000	0.957	5.5	±	0.1
	2.8	±	0.2		I.000 – 0.982	0.902	2.7	±	0.5
	0.72	±	0.06		I.000 – 0.957		1.147	±	0.014
	6.5	±	0.3		1.000		0.738	±	0.015
0.232 ± 0.037	0.24	±	0.03	I.000	0.984 – 1.000	0.965	5.19	±	0.03
	2.76	±	0.10		I.000 – 0.985	0.917	1.84	±	0.16
	0.76	±	0.03		1.000 – 0.964		1.172	±	0.004
	5.95	±	0.11		I.000		0.782	±	0.006
0.248 ± 0.040	0.28	±	0.14	I.000	0.983 – I.000	0.984	4.99	±	0.09
	2.7	±	0.5		I.000 – 0.984	0.943	2.1	±	0.7
	0.71	±	0.14		I.000 – 0.983		2	±	0.018
	5.9	±	0.5		I.000			±	0.03
0.298 ± 0.042	0.18	±	0.05	I.000	0.950 – 0.989	0.961	4.93	±	0.08
	1.8	±	0.3		I.000 – 0.960	0.868	2.I	±	0.4
	0.82	±	0.05		I.000 – 0.957		I.2I	±	0.03
	5.6	±	0.3		I.000		0.6I	±	0.05
0.349 ± 0.041	0.28	±	0.11	I.000	0.977 – I.000	0.979	4.98	±	0.08
	2.5	±	0.4		I.000 – 0.979	0.925	2.4	±	0.6
	0.72	±	0.11		I.000 – 0.978		I.I6	±	0.02
	5.9	±	0.5		I.000		0.72	±	0.04
0.644 ± 0.16	0.047	±	0.015	I.000	0.984 – I.000	0.879	3.90	±	0.04
	1.69	±	0.15		I.000 – 0.984	0.8I4	0.24	±	0.05
	0.953	±	0.015		I.000 – 0.870		I.035	±	0.004
	4.00	±	0.07		I.000		0.900	±	0.008
0.857 ± 0.14	0.08	±	0.09	I.000	0.990 – I.000	0.950	3.2I	±	0.07
	1.7	±	0.5		I.000 – 0.990	0.9I4	0.I9	±	0.I4
	0.92	±	0.09		I.000 – 0.950		I.034	±	0.0I3
	3.34	±	0.I8		I.000		0.9I5	±	0.0I8
1.43 ± 0.16	0.946	±	0.016	I.000 – 0.896	- I.000 – 0.985		3.05	±	0.03
	3.15	±	0.06		I.000 0.896	0.839	0.I6	±	0.03
	0.054	±	0.016		I.000	0.985	I.037	±	0.004
	I.38	±	0.12			I.000	0.898	±	0.008

Z I N C

0.05 ± 0.03	0.436	±	0.050	I.000	0.979 – I.000	0.940	8.45	±	0.34
	3.52	±	0.27		I.000 – 0.983	0.888	I8.8	±	4.2
	0.564	±	0.052		I.000 – 0.937		I.44	±	0.04
	I2.3	±	I.I		I.000		0.5I6	±	0.0I9
0.085 ± 0.03	0.705	±	0.056	I.000	0.967 – I.000	0.922	8.60	±	0.75
	4.77	±	0.22		I.000 – 0.97I	0.853	35	±	I9
	0.295	±	0.058		I.000 – 0.920		I.4I	±	0.II
	I7.7	±	4.3		I.000		0.599	±	0.049
0.I25 ± 0.030	0.3I6	±	0.066	I.000	0.975 – I.000	0.926	7.I0	±	0.29
	3.42	±	0.26		I.000 – 0.975	0.858	6.3	±	I.9
	0.684	±	0.067		I.000 – 0.925		I.2I	±	0.03
	8.80	±	0.78		I.000		0.668	±	0.028
0.I70 ± 0.030	0.470	±	0.085	I.000 – 0.944	I.000 – 0.98I		7.45	±	0.37
	II.I	±	I.6		I.000 0.944	0.890	II.9	±	4.5
	0.530	±	0.084		I.000	0.980	I.25	±	0.05
	4.2I	±	0.27		I.000		0.669	±	0.032
0.200 ± 0.030	0.70	±	0.I3	I.000	0.984 – I.000	0.957	6.6	±	0.4
	4.7	±	0.3		I.000 – 0.985	0.9I0	9	±	6
	0.30	±	0.I3		I.000 – 0.956		I.I7	±	0.06
	II.0	±	3.2		I.000		0.777	±	0.046
0.24 ± 0.03	0.57	±	0.I5	I.000	0.988 – I.000	0.972	5.93	±	0.22
	4.08	±	0.34		I.000 – 0.988	0.934	4.5	±	2.2
	0.43	±	0.I5		I.000 – 0.972		I.I3	±	0.03
	8.3	±	I.5		I.000		0.799	±	0.028
0.28 ± 0.03	0.456	±	0.033	I.000	0.756 – I.000	0.6I9	5.85	±	0.I4
	3.7I	±	0.I0		I.000 – 0.766 – 0.I0I		4.0	±	0.8
	0.534	±	0.033		I.000 – 0.6II		I.I4	±	0.02
	7.7I	±	0.39		I.000		0.748	±	0.027

G A L L I U M

0.09I ± 0.052	0.I0	±	0.05	I.000	0.993 – I.000	0.969	6.47	±	0.07
	2.9	±	0.6		I.000 – 0.994	0.946	I.4	±	0.3
	0.90	±	0.05		I.000 – 0.968		I.070	±	0.005
	6.8	±	0.2		I.000		0.83	±	0.02
0.I36 ± 0.056	0.05I	±	0.0I7	I.000	0.989 – I.000	0.952	6.37	±	0.05
	2.0	±	0.5		I.000 – 0.992	0.9I9	I.0I	±	0.I3
	0.950	±	0.0I8		I.000 – 0.948		I.075	±	0.009
	6.60	±	0.I0		I.000		0.78	±	0.05
0.I82 ± 0.063	0.048	±	0.0I7	I.000	0.990 – I.000	0.954	6.08	±	0.05
	I.9	±	0.5		I.000 – 0.993	0.9I9	0.90	±	0.II
	0.95I	±	0.0I9		I.000 – 0.950		I.075	±	0.0I2
	6.29	±	0.I0		I.000		0.78	±	0.06

0.291 ± 0.059	0.94	±	0.03	I.000	–	0.945	–	I.000	–	0.990	5.80	±	0.05
	6.02	±	0.12			I.000		0.948		0.904	0.81	±	0.14
	0.06	±	0.02					I.000		0.988	I.062	±	0.008
	2.3	±	0.6							I.000	0.82	±	0.04
0.277 ± 0.066	0.10	±	0.04	I.000		0.993	–	0.999		0.982	5.58	±	0.03
	2.8	±	0.4			I.000	–	0.994		0.959	0.88	±	0.13
	0.90	±	0.04					I.000	–	0.981	I.050	±	0.003
	5.89	±	0.11							I.000	0.87	±	0.01
0.322 ± 0.054	0.63	±	0.03	I.000	–	0.995	–	I.000	–	0.997	5.50	±	0.06
	6.1	±	0.7			I.000		0.995		0.985	I.I	±	0.5
	0.4	±	0.3					I.000		0.997	I.045	±	0.009
	3.9	±	0.6							I.000	0.912	±	0.009
0.365 ± 0.052	0.92	±	0.07	I.000	–	0.987	–	I.000	–	0.996	4.99	±	0.05
	5.20	±	0.19			I.000		0.988		0.973	0.53	±	0.16
	0.08	±	0.07					I.000		0.996	I.042	±	0.006
	2.4	±	0.9							I.000	0.89	±	0.04
0.406 ± 0.015	0.95	±	0.05	I.000	–	0.980	–	I.000	–	0.994	4.79	±	0.03
	4.91	±	0.12			I.000		0.981		0.955	0.32	±	0.09
	0.05	±	0.05					I.000		0.993	I.028	±	0.007
	2.3	±	I.I							I.000	0.92	±	0.04

Z I R C O N I U M

0.070 ± 0.018	0.31	±	0.06	I.000		0.987	–	I.000		0.970	8.72	±	0.08
	5.1	±	0.3			I.000	–	0.988		0.938	5.9	±	0.8
	0.69	±	0.06					I.000	–	0.976	I.II2	±	0.007
	I0.4	±	0.4							I.000	0.794	±	0.009
0.I00 ± 0.019	0.28	±	0.04	I.000		0.971	–	I.000		0.952	9.07	±	0.I0
	5.I2	±	0.I8			I.000	–	0.971		0.877	6.2	±	0.8
	0.72	±	0.04					I.000	–	0.952	I.II	±	0.0I
	I0.6	±	0.3							I.000	0.79	±	0.0I
0.I39 ± 0.019	0.52	±	0.II	I.000		0.991	–	I.000		0.983	9.34	±	0.I3
	6.5	±	0.4			I.000	–	0.991		0.957	9.0	±	2
	0.48	±	0.I2					I.000	–	0.985	I.I08	±	0.0I2
	I2.4	±	I.2							I.000	0.825	±	0.0II
0.I80 ± 0.019	0.3I	±	0.06	I.000		0.982	–	I.000		0.975	9.I	±	0.I
	5.2	±	0.3			I.000	–	0.982		0.923	7	±	I
	0.68	±	0.06					I.000	–	0.974	I.I24	±	0.0I0
	I0.9	±	0.5							I.000	0.777	±	0.0I0
0.209 ± 0.018	0.44	±	0.I2	I.000		0.976	–	I.000		0.983	9.I2	±	0.I5
	5.5	±	0.5			I.000	–	0.976		0.925	I0	±	3
	0.56	±	0.I2					I.000	–	0.983	I.I5	±	0.02
	II.9	±	I.2							I.000	0.756	±	0.0I9

0.257 ± 0.017	0.39 ± 0.08		I.000	0.984 – I.000	0.982	8.79 ± 0.09		
	5.7 ± 0.3			I.000 – 0.984	0.936	6.2 ± I.2		
	0.6I ± 0.08			I.000 – 0.98I		I.IOI ± 0.0I0		
	I0.8 ± 0.6			I.000		0.822 ± 0.0I0		
0.293 ± 0.019	0.68 ± 0.06		I.000	0.972 – I.000	0.973	8.64 ± 0.I8		
	6.06 ± 0.20			I.000 – 0.973	0.904	I4 ± 4		
	0.32 ± 0.06			I.000 – 0.972		II.66 ± 0.020		
	I4 ± 2			I.000		0.775 ± 0.0I6		
0.334 ± 0.028	0.06 ± 0.02		I.000	0.982 – I.000	0.946	8.44 ± 0.05		
	3.6 ± 0.4			I.000 – 0.982	0.900	I.6 ± 0.3		
	0.94 ± 0.02			I.000 – 0.945		I.050 ± 0.005		
	8.77 ± 0.I4			I.000		0.866 ± 0.008		
0.45 ± 0.I5	0.37 ± 0.27		I.000 – 0.988	– I.000 – 0.99I		8.28 ± 0.I8		
	II ± 2			I.000 0.988	0.963	4 ± 2		
	0.63 ± 0.27			I.000	0.99I	I.048 ± 0.0I9		
	6.8 ± 0.5				I.000	0.9I7 ± 0.022		

N I O B I U M

0.025 ± 0.020	0.366 ± 0.050		I.000 – 0.964 – I.000 – 0.969			8.04 ± 0.20		
	I2.3 ± I.0			I.000 0.964	0.883	I0.4 ± 2.3		
	0.633 ± 0.050			I.000	0.968	I.I5 ± 0.02		
	5.58 ± 0.I4				I.000	0.783 ± 0.020		
0.050 ± 0.0I8	0.44 ± 0.II		I.000	0.987– I.000	0.980	8.69 ± 0.20		
	5.0 ± 0.6			I.000 – 0.988	0.944	I0.7 ± 2.8		
	0.56 ± 0.I0			I.000 – 0.979		I.I6 ± 0.02		
	II.6 ± I.2			I.000		0.72 ± 0.02		
0.099 ± 0.0I8	0.49 ± 0.I0		I.000	0.990 – I.000	0.982	8.79 ± 0.I2		
	6.0 ± 0.4			I.000 – 0.987	0.952	7.6 ± I.8		
	0.5I ± 0.I0			I.000 – 0.982		I.II ± 0.0I		
	II.5 ± I.0			I.000		0.8I7 ± 0.0I0		
0.I2I ± 0.020	0.28 ± 0.20		I.000	0.994 – I.000	0.988	8.85 ± 0.I6		
	5.3 ± I.0			I.000 – 0.994	0.970	5 ± 2		
	0.72 ± 0.I6			I.000 – 0.988		I.09 ± 0.03		
	I0.2 ± I.0			I.000		0.82 ± 0.02		
0.I44 ± 0.026	0.23 ± 0.04		I.000	0.986 – I.000	0.960	9.I3 ± 0.08		
	5.00 ± 0.25			I.000 – 0.986	0.920	5.2 ± 0.7		
	0.77 ± 0.04			I.000 – 0.960		I.099 ± 0.007		
	I0.4 ± 0.3			I.000		0.804 ± 0.008		
0.I83 ± 0.027	0.24 ± 0.05		I.000	0.977 – I.000	0.969	9.I8 ± 0.08		
	5.2 ± 0.3			I.000 – 0.978	0.908	5.I ± 0.8		
	0.76 ± 0.05			I.000 – 0.969		I.095 ± 0.008		
	I0.4 ± 0.3			I.000		0.8I ± 0.0I		

0.24	±	0.02	0.22	±	0.06	I.000	0.990 - I.000	0.978	8.90	± 0.09
			5.2	±	0.4		I.000 - 0.990	0.945	3.9	± 0.7
			0.78	±	0.06		I.000 - 0.978		I.074	± 0.007
			I0.0	±	0.4		I.000		0.848	± 0.008
0.26	±	0.0I	0.I0	±	0.05	I.000	0.984 - I.000	0.973	8.82	± 0.08
			4.2	±	0.8		I.000 - 0.986	0.929	2.4	± 0.6
			0.90	±	0.05		I.000 - 0.972		I.053	± 0.006
			9.3	±	0.3		I.000		0.847	± 0.0I9
0.320	±	0.03I	0.06	±	0.03	I.000	0.988 - I.000	0.940	8.80	± 0.II
			3.5	±	0.7		I.000 - 0.990	0.890	I.8	± 0.5
			0.94	±	0.03		I.000 - 0.930		I.058	± 0.005
			9.I	±	0.2		I.000		0.84	± 0.02
0.37	±	0.04	0.075	±	0.025	I.000	0.986 - I.000	0.968	8.50	± 0.05
			3.8	±	0.5		I.000 - 0.985	0.924	I.8	± 0.3
			0.92	±	0.02		I.000 - 0.967		I.053	± 0.004
			8.88	±	0.I5		I.000		0.860	± 0.0II
0.42	±	0.03	0.08	±	0.03	I.000	0.984 - I.000	0.965	8.59	± 0.06
			3.7	±	0.6		I.000 - 0.986	0.925	2.0	± 0.4
			0.92	±	0.03		I.000 - 0.964		I.062	± 0.005
			9.0I	±	0.I8		I.000		0.838	± 0.0I6
0.50	±	0.03	0.056	±	0.0I4	I.000	0.982 - I.000	0.948	7.95	± 0.03
			3.3	±	0.3		I.000 - 0.983	0.90I	I.29	± 0.I8
			0.944	±	0.0I4		I.000 - 0.947		I.048	± 0.003
			0.23	±	0.08		I.000		0.866	± 0.008

M O L Y B D E N U M

0.044	±	0.02I	0.4I	±	0.I2	I.000	0.985 - I.000	0.987	8.92	± 0.II
			5.8	±	0.5		I.000 - 0.985	0.949	6.9	± I.8
			0.59	±	0.I2		I.000 - 0.986		I.I07	± 0.0I2
			II.I	±	0.9		I.000		0.8I6	± 0.0I3
0.060	±	0.033	0.36	±	0.20	I.000	0.988 - I.000	0.987	8.89	± 0.20
			5.5	±	I.0		I.000 - 0.988	0.955	6.5	± 3.0
			0.64	±	0.20		I.000 - 0.987		I.II	± 0.02
			I0.8	±	I.5		I.000		0.80	± 0.02
0.I32	±	0.026	0.I4	±	0.07	I.000	0.986 - I.000	0.984	8.78	± 0.07
			4.5	±	0.7		I.000 - 0.986	0.948	2.9	± 0.7
			0.86	±	0.07		I.000 - 0.984		I.067	± 0.007
			9.5	±	0.3		I.000		0.847	± 0.0I6
0.2I7	±	0.0I7	0.I2	±	0.I5	I.000	0.988 - I.000	0.988	8.89	± 0.I0
			5.0	±	I.7		I.000 - 0.989	0.957	2.2	± I.2
			0.88	±	0.I5		I.000 - 0.988		I.046	± 0.0I0
			9.4	±	0.6		I.000		0.892	± 0.025

0.340 ± 0.020	0.06	±	0.06	I.000	0.992 - I.000	0.988	8.66	±	0.05
	4.I	±	I.6		I.000 - 0.992	0.964	I.2	±	0.4
	0.94	±	0.06		I.000 - 0.986		I.033	±	0.005
	8.9	±	0.2		I.000		0.9I	±	0.03

C A D M I U M

0.04 ± 0.03	0.76	±	0.I8	I.000	0.987 - I.000	0.973	7.3	±	0.4
	5.8	±	0.4		I.000 - 0.988	0.937	7	±	7
	0.24	±	0.I8		I.000 - 0.973		I.I0	±	0.05
	I2	±	5		I.000		0.85	±	0.0I
0.I2 ± 0.04	0.89	±	0.I8	I.000	0.987 - I.000	0.979	7.2	±	0.3
	6.6	±	0.4		I.000 - 0.987	0.942	3	±	6
	0.II	±	0.I8		I.000 - 0.979		I.04	±	0.04
	I3	±	I0		I.000		0.94	±	0.04
0.I7 ± 0.04	0.5	±	0.8	I.000	0.996 - I.000	0.994	7.35	±	0.I9
	6	±	2		I.000 - 0.996	0.980	2	±	2
	0.4	±	0.7		I.000 - 0.993		I.044	±	0.0I9
	9	±	9		I.000		0.92	±	0.02
0.20 ± 0.04	0.79	±	0.25	I.000	0.994 - I.000	0.989	7.64	±	0.I8
	6.7	±	0.5		I.000 - 0.994	0.970	3	±	3
	0.2I	±	0.25		I.000 - 0.989		I.046	±	0.020
	II	±	4		I.000		0.926	±	0.020
0.24 ± 0.04	0.93	±	0.06	I.000	0.975 - I.000	0.954	7.8	±	0.5
	7.I0	±	0.I7		I.000 - 0.976	0.896	6	±	II
	0.07	±	0.06		I.000 - 0.744		I.05	±	0.05
	I7	±	I2		I.000		0.93	±	0.05

T U N G S T E N

0.025 ± 0.0I0	0.64	±	0.I2	I.000	0.959 - I.000	0.953	I6	±	I
	8.5	±	I.I		I.000 - 0.965	0.856	92	±	47
	0.36	±	0.I2		I.000 - 0.950		I.38	±	0.0I8
	28	±	7		I.000		0.60	±	0.05
0.035 ± 0.0I5	0.8I	±	0.07	I.000	0.9I9 - 0.999	0.896	I6	±	2
	8.9	±	0.7		I.000 - 0.929	0.757	207	±	I78
	0.I9	±	0.07		I.000 - 0.892		I.52	±	0.20
	45	±	20		I.000		0.58	±	0.08
0.052 ± 0.0I5	0.84	±	0.06	I.000	0.93I - 0.999	0.898	I4	±	2
	9.0	±	0.5		I.000 - 0.940	0.775	I64	±	I38
	0.I6	±	0.06		I.000 - 0.894		I.4I	±	0.I6
	44	±	20		I.000		0.64	±	0.07

0.070	±	0.015	0.73	±	0.11	I.000	0.972 - I.000	0.980	II.8	±	0.4
			8.4	±	0.6		I.000 - 0.974	0.904	51	±	I4
			0.27	±	0.I2		I.000 - 0.970		I.I8	±	0.04
			2I	±	5		I.000		0.77	±	0.03
0.090	±	0.015	0.63	±	0.20	I.000	0.985 - I.000	0.986	I0.9	±	0.3
			7.5	±	I.0		I.000 - 0.986	0.943	I9	±	9
			0.37	±	0.2I		I.000 - 0.985		I.I5	±	0.03
			I6	±	4		I.000		0.78	±	0.03

L E A D

0.46	±	0.I6	0.8I	±	0.09	I.000 - 0.959 - I.000 - 0.990			7.0	±	0.2
			7.8	±	0.6		I.000	0.960	0.922	3	±	I
			0.I9	±	0.08			I.000	0.990	I.I04	±	0.0I8
			3.5	±	0.5				I.000	0.786	±	0.020
0.72	±	0.I5	0.5	±	0.3	I.000	0.996 - I.000	0.994		5.7I	±	0.09
			4.6	±	0.5		I.000 - 0.995	0.98I		I.2	±	0.7
			0.5	±	0.3			I.000 - 0.994		I.039	±	0.0I3
			6.8	±	I.I				I.000	0.927	±	0.0I6
I.08	±	0.I2	0.26	±	0.I2	I.000 - 0.980 - I.000 - 0.993				5.45	±	0.II
			7.75	±	I.40		I.000	0.980	0.957	I.8	±	I.0
			0.74	±	0.I2			I.000	0.993	I.050	±	0.0I6
			4.66	±	0.I5				I.000	0.9I7	±	0.0I9
I.27	±	0.I2	0.02	±	0.04	I.000 - 0.904 - I.000 - 0.908				5.3	±	0.3
			I6	±	24		I.000	0.904	0.736	3	±	8
			0.58	±	0.04			I.000	0.907	I.03	±	0.06
			5.06	±	0.07				I.000	0.96	±	0.06
I.56	±	0.I0	0.26	±	0.22	I.000	0.984 - I.000	0.977		5.4	±	0.4
			5.I	±	0.5		I.000 - 0.985	0.934		2	±	I0
			0.04	±	0.23			I.000 - 0.976		I.03	±	0.07
			I2	±	36				I.000	0.96	±	0.07
1.75	±	0.10	0.012	±	0.015	1.000 - 0.761 - 0.219			0.318	5.68	±	0.28
			0.4	±	0.4		1.000 - 0.464		0.288	0.20	±	0.60
			0.948	±	0.010			1.000 -	0.896	1.6	±	1.4
			5.94	±	0.09				1.000	0.2	±	0.3
2.I2	±	0.I2	0.002	±	0.00I	I.000	0.974 - 0.994	0.895		6.07	±	0.03
			I	±	I		I.000 - 0.993	0.8I5		0.06	±	0.03
			0.998	±	0.002			I.000 -	0.863	I.0I0	±	0.0I2
			6.08	±	0.03				1.000	0.93	±	0.I2
2.52	±	0.08	0.98	±	0.I2	I.000 - 0.994 - I.000 - 0.998				6.58	±	0.08
			6.62	±	0.30		I.000	0.994	0.986	0.I3	±	0.34
			0.02	±	0.I2			I.000	0.998	I.005	±	0.004
			4	±	6				I.000	0.986	±	0.006

2.67 ± 0.09	0.993	±	0.001	I.000	-	0.702	-	0.100	-	0.612	6.89	±	0.03
	6.93	±	0.03			I.000		0.291		0.248	0.28	±	0.02
	0.007	±	0.002					I.000	-	0.726	I.09	±	0.06
	0.47	±	0.20							I.000	0.45	±	0.25
2.84 ± 0.03	0.94	±	0.15	I.000	-	0.993	-	I.000	-	0.998	7.09	±	0.11
	7.26	±	0.43			I.000		0.993		0.983	0.45	±	0.30
	0.06	±	0.15					I.000		0.998	I.014	±	0.007
	4.38	±	2.42							I.000	0.965	±	0.008
2.99 ± 0.05	0.982	±	0.001	I.000	-	0.786		0.043	-	0.442	7.35	±	0.03
	7.48	±	0.04			I.000		0.116		0.203	0.97	±	0.05
	0.018	±	0.012					I.000	-	0.915	I.5	±	0.8
	0.55	±	0.21							I.000	0.09	±	0.15

T H O R I U M

0.020 ± 0.010	0.10	±	0.05	I.000	-	0.957	-	0.998	-	0.972	I3.5	±	0.4
	28	±	I0			I.000		0.957		0.874	23	±	18
	0.90	±	0.05					I.000		0.974	I.07	±	0.03
	I2.0	±	0.2							I.000	0.90	±	0.03
0.040 ± 0.020	0.09	±	0.05	I.000	-	0.942	-	I.000	-	0.969	I3.6	±	0.8
	33	±	I7			I.000		0.944		0.883	40	±	45
	0.9I	±	0.05					I.000		0.969	I.I0	±	0.06
	II.6	±	0.2							I.000	0.87	±	0.05
0.055 ± 0.020	0.85	±	0.07	I.000		0.980	-	I.000		0.964	I3.I	±	0.3
	II.4	±	0.3			I.000	-	0.980		0.910	I7	±	9
	0.I5	±	0.07					I.000	-	0.964	I.067	±	0.020
	23	±	6							I.000	0.902	±	0.020
0.080 ± 0.020	0.4	±	0.4	I.000	-	0.988	-	0.999	-	0.998	I2.8	±	0.4
	I7	±	5			I.000		0.988		0.977	I0	±	9
	0.6	±	0.4					I.000		0.999	I.058	±	0.025
	I0	±	2							I.000	0.900	±	0.025
0.I3 ± 0.04	0.I	±	3.5	I.000	-	0.993	-	I.000	-	0.998	II.4	±	0.8
	I3	±	46			I.000		0.993		0.993	0.6	±	5.2
	0.9	±	3.5					I.000		0.998	I.004	±	0.020
	II	±	4							I.000	0.99	±	0.03
0.2I ± 0.04	0.2I	±	0.25	I.000	-	0.995	-	I.000	-	0.996	I0.85	±	0.I3
	I5	±	5			I.000		0.995		0.984	4	±	3
	0.79	±	0.25					I.000		0.996	I.029	±	0.0I2
	9.8	±	0.5							I.000	0.950	±	0.0I2
0.27 ± 0.04	0.98	±	0.05	I.000		0.937	-	I.000		0.918	I0.2	±	0.6
	I0.0	±	0.2			I.000	-	0.939		0.804	6	±	36
	0.02	±	0.05					I.000	-	0.9I7	I.02	±	0.06
	30	±	85							I.000	0.97	±	0.06
0.35 ± 0.04	0.3	±	0.7	I.000	-	0.99I	-	I.000	-	0.997	9.5	±	0.5
	I3	±	I0			I.000		0.99I		0.978	4	±	8
	0.7	±	0.7					I.000		0.997	I.04	±	0.04
	8	±	2							I.000	0.94	±	0.04

U R A N I U M

0.010	±	0.005	0.22	±	0.06	I.000	-	0.964	-	I.000	-	0.964	I4.8	±	0.5
			30	±	6			I.000		0.965		0.890	65	±	28
			0.78	±	0.06					I.000		0.962	I.20	±	0.04
			I0.6	±	0.4							I.000	0.76	±	0.02
0.025	±	0.010	0.24	±	0.2I	I.000		0.986	-	I.000		0.970	I4.4	±	0.8
			7.4	±	2.4			I.000	-	0.987		0.927	I7	±	II
			0.76	±	0.2I					I.000	-	0.970	I.I3	±	0.04
			I7	±	3							I.000	0.76	±	0.05
0.035	±	0.015	0.55	±	0.08	I.000	-	0.983	-	I.000	-	0.989	I2.99	±	0.I4
			I6	±	I			I.000		0.983		0.952	I4	±	3
			0.45	±	0.08					I.000		0.989	I.099	±	0.009
			8.8	±	0.4							I.000	0.830	±	0.009
0.050	±	0.015	0.I779	±	0.000I	I.000	-	0.233	-	0.778		0.I06	I2.32	±	0.04
			6.89	±	0.05			I.000	-	0.266	-	0.552	6.37	±	0.I7
			0.8221	±	0.0001					I.000		0.06I	I.068	±	0.002
			I3.49	±	0.05							I.000	0.852	±	0.004
0.070	±	0.015	0.946	±	0.0I2	I.000	-	0.948	-	I.000	-	0.980	I2.20	±	0.06
			I2.64	±	0.I2			I.000		0.950		0.890	3.I	±	0.4
			0.054	±	0.0I2					I.000		0.977	I.057	±	0.003
			4.6	±	0.5							I.000	0.836	±	0.0I2
0.085	±	0.015	0.95	±	0.03	I.000	-	0.964	-	I.000	-	0.985	II.56	±	0.I2
			II.9	±	0.3			I.000		0.966		0.9I7	2.5	±	2.5
			0.05	±	0.03					I.000		0.983	I.05	±	0.0I
			4.65	±	0.I2							I.000	0.87	±	0.03
0.II	±	0.02	0.955	±	0.0I2	I.000	-	0.952	-	I.000	-	0.982	II.6	±	0.I
			II.92	±	0.I3			I.000		0.953		0.898	2.4	±	0.4
			0.045	±	0.0I2					I.000		0.980	I.046	±	0.003
			4.4	±	0.4							I.000	0.862	±	0.0I2
0.I35	±	0.02	0.93	±	0.02	I.000	-	0.970	-	I.000	-	0.984	I0.92	±	0.07
			II.35	±	0.I9			I.000		0.970		0.922	2.6	±	0.5
			0.07	±	0.02					I.000		0.983	I.046	±	0.004
			4.9	±	0.7							I.000	0.878	±	0.0II
0.I6	±	0.02	0.984	±	0.0I2	I.000	-	0.946		0.994		0.989	I0.88	±	0.II
			II.2	±	0.2			I.000		0.960		0.906	I.2	±	0.2
			0.0I6	±	0.009					I.000		0.968	I.05	±	0.05
			2	±	2							I.000	0.8	±	0.3
0.20	±	0.I2	0.85	±	0.06	I.000	-	0.985	-	I.000	-	0.995	I0.99	±	0.05
			II.6	±	0.2			I.000		0.985		0.965	2.I	±	0.4
			0.I5	±	0.06					I.000		0.995	I.024	±	0.003
			7.5	±	0.5							I.000	0.947	±	0.004

U R A N I U M (continued)

0.20	±	0.02	0.3	±	0.3	I.000	0.997 - I.000	0.994	I0.76	±	0.I4
			8	±	I		I.000 - 0.997	0.985	3	±	2
			0.7	±	0.3		I.000 -	0.994	I.035	±	0.009
			I2	±	I			I.000	0.93	±	0.0I
0.2I5	±	0.020	0.97	±	0.02	I.000 -	0.965 - I.000 -	0.99I	I0.39	±	0.08
			I0.5	±	0.2		I.000	0.969	0.99I	I.4	±	0.6
			0.03	±	0.02			I.000	0.987	I.04	±	0.02
			3	±	2				I.000	0.86	±	0.II
0.24	±	0.02	0.6	±	0.4	I.000 -	0.989 - I.000 -	0.994	I0.60	±	0.I4
			I2	±	2		I.000	0.990	0.969	4	±	2
			0.4	±	0.4			I.000	0.994	I.036	±	0.0I2
			8	±	I				I.000	0.930	±	0.0I6
0.295	±	0.020	0.84	±	0.20	I.000 -	0.989 - I.000 -	0.994	I0.I6	±	0.I5
			II.0	±	0.8		I.000	0.989	0.969	3.6	±	I.8
			0.I6	±	0.20			I.000	0.994	I.052	±	0.009
			5.9	±	2.3				I.000	0.88	±	0.03

Figure captions

Figure 1. Experimental arrangement for measurement of transmission functions of neutrons emitted in the direction of a beam of charged particles: (1) tank with water; (2) back shield; (3) organic glass insert; (4) detector; (5) boron counters; (6) collimator; (7) boron carbide layer; (8) diffuser; (9) support; (10) wheels; (11) rails; (12) small motors; (13) bracket; (14) samples; (15) target holder; (16) location of target; (17) [missing in original]; (18) diaphragm on proton beam path; (19) filaments for suspending samples; (20) limit switches; (21) counterweight.

Figure 2. Experimental arrangement for measurement of transmission functions of neutrons escaping at an angle of 100° to the proton beam: (1) detector; (2) boron layer; (3) water shield; (4) collimator insert; (5) samples; (6) target; (7) boron monitor; (8) collimator; (9) shield of boron carbide and paraffin; (10) thin-walled guide pipe; (11) air blower.

Figure 3. Total neutron cross-section of beryllium at energies around 200 keV. White circles represent the atlas data [7] and both kinds of crosses the data of Ref. [8]. Our data are represented by dark circles for resolutions of 8–10 keV and triangles for a resolution of ~ 40 keV. The squares in the lower part of the diagram represent the dispersion values obtained for ~ 40 keV intervals. The dashed line (and letter P) and the dot-dash line show dispersion values calculated from the data of the atlas [7] and of Ref. [8].

Figure 4. Total cross-section of magnesium.

Figure 5. Dispersion of the total cross-section of magnesium.

Figure 6. Cross-sections (sub-groups) describing the total cross-section structure of aluminium.

Figure 7. Total cross-section of aluminium.

Figure 8. Dispersion of the total cross-section of aluminium.

Figure 9. Total cross-section structure of silicon.

Figure 10. Dispersion of the total cross-section of silicon.

Figure 11. Total cross-section of phosphorus. The solid line and triangles represent the data of the atlas [7] and the dots refer to the present work.

Figure 12. Total cross-section of sulphur.

Figure 13. Dispersion of the total cross-section of sulphur.

Figure 14. Total cross-section of potassium. The triangles represent the data of the present work and other symbols the atlas data [7].

Figure 15. Total cross-section structure of titanium.

Figure 16. Total cross-section of titanium. White circles represent the data of the present work and other symbols the atlas data [7].

Figure 17. Dispersion of the total cross-section of titanium.

Figure 18. Total cross-section structure of vanadium.

Figure 19. Dispersion of the total cross-section of vanadium. The dashed line shows the results of calculations based on the data of Ref. [9] and the dots those based on the atlas data [7].

Figure 20. Total cross-section of vanadium. The solid line represents the data of the present work.

Figure 21. Cross-sections (sub-groups) describing the total cross-section structure of chromium.

Figure 22. Contribution of the larger of the cross-sections describing the total cross-section structure of chromium.

Figure 23. Dispersion of the total cross-section of chromium. The points represent the results of calculations based on the atlas data [7].

Figure 24. Total cross-section of chromium. The solid and dashed lines represent the atlas data [7] and the points those of the present work.

Figure 25. Cross-sections (sub-groups) describing the total cross-section structure of iron (see the text).

Figure 26. Contributions of the cross-sections describing the total cross-section structure of iron.

Figure 27. Total cross-section of iron. The solid line represents the average of the atlas data [7] and the dashed line calculations from Ref. [9].

Figure 28. Dispersion of the total cross-section of iron. The dashed line represents calculations from Ref. [9].

Figure 29. Total cross-section structure of nickel.

Figure 30. Total cross-section of nickel. The dashed line represents calculations from Ref. [9].

Figure 31. Dispersion of the total cross-section of nickel. The dashed line represents calculations from Ref. [9] and the points calculations based on the atlas data [7].

Figure 32. Cross-sections (sub-groups) describing the cross-section structure of copper. The dashed line represents the calculations from Ref. [9].

Figure 33. Contribution of the larger of the cross-sections describing the total cross-section structure of copper. The dashed line represents calculations based on data from Ref. [9].

Figure 34. Top: total cross-section of gallium. The solid line and dark circles represent the atlas data [7], the white circles represent our values. Below: dispersion values obtained with the average cross-sections shown above.

Figure 35. Total cross-section structure of gallium.

Figure 36. Dispersion of the total cross-section of gallium.

Figure 37. Total cross-section of zirconium. The dashed line represents the atlas data [7], the squares calculations based on the optical model [10] and the points the data of the present work.

Figure 38. Cross-sections (sub-groups) describing the total cross-section structure of niobium.

Figure 39. Contribution of the larger of the cross-sections describing the total cross-section structure of niobium.

Figure 40. Total cross-section of niobium. The dashed line and white circles denote the atlas data [7], the squares represent calculations based on the optical model [10] and the points the data of the present work.

Figure 41. Cross-sections (sub-groups) describing the total cross-section structure of molybdenum.

Figure 42. Contribution of the larger of the cross-sections describing the total cross-section structure of molybdenum.

Figure 43. Dispersion of the total cross-section of molybdenum.

Figure 44. Total cross-section of molybdenum. The dashed line and white circles represent the atlas data [7] and the points the data of the present work.

Figure 45. Total cross-section of cadmium. The black triangles and points show the atlas data [7] and the white circles the data of the present work.

Figure 46. Total cross-section of rhenium. White circles and crosses represent the atlas data [7]. The dashed line shows the values recommended in Ref. [7] and the dark circles those of the present work.

Figure 47. Total cross-section of osmium. The solid line and the dark circle represent the atlas data [7]. The dashed line shows the values recommended in Ref. [7] and the white circles those of the present work.

Figure 48. Total cross-section of iridium. The dashed line represents the values recommended in Ref. [7], and the squares show the cross-section of platinum [7].

Figure 49. Cross-section structure of lead.

Figure 50. Cross-sections (sub-groups) describing the total cross-section structure of uranium.

Figure 51. Contribution of the larger of the cross-sections describing the total cross-section structure of uranium.

Figure 52. Dispersion of the total cross-section of uranium.

Figure 53. Total cross-section of uranium. Rhombuses, triangles, crosses and half-shaded circles represent the atlas data [7], and the rectangles the data of the present work.

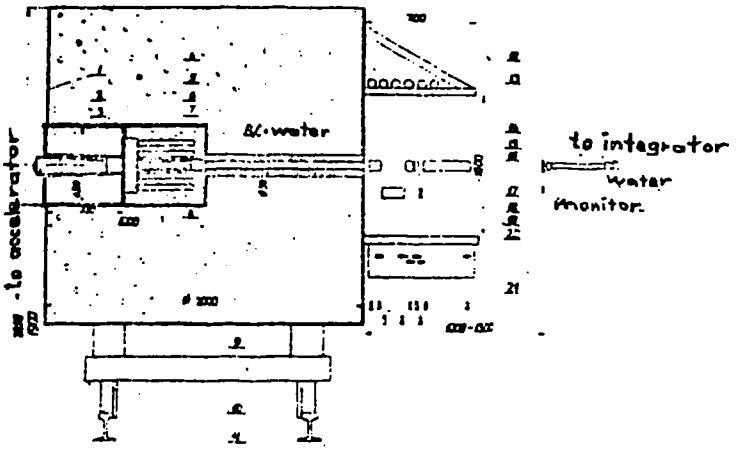

Fig. 1

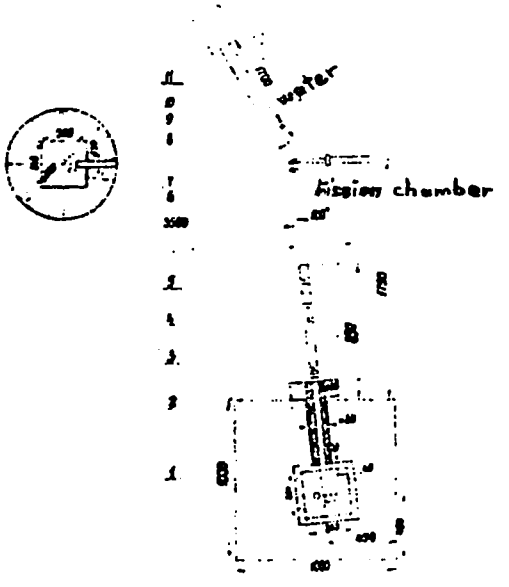

Fig. 2

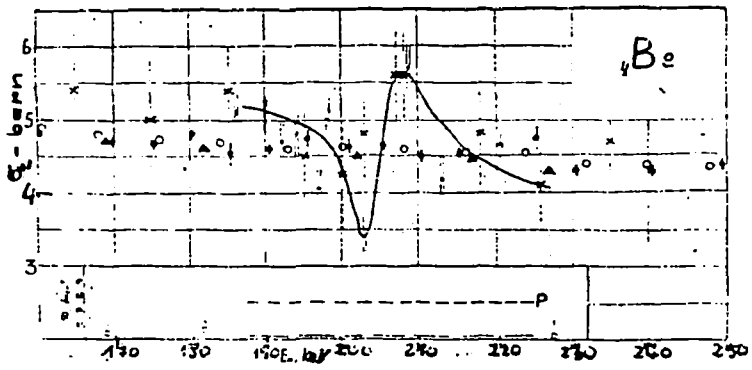

Fig. 3

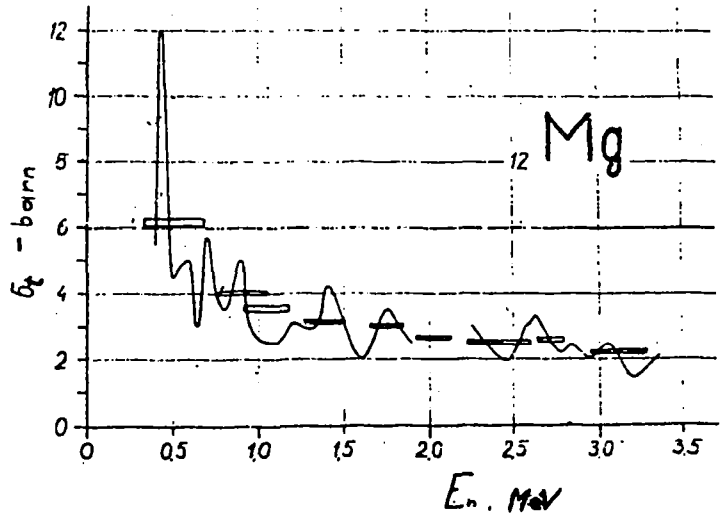

Fig. 4

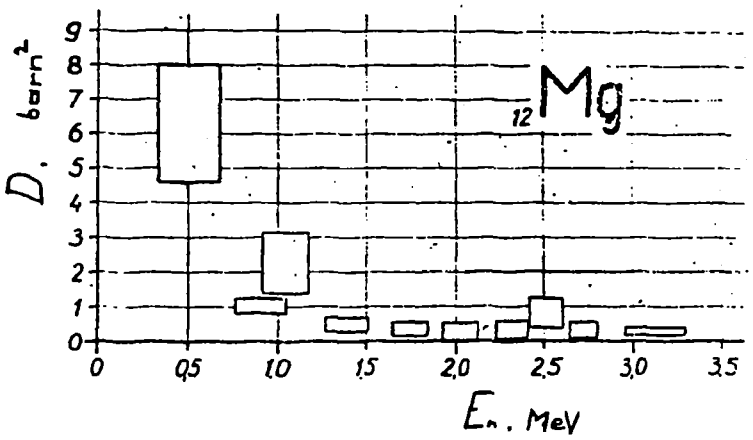

Fig. 5

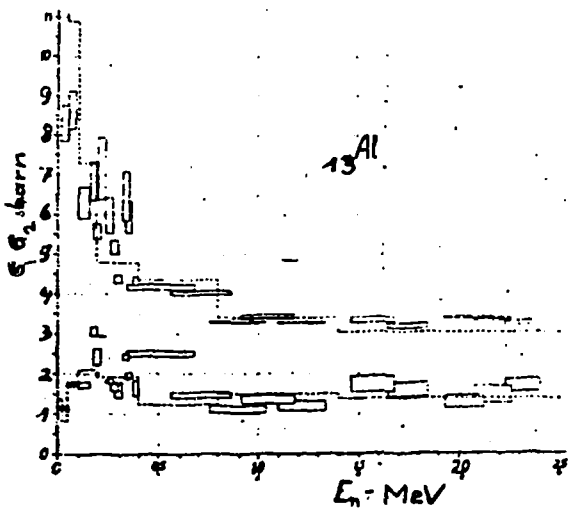

Fig. 6

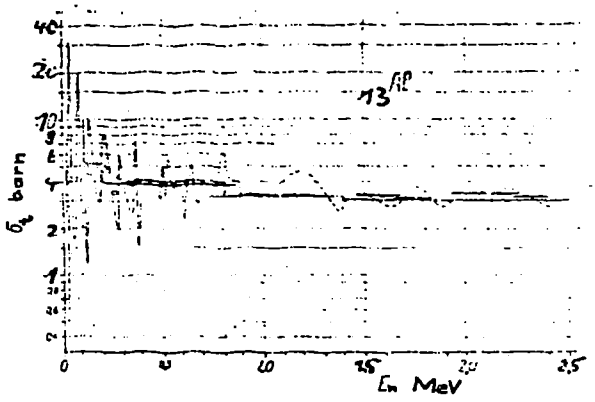

Fig. 7

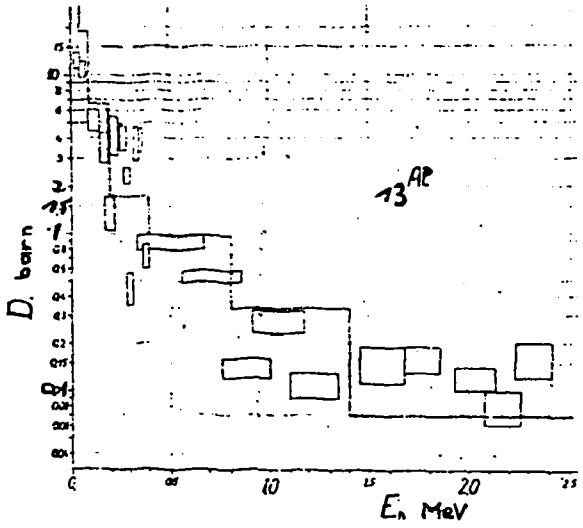

Fig. 8

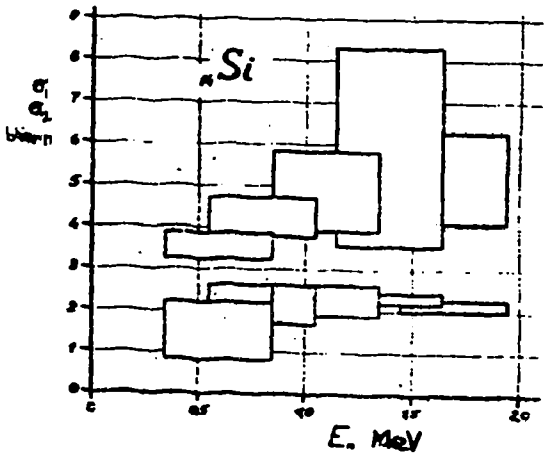

Fig. 9

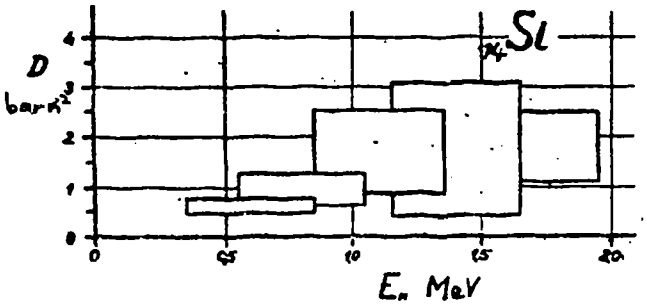

Fig. 10

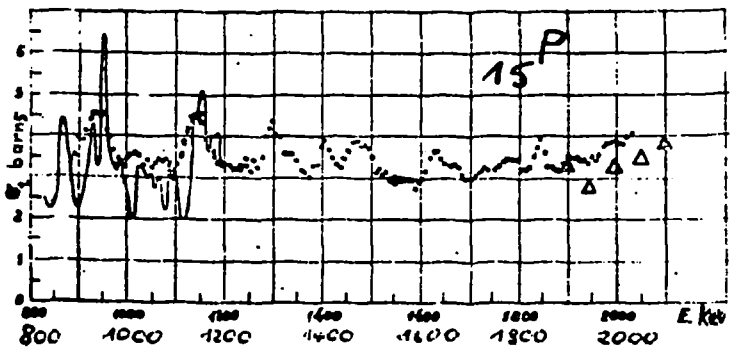

Fig. 11

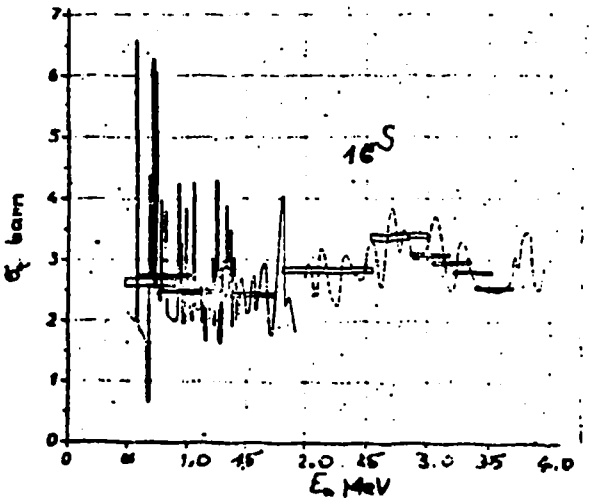

Fig. 12

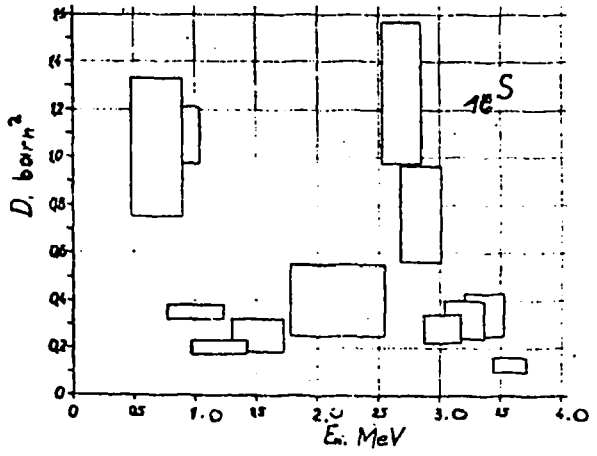

Fig. 13

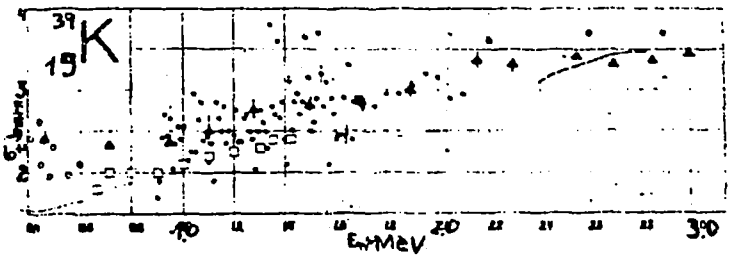

Fig. 14

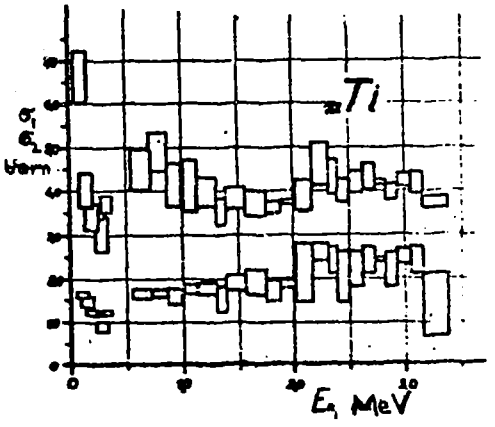

Fig. 15

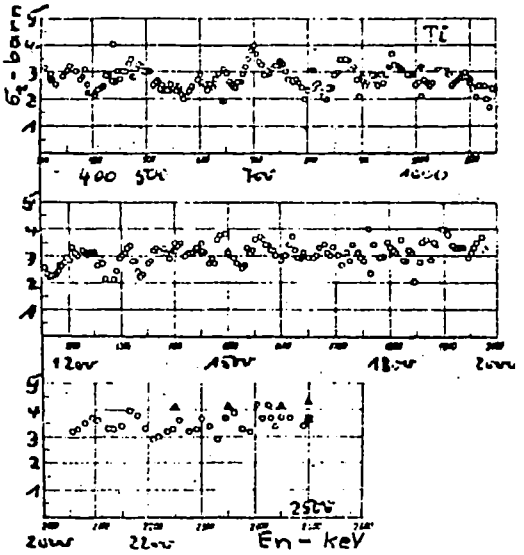

Fig. 16

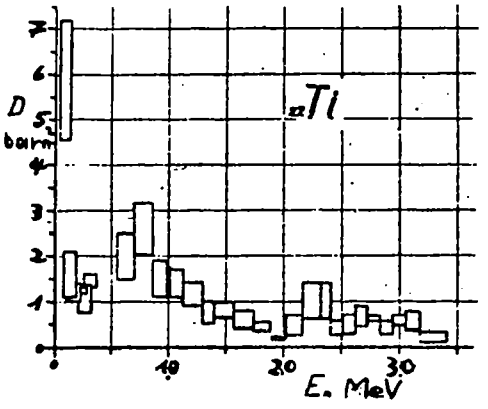

Fig. 17

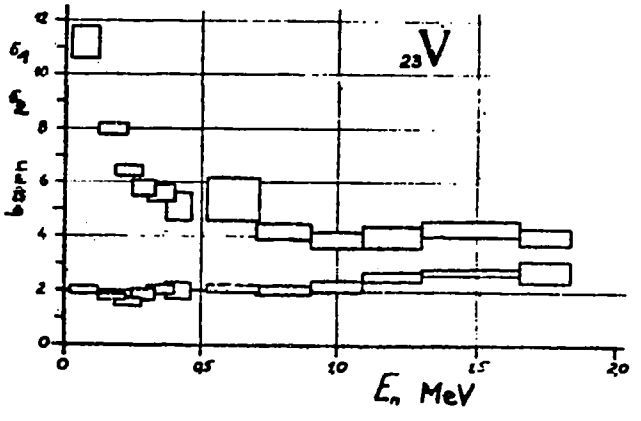

Fig. 18

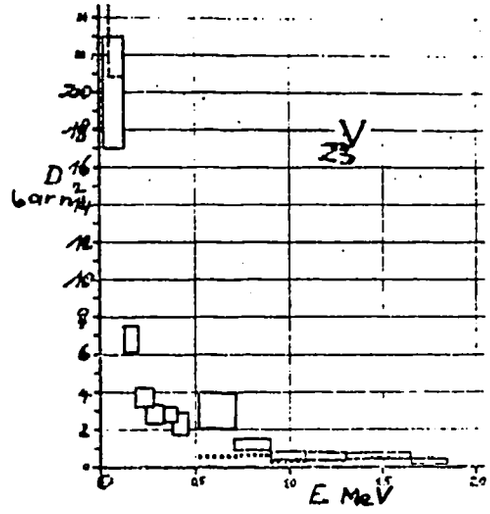

Fig. 19

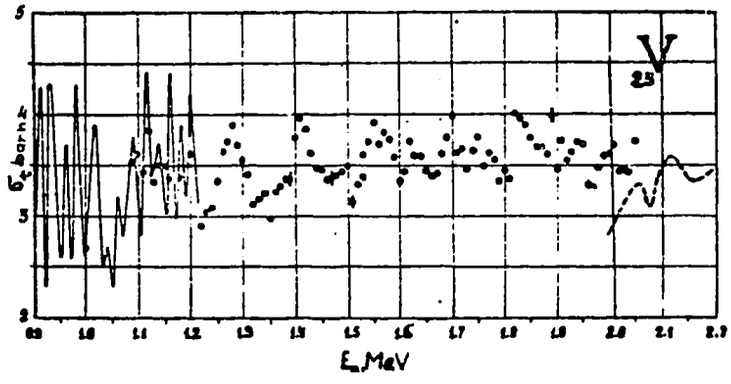

Fig. 20

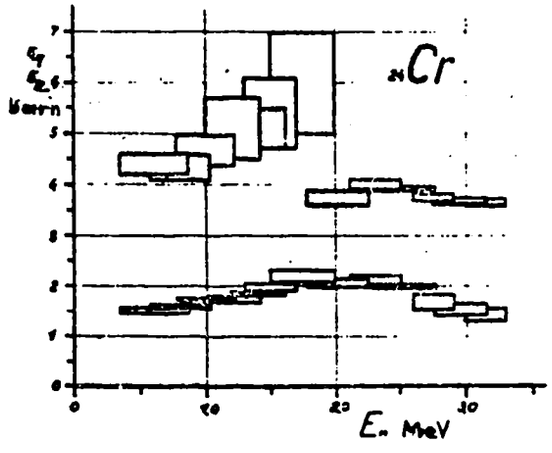

Fig. 21

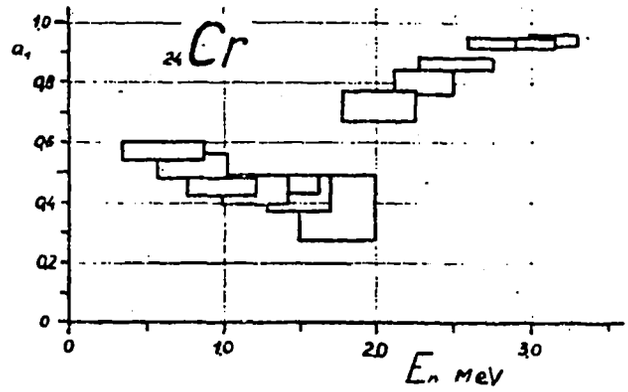

Fig. 22

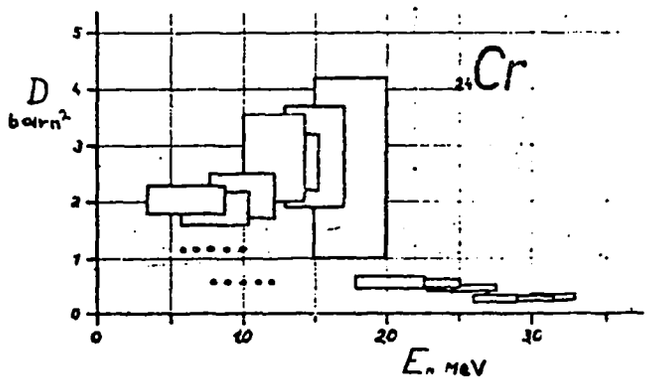

Fig. 23

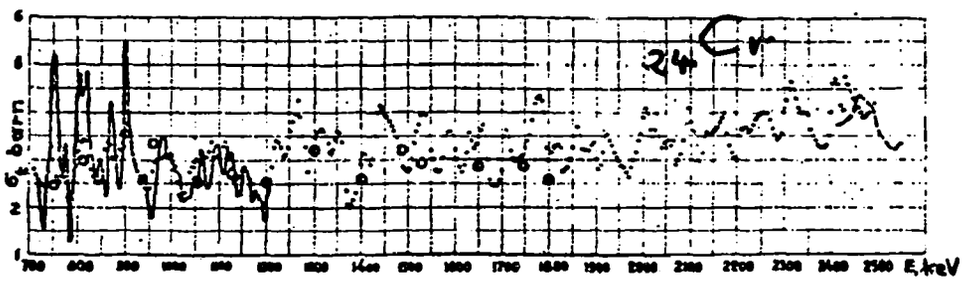

Fig. 24

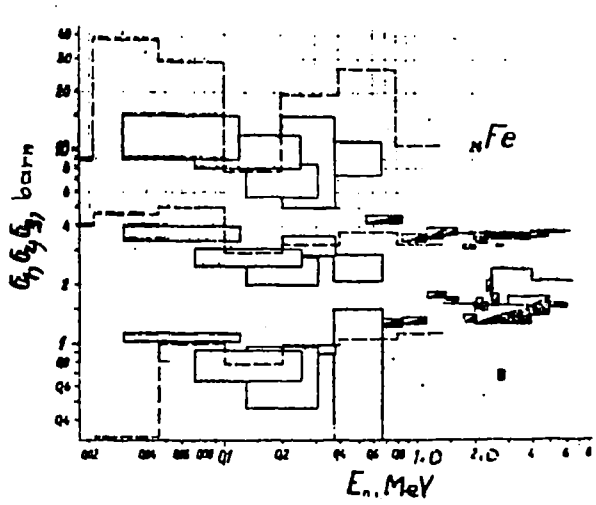

Fig. 25

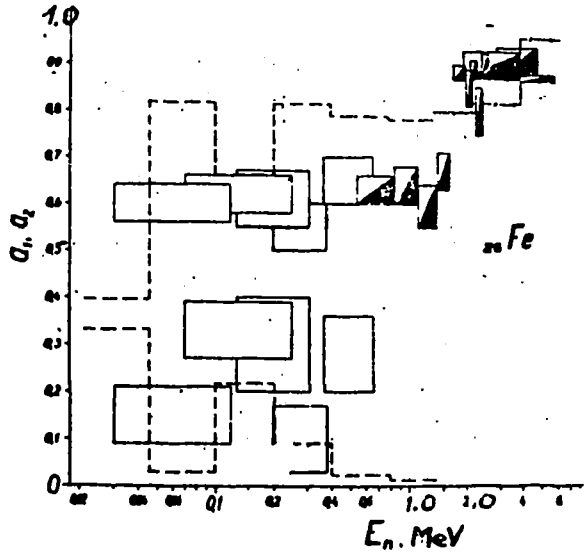

Fig. 26

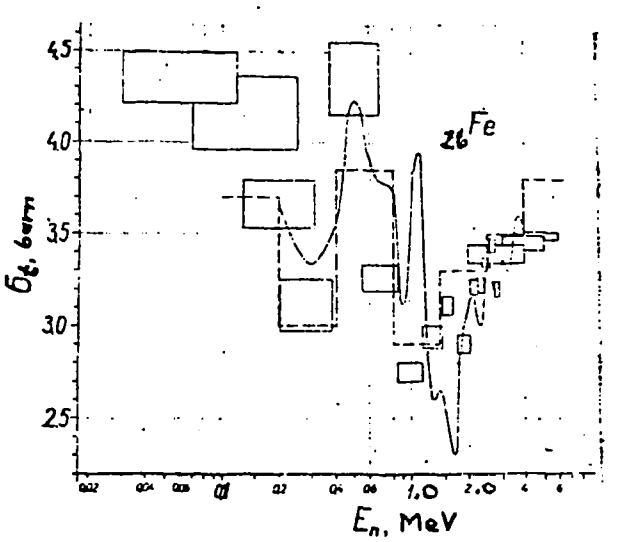
4.5
4.0
3.5
3.0
2.5
σ_t, barn
^{26}Fe
1.0
2.0
E_n, MeV

Fig. 27

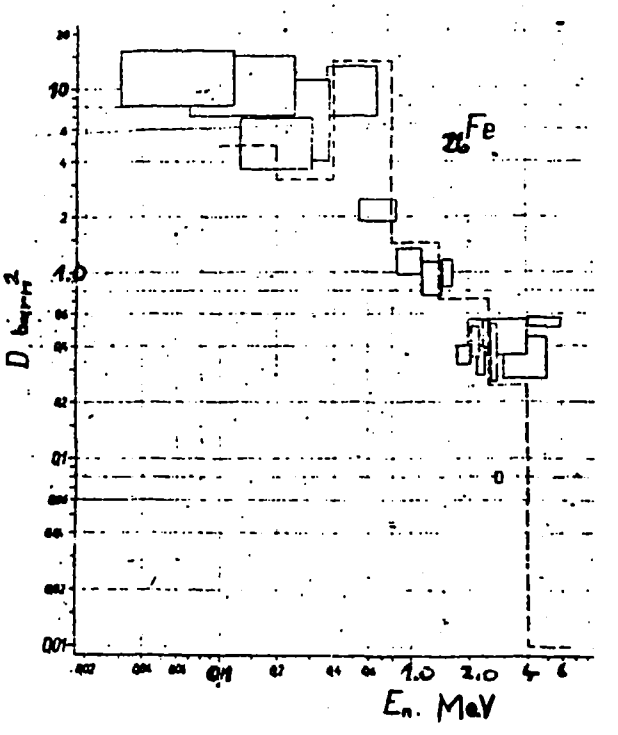
10
4
2
1.0
0.2
0.1
0.01
D, barn^2
^{26}Fe
1.0
2.0
4
E_n, MeV

Fig. 28

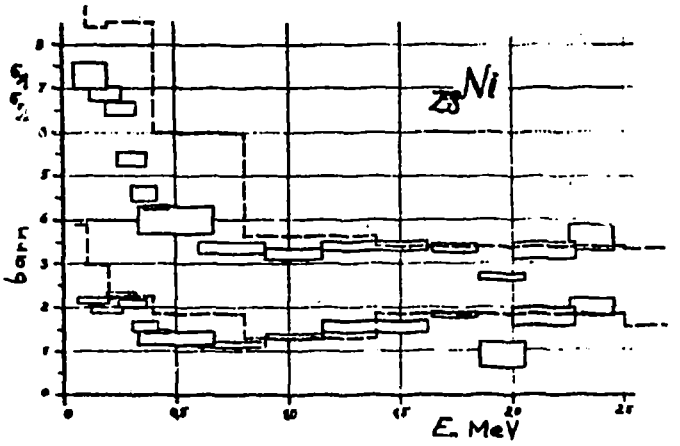

Fig. 29

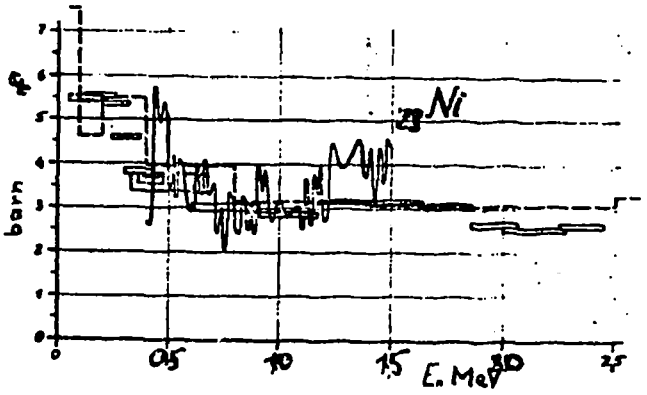

Fig. 30

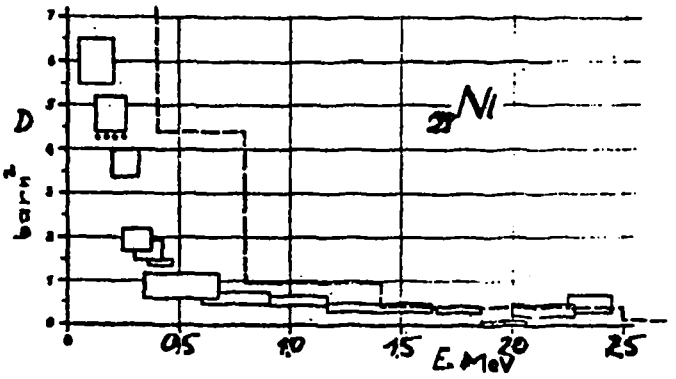

Fig. 31

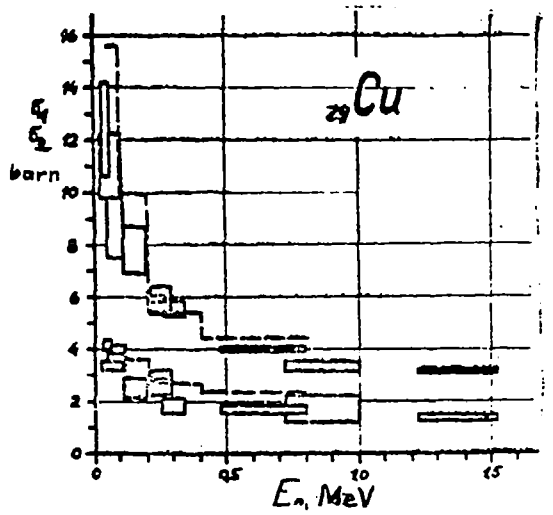

Fig. 32

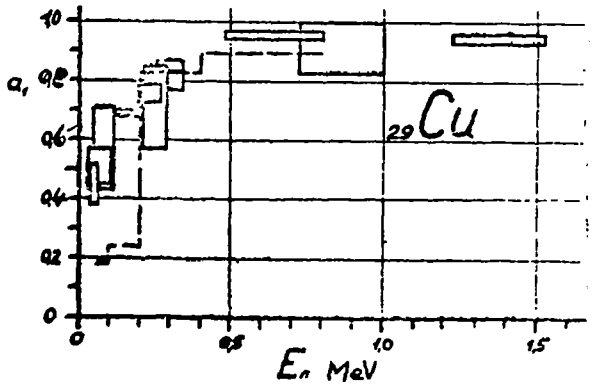

Fig. 33

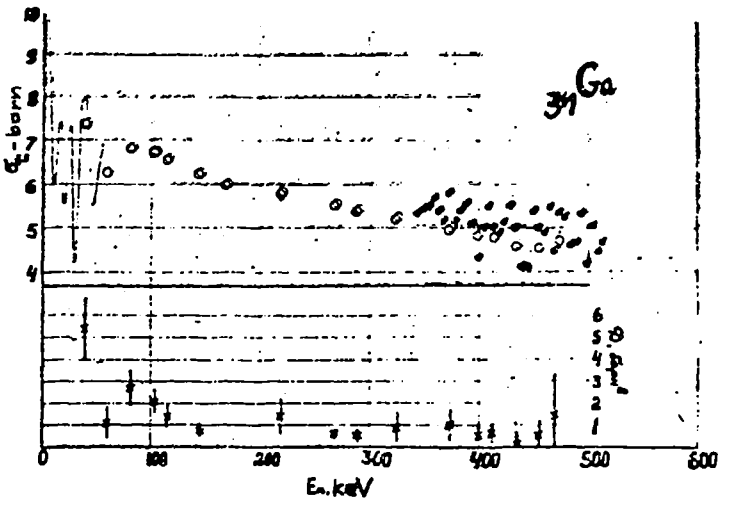

Fig. 34

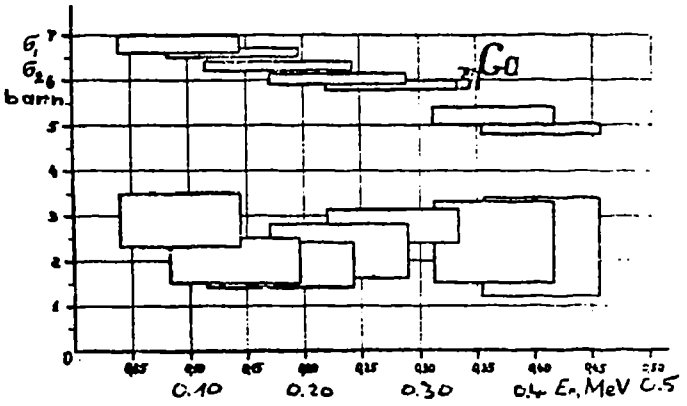

Fig. 35

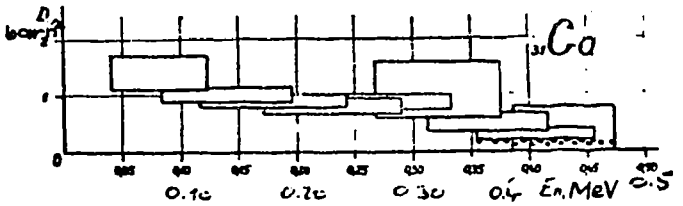

Fig. 36

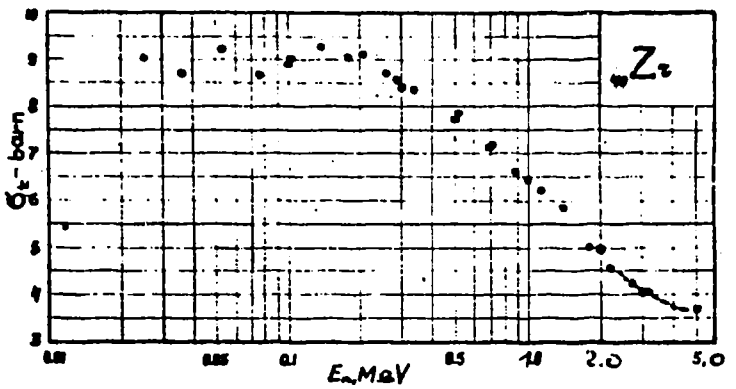

Fig. 37

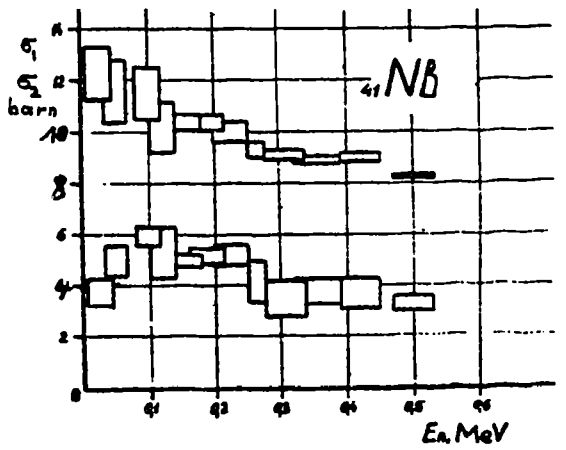

Fig. 38

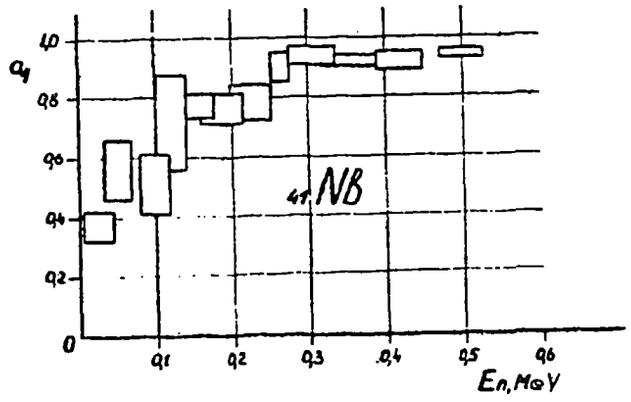

Fig. 39

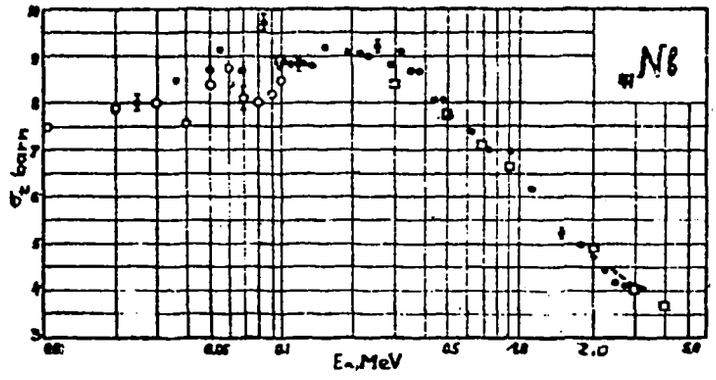

Fig. 40

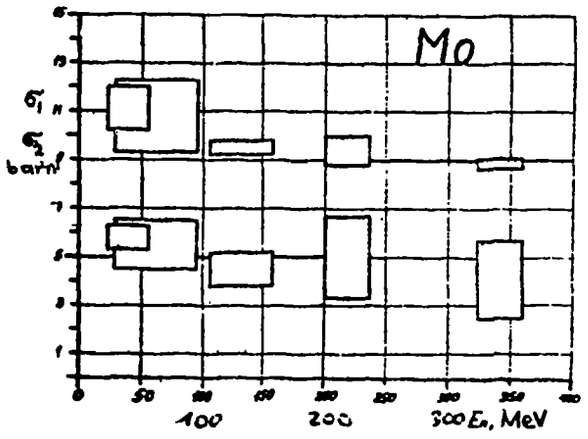

Fig. 41

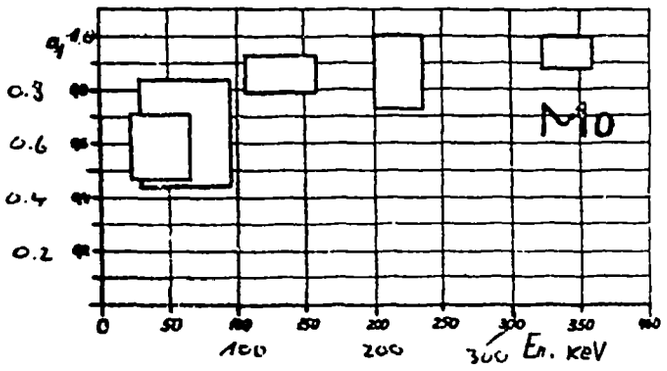

Fig. 42

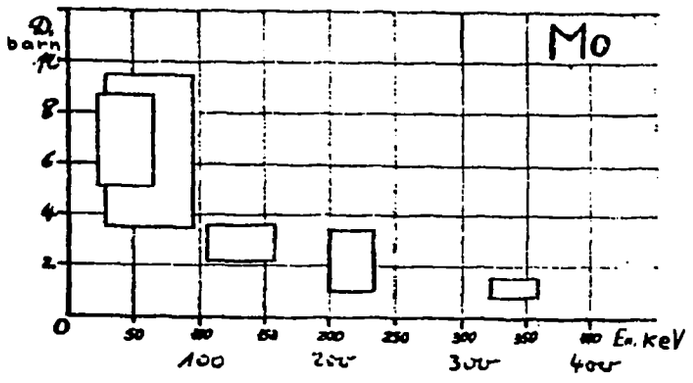

Fig. 43

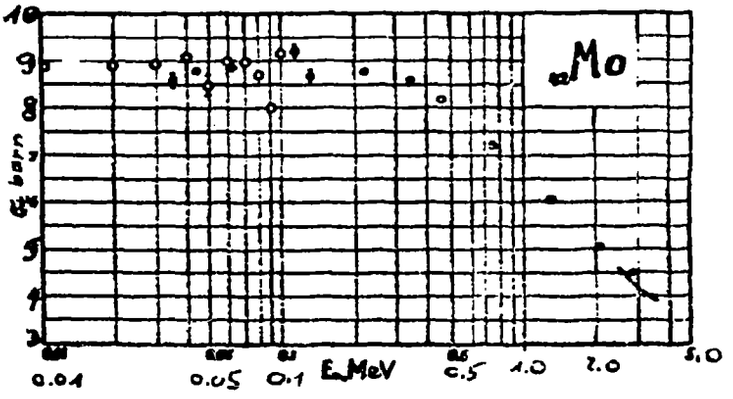

Fig. 44

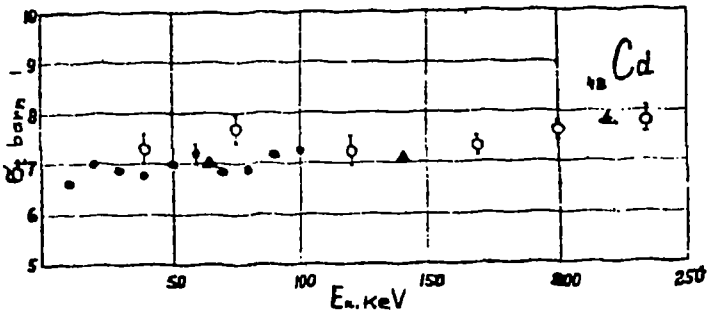

Fig. 45

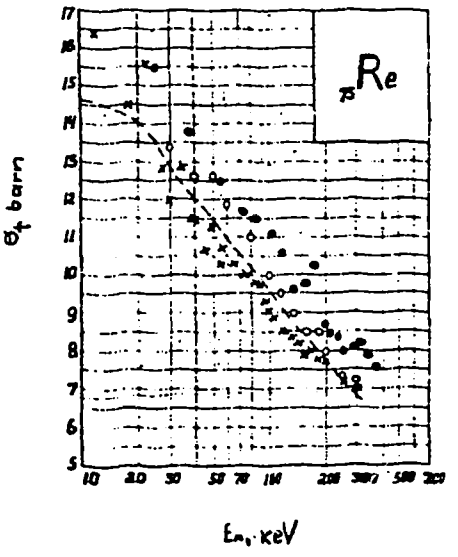

Fig. 46

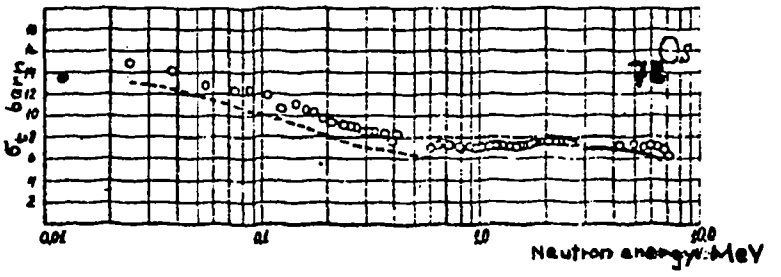

Fig. 47

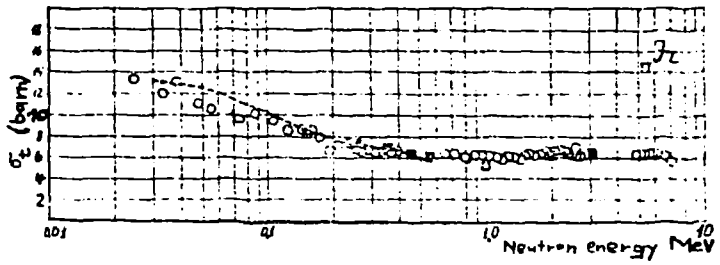

Fig. 48

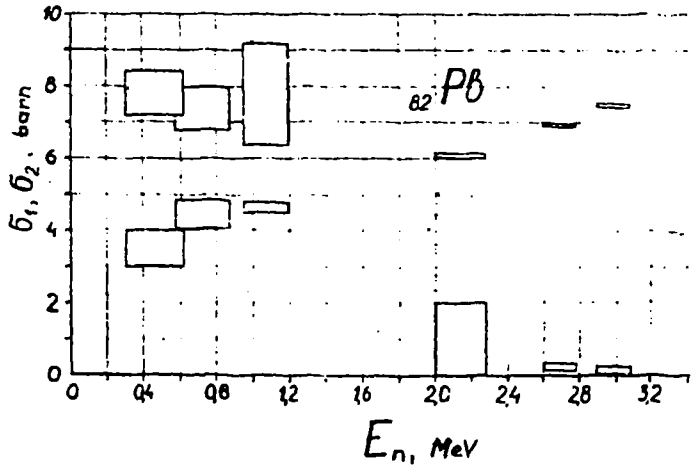

Fig. 49

Fig. 50

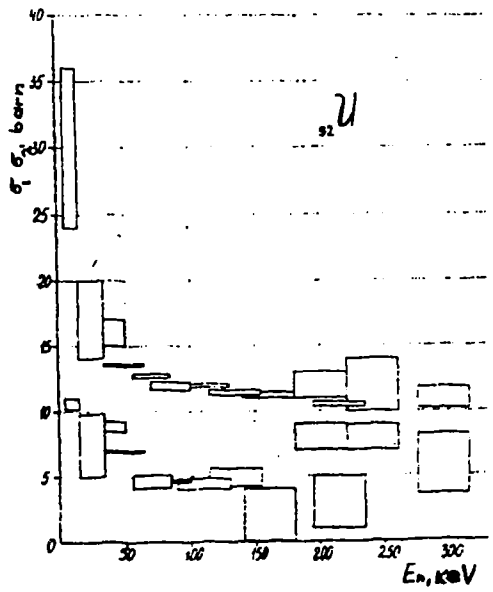

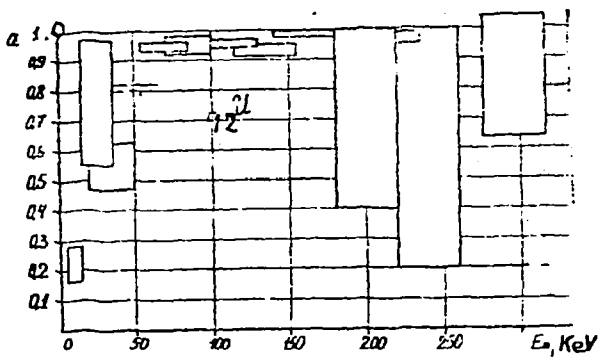

Fig. 51

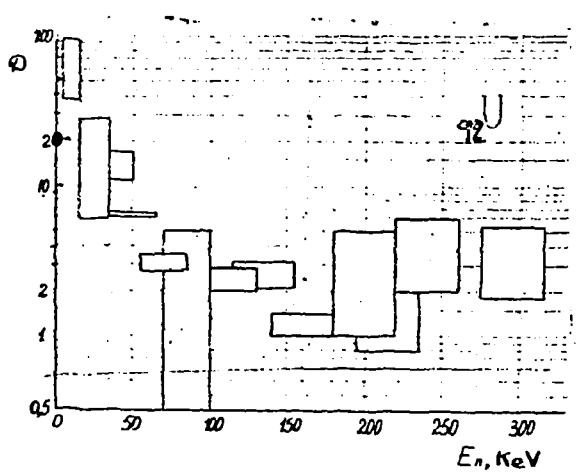

Fig. 52

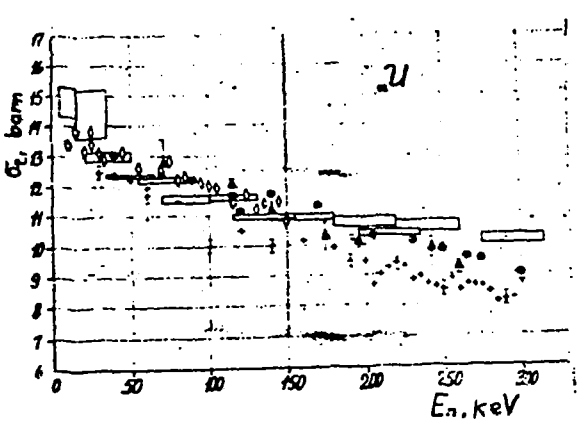

Fig. 53

INVESTIGATION OF THE REACTIVITY WORTH OF DIFFERENT MATERIALS IN THE FAST ASSEMBLY BFS-16

Gorbatov N.E., Mamontov V.F., Matveev V.I.,
Orlov V.V., Pshakin G.M.

Institute of Physics and Power Engineering
Obninsk, USSR

Translation made at Obninsk
Edited by NDS

Abstract

The paper presents results of experimental investigations of perturbations for different materials in the BFS-16 fast assembly.

The comparison between calculated and experimental values has been carried out with due account for the effects of the sample resonance self-shielding and perturbations of the neutron field by the sample.

The method and calculation results of the scattering sample influence on the change of resonance cross-sections near the sample are also given in the paper.

Introduction

One of the methods for checking nuclear-physical constants used for reactor calculations is the analysis and comparison of calculation results with measurements of the reactivity effects from different materials. Such an analysis together with that of other macroscopic characteristics (critical mass, ratios of average cross-sections, etc.) can point out the inaccuracies of the multigroup cross-sections used in the calculations.

For this purpose we studied the reactivity effects from different materials in BFS assemblies. The results of such investigations were given in the papers [1,2]. The investigations were carried out in considerable detail in the BFS-16 assembly which is the model of BN-350.

In contrast with earlier models this assembly had more uniform composition which allowed more exact calculations. Detailed information on the assembly composition and its sizes is given in reference [2] and also in the appendix of this paper.

When making the indicated experiments it is rather important to choose sample weights and sizes so that the influence on the neutron field is as small as possible. In this case one can use the 1^{st} approximation of the perturbation theory. But the decrease of the sample size results in an increase of the experimental error. Therefore in practical measurements one uses samples having an influence on the neutron field (this influence cannot be neglected) which demands the introduction of suitable corrections to the perturbation theory calculations.

Together with the experimental results, the paper presents a discussion of the calculated values obtained from the first approximation of the perturbation theory, taking into account the corrections for the neutron field

disturbance (depression), the sample resonance self-shielding and its influence on resonance shielding in the nearby region. Inclusion of such corrections for a number of materials allows considerable improvement in the agreement between experimental and calculated values.

Aside from the efficiencies of homogeneous materials we used BFS-16 for investigating several mixtures of absorber materials which are of interest from the viewpoint of their application in fast reactor control rods.

1. Experimental Technique

When measuring reactivity effects produced by the materials studied we used the method of measuring the stable reactor start-up period. The measurements of the start-up period were carried out before and after placing the sample into the reactor. The reactor, which has a void in the core centre, was driven to above-critical state by moving the control rods. The start-up period ($T \approx 50 \div 150$ sec.) was selected depending on the value and sign of the reactivity effect produced by the experimental sample.

After measuring the value of the stable period the reactor was shut down by means of one or several control rods. The sample to be studied was placed in the void of the channel removed from the reactor. After replacing the channel with the sample into the reactor the control rods were moved to the initial position and the stable start-up period was measured. The difference in the reactor reactivity before and after placing a sample is the reactivity effect produced by the sample. The reactor reactivity

was calculated by the "inhour formula":

$$\frac{\rho}{\beta_{eff}} \cong \sum \frac{a_i}{1 + \lambda_i T}$$

where T is the stable reactor start-up period; $a_i = \beta_i / \beta_{eff}$ is the relative contribution of the i-th-group of delayed neutrons; and λ_i is the decay constant of delayed neutrons of the i-th-group.

The quantities β_i were determined by averaging over the fluxes and importances obtained from the multigroup diffusion calculation; in this case the data of delayed neutron yield were taken from reference [3].

i	1	2	3	4	5	6
a_i	0.328	0.19478	0.18171	0.40248	0.15071	0.03751

The value of $\beta_{eff} = \sum_1^6 \beta_i$ obtained from the calculations will be equal to β_{eff} =0.0072 for BFS-16 assembly.

The start-up period was measured by the electronic equipment consisting of a normal boron chamber, current integrator, two scalers and a quartz stopwatch.

The integrator transforms the chamber current into a pulse train and the pulse frequency is proportional to the current. The quartz stopwatch switches on scalers in turn in equal time intervals of Δt = 20,40,80,100 sec. Successive readings at equal successive time intervals are used for determining the start-up period.

$$T = \frac{\Delta t}{\ln(\overline{n_k / n_{k-1}})}$$

where Δt is the measurement time interval, and n_k, n_{k-1} are the quantity readings from adjacent intervals.

When calculating the period we used 6 to 10 successive readings obtained at the stable start-up period. The measurement error of the reactivity effect is caused by many reasons. The main ones are:

1. Mechanical oscillations of the core during channel rechargings.
2. Displacement of the reactor materials in the central channel during sample rechargings.
3. Reactor temperature effect.
4. Accuracy of returning the control rods into the initial state.
5. Accuracy of the period measurement.

The indicated errors were not differentiated in detail. The measurements with one sample were repeated successively several times alternating between sample and chamber. The inaccuracy in the result obtained from the measurement series contains probably all the possible errors.

When applying methods to provide sufficient core stiffness, and thus eliminating material displacement in the central channel, the measurement accuracy of reactivity introduced by a single sample in the BFS-16 was equal to $\sim 1.10^{-6} \Delta k/k$. In this case, with the use of the mentioned technique, the error in the period measurements equals about 0.1%.

Characteristics of the samples exploited for measuring the reactivity effects are presented in Table 1.

The results of the experiments are given in Table 2.

2. Comparison of experimental and calculated results

The reactivity effects were calculated by means of the 1st order perturbation theory by means of computer programmes written for the M-20 computer. This programme uses neutron fluxes and importances obtained from solution of multigroup diffusion equations in one-dimensional geometry. The formula for calculating the reactivity produced by the studied material sample placed in the reactor at point ($\vec{r}$) is of the form

$$\left[\frac{\Delta k}{k}\right](\vec{r}) = \frac{\rho_0}{4HD}\int_{V_0}\Big\{\sum_{k=1}^{m} 3\sigma_{tr}^{k}\cdot i_k^{+}(\vec{r})\cdot i_k(\vec{r}) - \sum_{k=1}^{m}\sigma_a\cdot\Phi_k(\vec{r})\Phi_k^{+}(\vec{r}) - \sum_{k=1}^{m}\sigma_{cf}^{k}\cdot\Phi_k(\vec{r})\Phi_k^{+}(\vec{r}) + \sum_{k=1}^{m}\sum_{j=1}^{k-1}\sigma^{j\to k}\Phi_j(\vec{r})\Phi_k^{+}(\vec{r}) + \frac{1}{k_\infty\Phi}\sum_{k=1}^{m}\nu_f\sigma_f\cdot\Phi_k(\vec{r})\sum_{k=1}^{m}\Phi_k^{+}(\vec{r})\chi_k\Big\}dV_0$$

where $4HD = \int_V \sum_{k=1}^{m}\nu_f\Sigma_f\Phi_k(\vec{r})\cdot\sum_{k=1}^{m}\chi_k\cdot\Phi_k^{+}(\vec{r})dV$

is the importance of fission neutrons in the whole reactor volume.

$\Phi_k(\vec{r})$, $\Phi_k^{+}(\vec{r})$ is the distribution of fluxes and importances of the Kth energy group in the reactor. V_0, ρ_0 are volume and nuclear density of the material studied respectively. σ_{tr}, σ_{cf}, σ_a, $\sigma^{j\to k}$, $\nu_f\sigma_f$ are microscopic cross-sections of the studied material.

For solving the diffusion equations we used the conventional method of the separation of variables; $\Phi_k(\vec{r})$ and $\Phi_k^{+}(\vec{r})$ were presented in the form:

$$\Phi_k(\vec{r}) = \Phi(r)\cdot\Phi(z)$$

$$\Phi_k^{+}(\vec{r}) = \Phi^{+}(r)\cdot\Phi^{+}(z)$$

and $\Phi(z) = \Phi^{+}(z) = \cos\beta z$ where $\beta = \left|\sqrt{\chi^2_{\tau}}\right|$

Parameter $\mathcal{X}_r^2$ determining axial leakage was taken to be the same for all assembly zones ($\mathcal{X}_r^2 = 0.03518$).

In the calculation we used an 18-group constant set obtained from the 26-group set [4] by combining a number of energy intervals below the 12th group. The coefficients of cross-section resonance self-shielding for new energy intervals were derived simply by averaging over lethargy. The results of these calculations are presented in Table 2. The results for the reactivity effects obtained by the perturbation theory formula were corrected for resonance self-shielding of the samples taking into account heterogeneity as well as the flux depression near and within the sample. The resonance self-shielding of a single sample was taken into account according to the method described in reference [4], where the shielding coefficients are considered to be functions of the dilution characteristic G_0 which is the sum of the total cross-sections of all the sample elements per nucleus of the given element. For the sample containing only one element $\sigma_0 = 0$ the finiteness of the sample sizes is taken into account by adding the term $1/\rho\bar{\ell}$ to σ_0, where ρ is the nuclear density of the material in the sample, $\bar{\ell}$ is the 4V/S characteristic sample size ($\bar{\ell} = 4V/S$), V being the sample volume, and S its surface area.

As the calculations have shown, consideration of the sample resonance self-shielding effect gives important corrections to the results carried out with the use of un-shielded cross-sections.

We used such corrections for those materials having a noticeable resonance part in the cross-sections (e.g. U-238, Fe and others).

material:	U-238	Ta	Nb	Mo	W	Fe	Re	Eu
Corrections %:	6.3	25	13.2	6.2	8.7	17.3	18	10.3

For U-238 and Fe, which enter into the composition of the assembly, the calculations of the corrections were applied to the cross-sections shielded over the assembly core composition. In this case the calculations produced too low results. However, the under-estimate was not too great because the calculations which assumed infinite sample size give a correction of 8% for U-238 and 21.4% for Fe. In addition to the corrections which take account of the sample resonance self-shielding one must also introduce the corrections related to the neutron field depression produced by a sample. This effect was experimentally determined for boron carbide samples, see reference [6]. In order to determine the non-shielded reactivity effect we used boron carbide samples of natural enrichment with weights ranging from ~120g to ~0.9g. The 30g to 120g samples were composed of standard slugs of the BFS assembly (1 - 4 slugs 46 mm D). The samples, weighing less than 30g, represented thin-walled aluminium containers which were filled up with boron carbide powder. All the containers had the same diameter-(46 mm) but different height. The measurement results are presented in Table 4. The value of boron carbide non-shielded reactivity effect was obtained by extrapolation from the tabulated data. This value is equal to $(5.76 \pm 0.10) \cdot 10^{-3}$ $\Delta K/K/kg$. In this connection the value of the shielding effect related to the neutron field depression for the boron carbide sample, presented in Table 2 will be equal to about 14%. We also obtained the calculated data for evaluating the shielding effect of the boron carbide sample. These calculations in P_1 and P_3 approximations for the spherical sample whose weight and volume are similar to sample No. 1 of Table 4 gave a corrected value near to the experimental one. In the same way we evaluated the corrections for the neutron field depression for tantalum and U-238 samples. This correction is about 10 per cent for the tantalum sample and about 4 per cent for the U-238 sample, being a less strong absorber.

The correlation between experimental and calculated results, taking into account both resonance self-shielding and neutron field depression, shows that the difference between the calculated and experimental values is about 10 per cent for most of the materials studied (U^{235}, U^{238}, Ta, Mo). Such accuracy may be considered good considering the errors in the calculation methods and the multigroup cross-sections used. For a series of other materials a greater difference (~30%) is observed. In particular, for boron carbide it is about 25 per cent and cannot be explained by cross-section inaccuracies. Apparently it is related to the softer neutron spectrum of the real assembly in comparison with the calculated one. Some spectrum softening occurs due to the heterogeneous assembly structure. However, the calculations show that the neutron spectrum softening due to heterogeneity can increase the calculated boron carbide efficiency not more than 5 per cent. The greatest difference is observed for carbon and it demands further analysis.

3. Calculation of the Effect on the Resonance Cross-Sections of the surrounding medium when Introducing Scattering Samples in a Fast Reactor

The effective widths of uranium and plutonium resonances (the main elements with strongly pronounced resonance structure in the cross-sections) do not exceed about 1 eV, while the neutron energy losses upon scattering on the same elements considerably exceed this value at $E \geq 100$ eV (if $\Delta \bar{E} \simeq \frac{2}{A} E$, then for mass numbers A=200, $\Delta \bar{E} \simeq \frac{E}{100}$). Therefore when introducing a sample with any atomic weight into a fast reactor, there occurs an effect connected with an additional resonance absorption of the neutrons being scattered on the sample nuclei. This leads to a decrease of the self-shielding of the surrounding element resonance cross-sections, i.e. to an increase of neutron absorption in uranium and plutonium near the sample. It should be noted

that the magnitude of this effect is comparable to the other components of the reactivity effect due to sample-scatter and must be taken into account in the perturbation theory calculations.

Let us consider a sample of small sizes ($\ell \ll \lambda$, where ℓ is the sample size, λ is the neutron meanfree path in it). For the sake of simplicity we shall not take into account effects connected with absorption in the sample itself, with the change of the average neutron importance due to moderation, and with diffusion. These effects are included in the general perturbation theory equation.

Consider the relation of the reaction cross-section $\overline{\Sigma}_x^i$ (i=element of the surrounding medium) averaged over the neutron flux $\phi(E) \sim 1/\Sigma(E)$ to the scattering cross-section, Σ_s, of the surrounding medium. Since $\overline{\Sigma}_x^i$ is a function of (Σ_s), then the change of $\overline{\Sigma}_x^i$ due to the introduction of a single nucleus with the scattering cross-section σ_s^{od} in the surrounding unit volume, will be

$$\delta\overline{\Sigma}_x^i = \sigma_s^{o\delta} \cdot \frac{\partial \overline{\Sigma}_x^i}{\partial \Sigma_s}$$

As the sample is small, the influence of the scattering process on the reactivity change, when introducing a sample of volume V_{od} and nuclear density ρ, will be equal to:

3.1. $$\left[\frac{\Delta K}{K}\right] = -\sum_i \frac{1}{4\pi H^2} \cdot V_{o\delta} \cdot \rho \int_E dE \cdot \Phi(E) \cdot \Phi^+(E) \times \sigma_s^{o\delta}(E) \cdot \frac{\partial \overline{\Sigma}_x^i}{\partial \Sigma_s}$$

If X-reaction is fission then the formula (3.1.) changes sign and acquires (if K_{eff}=1.0) the factor equal to $\left(\nu_f \frac{\phi_f^+}{\phi^+} - 1\right)$, where ϕ^+ is the neutron importance, and $\phi_f^+ = \sum_k \chi_k \phi_k^+ \cdot \delta\Sigma_x^i / \delta\Sigma_s$, which can be either obtained from the known values of the shielding cross-sections [4],

or be evaluated from the consideration of two cases of the cross-sections with resonance form (strong and weak resonances). This consideration is similar to that given by the authors in reference [5].

Taking these considerations into account, formula (3.1.) can be written as:

$$\frac{\Delta K}{K} = -\sum_i \frac{1}{4\pi\omega} \cdot V_{o\delta} \int dE\, \Phi(E) \cdot \Phi^{+}(E) \times$$

$$\times \bar{\Sigma}_x^i \cdot \frac{\Sigma_s^{o\delta}}{\Sigma} \cdot \frac{1 - f_x^{i2}}{2} \qquad 3.2.$$

where f_x^i is the factor of the resonance shielding cross-section $\bar{\Sigma}_x^i$.

All the above mentioned considerations are valid for a sample which is small in comparison to the neutron meanfree path length so that neutrons undergo not more than one collision within the sample. Therefore, the reactivity effect appears to be proportional to the number of scattering neutron collisions in the sample $\phi(E) \cdot V_{o\delta} \cdot \Sigma_s^{o\delta}$. Also, when measuring the reactivity coefficients one is obliged to use rather large samples to obtain noticeable reactivity values. If the sample is of the order of one meanfree path or more, then double or multiple scattering becomes possible. However, just after single collisions the neutrons are distributed uniformly over energy, and further collisions do not alter the situation. For large samples, therefore, one observes a decrease of the self-shielding effect with the increase of the sample sizes. Therefore, in order to consider the effect of the sample size it is necessary to know the ratio of the number of neutron collisions in the sample $\phi(E) \cdot V_{o\delta} \cdot \Sigma_s^{o\delta}$ to that of the first neutron collisions which fall upon the surface S of the sample.

It is known that $\phi(E) \cdot \frac{S}{4}$ neutrons fall upon the sample surface, these can either undergo a first collision in the sample (total scattering cross-section of the sample nuclei is $V\Sigma_s^{o\delta}$) or pass through the sample without any collisions with the sample nuclei, and escape through the back surface

(the neutron collision "cross-section" with the sample surface is S/4). Thus, the probability that neutrons collide with the sample nuclei only once is equal to $V_{od}\,\Sigma_s^{od}/(V_{od}\,\Sigma_s^{od} + \frac{S}{4})$ and the number of first neutron collisions in the sample will be equal to $\phi(E)\cdot\frac{S}{4}\cdot V\cdot\Sigma_s'/(V\Sigma_s + \frac{S}{4})$ This is different from the total number of collisions $\phi(E)\cdot V_{od}\,\Sigma_s^{od}$ by the factor:

$$\frac{S/4}{V\cdot\Sigma_s + S/4} = \frac{1}{1 + \bar{\ell}\Sigma_s}$$

where $\bar{\ell} = 4V/S$

Thus, considering the sample size under the integral in formula (3,2) one ought to introduce this factor which, particularly for large size samples ($\bar{\ell}\Sigma_s^{od} \gg 1$), leads to $\delta k \sim \rho$ instead of $\delta k \sim V_{od}$ for small $\bar{\ell}$.

Finally, formula (3.2.) assumes the form:

$$\frac{\Delta k}{k} = -\sum_c \frac{1}{8HD}\cdot V\int_E \Phi(E)\cdot\Phi^+(E)\,x$$

3.3.

$$x\left\{\Sigma_a + \frac{\Sigma_s}{\Sigma_s(1+\bar{e}\Sigma_s)}\cdot\left[\bar{\Sigma}_a\cdot\frac{1-\beta a^2}{2} - \left(\nu_f\frac{\Phi_f^+(E)}{\Phi^+(E)} - 1\right)\Sigma_f\cdot\frac{1-\beta_f^2}{2}\right]\right\}dE$$

In our discussion we assumed that the average neutron flux is distributed uniformly in the sample and near it.

Large departures from this assumption in the resonance region can be expected only for the samples being either strong absorbers (Boron-10) or strong moderators (hydrogen). However, in these cases the effect considered plays a relatively small part in the total reactivity effect of the sample.

In the BFS-16 assembly we studied the reactivity effect produced by the materials for which the reactivity contribution of the absorption and scattering processes are approximately equal. The reactivity effects for these materials (carbon, iron), calculated from general formulae of the perturbation theory, are not in good agreement with experiment (see Table 2).

In our paper an attempt was made to consider the effect of the surrounding medium resonance cross-sections in the calculation of the reactivity worth of carbon and iron in the reactor center with the above described methods. In the calculations we used the resonance cross-sections and the self-shielding coefficients as given in reference [4].

The calculation results are given in the table below.

$\Delta K/K$ / kg.10^5

	characteristic sample size	experiment	perturbation theory calculation	calculation using equation (3.3)
Carbon	3.17	+19.1 ± 1.2	+1.9	1.64
Iron	3.78	- 2.6 ± 0.1	-4.04	-4.1

As seen from this table the consideration of the reactivity effect of the surrounding medium resonance cross-sections does not improve the agreement for moderating materials. One probable reason for the discrepancy between calculation and experiment for these materials may be due to the influence of the assembly heterogeneity on the distribution of the neutron importance.

References

1. Leipunskij, A.I. et al. Paper No. 368 at the Sixth Geneva Conference (1964)
2. Leipunskij, A.I. et al. "Experimental and theoretical investigations in the physics of fast reactors". (London,1966).
3. Keepin, G.R. "The physical basis of Nuclear Reactor Kinetics". Atomzdat (1967).
4. Abagjan, L.P., Bazazyants, N.O., Bondarenko, I.I., Nikolaev, M.N. "Group Constants for nuclear reactor calculations". Atomizdat (1964).
5. Orlov, V.V., Matveev, V.I., Zhukov A.V., Ivanov, A.P., Pshakin G.M. "The basic principles in the choice of control elements for fast power reactors". (4/1969).
6. Mamontov, V.I. et al. "Application of the Boron poison method to the prompt neutron lifetime measurement". FEI-125, (1968).

Table I

Characteristics of Samples

No.	Material	Sample weight, g	Sample type and sizes, mm
I.	Uranium-235 (90% U-235)	296,2	2 slugs d=46.7 h=5.6
2.	Uranium-238(0.42%U-235)	3220	A slug d=46.7 h=I00
3.	Tantalum	547.3	20 slugs d=46.7 h=I.0
4.	Rhenium	362	Powder in container
5.	Europia oxide	45.69	Powder in container d=45 h=40
6.	Boron carbide(of natural enrichment)	6I.I2	2 pellets d=46.7 h=I0
7.	Niobium	642.3	5 slugs d= 46.7 h=I0
8.	Molybdenum	8I7.25	discs d= 46.7 h=50
9.	Tungsten	II45.45	discs d= 46;7 h=50
I0.	Ferrum	I332	I slug d= 46.7 h=I00
II.	Carbon	I37.7	I slug d= 46.7 h=50
I2.	Tantalum diboride	282	pellets d= I0 h=I0 in container
I3.	(Boron of natural enrichment) Chrome diboride (Boron of natural enrichment)	I55	pellets d= I0 h=I0 in container

Continuation of Table I

No.	Material	Sample weight, g	Sample type and sizes, mm		
I4.	Rhenium boride (Boron of natural enrichment)	30I	pellets	d=I0	h=I0 in container
I5.	Europium hexaboride (Boron of natural enrichment)	5.I03	pellets	d=I0	h=I0 in container
I6.	Boron carbide (Boron is enriched up to 80% B-I0)	5.282	pellets	d= 8	h= 5 in container
I7.	Europium hexaboride (Boron is enriched up to 80% B-I0)	8.27	pellets	d= 8	h= 5 in container
I8.	Chrome diboride (Boron is enriched up to 80% B-I0)	9.878	pellets	d= 8	h= 5 in container

Table 2

Reactivity Effects Produced by Different Materials when Placed in EFS-I6 Assembly

No.	Material	$\Delta k/k$ / kg 10^3		Calculation / Experiment	*) **) Correction in % for calculated effect	Corrected Calculation / Experiment
		Experiment	Calculation by perturbation theory			
I	2	3	4	5	6	7
I.	U-235	+I.34 ± 0.02	I.48	I.I		
2.	U-238	-0.I0I ± 0.00I	-0.I2I	I.2	II%	I.07
3.	Ta	-0.424 ± 0.008	-0.562	I.33	35%	0.86
4.	Re	-0.668 ± 0.033	-0.7I0	I;06	I8%	0.87
5.	Eu_2O_3	-2.2 ± 0.0I	-I.89	0.86	I0%	0.78
6.	B_4C	-5.07 ± 0.02	-4.64	0.9I	I4%	0.78
7.	Nb	-0.235 ± 0.005	-0.360	I.53	I3%	I.33
8.	Mo	-0.I62 ± 0.00I	-0.I92	I.I8	6%	I.I2
9.	W	-0.I56 ± 0.00I	-0.22	I.4I	9%	I.28
I0.	Fe	-0.026 ± 0.00I	-0.0404	I.55	20%	I.24
II.	C	+0.I9I ± 0.0I2	+0.0I9	0.I		
I2.	TaB_2	-I.06 ± 0.0I	-I.I2	I.06		
I3.	CrB_2	-I.86 ± 0.02	-I.76	0.95		

Continuation of Table 2

I	2	3	4	5	6	7
I4.	ReB_3	-I.38 ± 0.06	-I.47	I.06		
I5.	EuB_6	-3.57 ± 0.I8	-3.0I	0.84		
I6.	B_4C*	-20.24 ±0.I8	-I9.I	0.94		
I7.	EuB_6*	-8.97 ± 0.I8	-8.3I	0.93		
I8.	CrB_2*	-7.45 ± 0.08	-6.74	0.90		

*) Boron compounds enriched by the isotope B-I0 up to 80%.

**) The correction containing resonance self-shielding effect and neutron field depression near sample and within it.

Table 3

Nuclear Concentration ($\times 10^{24}$) of Elements Entering into Composition of HFS-I6 Assembly Zones.

	Z.M.O.	ZBO	(Lateral shield) Side shield	Interlayers Top	Interlayers Bottom	End shield Top	End shield Bottom
U - 235	0^{2}I4I5	0^{2}2I85	0^{4}52	-	-	0^{4}57	0^{4}5
U - 238	0^{2}666	0^{2}5788	0.0II93	-	-	0^{2}998	0^{2}964
Oxygen	0.0I585	0.0I6II	0.02397	-	-	0.020I	0.0I94
Aluminium	0.0I056	0^{2}938	0^{2}8II	0.0I522	0.0I76	0.0I46	0.0I45
Stainless Steel[a)]	0.02067	0.0205	0.0I374	0.0368	0.0370	0^{2}58I	0^{2}58I

a) Stainless steel contains 73% Fe, I8% Cr, 9% Ni.

Table 4

Dependence of Reactivity Effect Produced by I kg of Boron Carbide of Natural Enrichment and Experimental Correction Value for Neutron Field Depression on Sample Thickness.

No.	Sample weight	Sample thickness, mm	Reactivity effect $\Delta K/K/kg \cdot 10^3$	Correction for neutron flux depression
I.	I22,48	40	4,78 ± 0,0I	I,I8
2.	9I,77	30	4,87 ± 0,0I	I,I6
3.	6I ,I2	20	5,07 ± 0,02	I,II4
4.	30,58	I0	5,24 ± 0,02	I,078
5.	I4,75	9	5,32 ± 0,02	I,06
6.	6,5I5	4	5,58 ± 0,03	I,0I
7.	6,I	4	5,50 ± 0,05	I,025
8.	3,I8I	2	5,6I ± 0,I7	I,005
9.	2,739	2	5,64 ± 0,08	I,0
I0.	0,935	0,6	5,83 ± 0,46	-

Design Diagram of BFS-16 Assembly

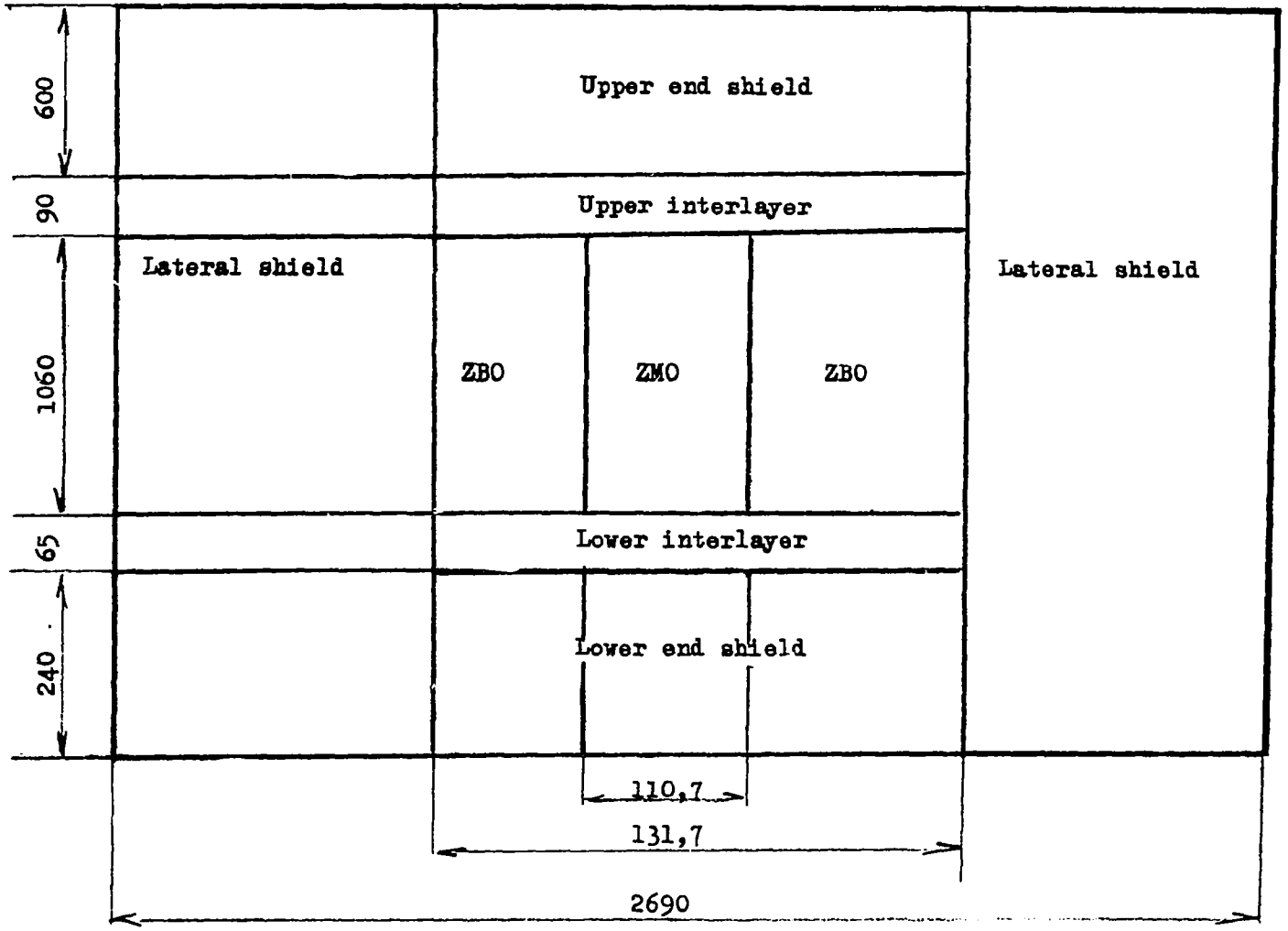

REEVALUATION OF THE U^{235} FISSION AND U^{238} CAPTURE CROSS-SECTIONS BASED ON ANALYSES OF CRITICAL PARAMETERS OF THE ZPR-III CRITICAL ASSEMBLIES

Antonova L.V., Bazazyants N.O., Bariba M.A.,
Markelov I.P., Nikolaev M.N., Troyanov M.F.

The Institute of Physics and Power Engineering
Obninsk, USSR

Translation made at Obninsk
Edited by NDS

Abstract

The present paper considers the changes in the 26-group cross-sections of U-235 fission and U-238 capture occasioned by new measurements and by the current analysis of the whole complex of microscopic data for the indicated cross-sections. Considerations of criticality calculations of the ZPR-III critical assemblies, using the BNAB* set, were also taken into account.

* Translater's note: the'BNAB set' refers to the group constants published in 1964 by Bazazyants, Nikolaev, Abagyan and Bondarenko.

1. Description of Initial Data.

The present paper is part of the program designed to revise and improve the 26-group BNAB set published in 1964 [1] on the basis of new nuclear data and the results of critical and exponential experiments. It was convenient to take advantage of the experimental results of the ZRP-III critical assemblies [2] for this purpose. To analyse the experimental data of the ZPR-III critical assemblies calculations of 22 assemblies using the 26-group P-3 approximation in spherical geometry was carried out with the computer programme M-26 [3] (a slightly corrected transport approximation with isotropic transitions was used [1]). The adequacy of the P-3 approximation to take into account the kinetic effect on k_{eff} of the considered assemblies is based on paper [4] presented at this Symposium. Altogether there were 4 series of calculations. The first series was calculated with the BNAB set; in the other three series the U^{235} fission cross-section of the BNAB set was changed in accordance with the recommendation of Davey [5] and Hart [9]. In addition the U^{238} capture cross-sections of the BNAB set were changed in the 3rd series according to L. Abagyan's recommendation (IPPE), and in the 4th one according to V. Tolstikov and L. Abagyan's recommendations (IPPE). In doing so σ_{tot} and of U^{235} as well as σ_{tot} of U^{238} remained the same and all of the changes introduced in the fission and capture cross-sections of the indicated elements were compensated by adjustment of the elastic scattering.

Table 1 lists the U^{235} fission and U^{238} capture cross-sections used in these calculations.

Tables 5 - 7 show all the group cross-sections of U^{235} and U^{238} used in the four calculation series.

ZPR-III critical assemblies are heterogeneous systems of near-cylindrical geometry having a central air gap. Therefore, in order to obtain the calculation model of these reactors it is necessary to introduce the following corrections into the experimental critical parameters:

a) heterogeneous effects,
b) irregularity of the core boundaries and the central gap,
c) difference between the calculated spherical geometry and the cylindrical one (form-factor).

In the present paper we proceeded from the homogeneous spherical calculation models of the ZPR-III critical assemblies calculated by Davey [2] taking account of structure peculiarities. The following corrections were introduced into the results of these k_{eff} calculations:

a) the difference between Davey's semi-empirically evaluated form-factors and those rigorously calculated by Zizin M.N. [4] using the P_1-approximation.

b) the difference between the corrections for heterogeneity introduced by Davey and the corrections calculated more exactly by Baker [6]. Introduction of these corrections has not influenced the conclusions which were drawn from the present analysis.

It should be noted that the evaluation of heterogeneous effects by Baker and Davey did not take into account neither the resonance heterogeneous effects nor the heterogeneous effects on the diffusion characteristics of the medium; therefore, the results of our calculations contain systematic errors caused by these effects. We hope, however, that these errors do not exceed 0.1 - 0.2% in k_{eff} for the considered critical assemblies have rather hard spectra.

Finally, we note one more reason of possible systematic errors in the calculated results. In the M-26 computer programme which we used [3] (as well as in paper [2]), the influence on the elastic neutron slowing down group cross-section of the difference between the spectral shape within the group, and the standard spectrum assumed in the construction of the group constants [1], was carried out by smoothing of the calculated histograms which were obtained by the P_1 approximation in the preliminary calculations. The errors inherent in this method to account for the elastic slowing down is estimated to be 0.2% to 0.4% in k_{eff}. Thus the resultant systematic error in k_{eff} can be $\sim 0.5\%$

The volumetric material fractions of the cores and reflectors of the ZPR-III critical assemblies are taken from paper [8]. These are given together with the results of the k_{eff} calculations in Table 3. Nuclear densities of the materials of the cores and reflectors are given in Table 2.

2. Discussion of the changes of the U^{235} and U^{238} cross-sections.

In the considered ZPR-III critical assemblies the principal effect on the value of k_{eff} is produced by inaccuracies of the U^{235} fission and U^{238} capture cross-sections. This conclusion is drawn both from the critical assembly analysis carried out by Baker [6] and from the perturbation theory analysis performed at our Institute. The determining influence of these isotopes on k_{eff} is clearly seen from Fig. 1a, where the values of $\Delta k_{eff} = k_{eff}^{-1}$, obtained in the 1st series of calculations (with the BNAB set) are plotted as a function of U^{238} nuclear concentration ratio ρ_8/ρ_5. It is evident that for the critical assemblies with low Uranium-238 content the calculated k_{eff} are over-evaluated by approximately 3 %. As the U^{238} concentration increases, these discrepancies decrease, and when $\rho_8/\rho_5 \approx 10$, they disappear completely. Hence we conclude that the U^{235} cross-sections are too "supercritical" and U^{238} cross-sections are too "subcritical", so that at $\rho_8/\rho_5 \sim 10$ there occurs an error compensation.

The perturbation theory analysis shows that in the case of U^{235}, k_{eff} is decisively affected by the fission cross-section (i.e. $\nu \cdot \sigma_f$), and in the case of U^{238} - by the capture cross-section. Influence of uncertainties in other cross-sections of these isotopes and the cross-sections of other elements is negligible.

The conclusion that the earlier adopted U^{235} fission and U^{238} capture cross-sections should be changed, is confirmed by analyzing the whole complex of the data of these cross-sections, taking the recent results into account. It follows from the above that the analysis of the criticality data of the ZPR-III critical assemblies gives the possibility to introduce corrections to the U^{235} fission and U^{238} capture cross-sections, or to confirm the changes in these cross-sections made on the basis of evaluating new nuclear data. In the present paper the second way of improving these constants is adopted.

To minimize the influence of experimental errors in critical parameters and inaccurate constants of other elements (Al, Na, C, O) contained in the core composition of separate critical assemblies we described the systematic dependence of Δk_{eff} on ρ_8/ρ_5 by a straight line.

It was intended that through the improvement of the constants, that this line generated by a least squares fit of the calculated points, deviates from the abscissa, in the considered range of ρ_8/ρ_5, by not more than a fraction of a percent, i.e. not exceeding the possible magnitude of the systematic error of the calculated results.

As it is seen from Fig. 1b, the change of the U^{235} fission cross-section according to Davey and Hart's recommendations (based primarily on the experimental results of White [7]) leads to the elimination of the systematic discrepancies between theoretical and experimental k_{eff} data, for critical assemblies of considerably low U^{238} content. However, as it should be expected, the calculated values of k_{eff} became considerably lower than unity for critical assemblies with high ρ_8/ρ_5 ratios.

In the 3rd series of calculations (see Fig. 1c) the U^{238} capture cross-sections in the resonance energy region were taken from L. Abagyan's reevaluation (FEI) performed on the basis of new U^{238} resonance parameter data, using sufficiently precise methods which took account of resonance self-shielding [10]. The re-evaluation of the capture cross-section extended also into the higher energy region. The agreement between theoretical and experimental data was markedly improved, as it is seen from Fig. 1c. Finally, the 4th series of calculations, included results of recent evaluations of the U^{238} capture cross-section, the resonance region (L. Abagyan, FEI) as well as in the region above 20 keV (V. Tolstikov, FEI); the results of these calculations are given in Fig. 2a. Fig. 2b shows the same data corrected for heterogeneous effects and form-factors (see Reference [2]) which were mentioned above. It is clear from the last two figures that due to the reevaluation of the U^{235} fission and U^{238} capture cross-sections we can describe the whole complex of k_{eff} of most ZPR-III critical assemblies down to accuracy limits of possible systematic errors. Further improvements of these cross-sections by minimizing the deviations of the calculated k_{eff} from experimental values will therefore be justified only if one performs more precise calculations taking resonance heterogeneous effects, elastic slowing down and other factors into acccunt, which could lead to systematic errors on the order of 1%. Presence of such errors in our calculations is demonstrated by the difference of the curves of Δk_{eff} dependence on ρ_8/ρ_5 given in Figs. 2a, 2b.

Proceeding from the above, we consider the U^{235} fission and U^{238} capture cross-sections adopted in the 4th series of calculations (see Table 1) as optimal and recommended for use in practical calculations. One should bear in mind, however, that rather coarse methods were used in adjusting the cross-sections; the criticality of the considered critical assemblies therefore, is a weak function of the choice of cross-sections in the comparatively low energy region. Table 4 shows the effect of changing the group cross-sections on k_{eff} for one of the assemblies with the softest spectrum. In this connection our recommendations are reliable only in the energy region above $\sim$ 1 keV.

3. Some considerations concerning oxygen, steel, carbon and sodium.

Among 22 critical assemblies under investigation there are 6 for which the calculated values of k_{eff} differ from unity by not more than 0.9 %; for three of them (nos. 30, 31, 35) k_{eff} differs from unity by more than 1.5%. Let us consider the possibility of explaining these discrepancies on the basis of inaccuracies of the nuclear data. One observed that k_{eff} exceeds unity considerably in all three assemblies containing oxygen in the core (the groups of assemblies 4 and 6; assemblies no. 29, 30, 35). However, this does not constitute evidence that the used oxygen constants are inaccurate, because all of these assemblies contain also much steel in the core. At the same time, in the 1st group of the assemblies which contain only steel in the core, except for the U^{235} and U^{238}, there is a tendency to increase Δk_{eff} as the iron volume fraction is increased. This tendency is consistent with the calculation results of k_{eff} for the second group of assemblies containing aluminium: for the assemblies containing $\sim 25\%$ of steel k_{eff} is higher than for the assemblies with 10 - 15 % of steel. Since the steel concentration and the concentration of other elements in these assemblies changes relatively slightly , it is reasonable not to expect a distinct manifestation of investigated effects in this group of assemblies. This tendency manifests itself most clearly in the results of the calculations of the 5th group of assemblies containing sodium. The substitution of U^{238} for steel, retaining the volume fractions of U^{235} and sodium in the core, led to a strong rise of k_{eff} in assembly no. 33 in comparison with assembly no. 36. Finally, oxygen influence on criticality manifests itself principally in a softened neutron spectrum at the expense of elastic slowing down. It is difficult to allow so great inaccuracies in the oxygen scattering cross-section that can lead to discrepancy of 1.5 % in k_{eff}. It would be more sensible to assume the existence of inaccuracies when taking into account elastic slowing down in a group approximation. However, this assumption must also be eliminated, because the criticality of those assemblies containing carbon in rather large concentrations (in the 4th group of assemblies) is not badly described.

On the basis of the above we suppose that those steel constants which we used are in need of improvement. The noted tendency for k_{eff} to increase with an increasing volume fraction of steel in the critical assemblies under consideration is not so pronounced that one can give any recommendations to change the steel cross-sections on the basis of their effect on criticality in this analysis.

REFERENCES

1. L.P. Abagyan, N.O. Bazaziantz, I.I. Bondarenko, M.N. Nikolaev, "Group Constants for Nuclear Reactor Calculations" Atomizdat, 1964.

2. W.G. Davey, "An Analysis of 23 ZPR-III Fast-Reactor Critical Experiments". Nucl. Sci. and Eng. 19, 259, 1964.

3. Sh.S. Nikolaishvili, V.G. Zolotukhin, I.P. Markelov, A.A. Bliskavka, "Methods and Programmes for Fast Reactors Calculation". See paper no. 1 of this Compilation.

4. M.N. Zizin, "Calculation of Integral Experiments on Fast Critical Assemblies ZPR-III, ZEBRA, VERA, and BFS".

5. W.G. Davey, "An Analysis of the Fission Cross-Section of Th^{232}, U^{333}, U^{235}, U^{234}, U^{236}, U^{238}, Np^{237}, Pu^{239}, Pu^{240}, Pu^{241} and Pu^{242} from 1 keV to 10 MeV".

6. A.R. Baker, "A Systematic Study of the Accuracy of Multigroup Criticality Calculations for Fast Critical Assemblies". The British Nuclear Energy Society. 6, 249, 1967.

7. P.N. White, "Measurements of the U^{235} Neutron Fission Cross-Section in the Energy Range 0.04 - 14 MeV". Journal of Nuclear Energy. P A/B, 19, 325, 1965.

8. W.G. Davey, "K Calculations for 22 ZPR-III Fast Reactor Assemblies Using ANL Cross-Sections set 635". ANL-657o, 1962.

9. W.Hart, "Fission Cross-Section Data Files for Th^{232}, U^{234}, U^{235}, U^{236}, U^{238}, Np^{237}, Pu^{239}, Pu^{240}, Pu^{241} in the Energy Range 1 keV to 14 MeV". AHSB(S) R 124, London, 1967.

10. L.P. Abagyan, M.N. Nikolaev, L.V. Petrova, "Calculation of the U-238 Cross-sections with the URAN Programme". Nuclear Data Centre Bulletin, Volume 4, Atomizdat, 1967.

Table 1

Group Values of U^{235} Fission and U^{238} Capture Cross-Sections Used in 4 Series of Calculation of the Critical Assemblies

№ № groups	E_n	$\sigma_f(U^{235})$ variants		$\sigma_c(U^{238})$ variants		
		I	2	I	2	3
		series of calculations		series of calculations		
		I	2,3,4	I,2	3	4
I	6.5 - I0.5 MeV	I.75	I,63	0.00	0.00	0.00
2	4.0 - 6.5	I.I5	I.II5	0.0I	0.0I	0.0I
3	2.5 - 4.0	I.25	I.200	0.02	0.02	0.02
4	I.4 - 2.5	I.28	I.280	0.06	0.06	0.06
5	0.8 - I.4	I.25	I.2I0	0.I3	0.I3	0.I4
6	0.4 - 0.8	I.23	I.I60	0.I3	0.I3	0.I3
7	0.2 - 0.4	I.4I	I.3I5	0.I5	0.I5	0.I4
8	0.I - 0.2	I.70	I.52I	0.22	0.I8	0.I8
9	46.5 - I00. kev	2.I0	I.802	0.35	0.27	0.26
I0	2I.5 - 46.5	2.65	2.257	0.46	0.45	0.4I
II	I0.0 - 2I.5	3.40	2.872	0.60	0.68	0.6I
I2	4.65- I0.0	4.40	3.722	0.78	0.9I	0.8I
I3	2.I5- 4.65	5.40	4.968	I.20	I.30	I.I6
I4	I.0 - 2.I5	7.30	6.838	2.I0	2.00	I.84
I5	465 - I000 ev	II.0	II.0	3.60	3.40	3.2
I6	2I5 - 465	I6.0	I6.0	4.50	4.35	4.4
I7	I00 - 2I5	22	22	I7.0	20.0	20
I8	46.5 - I00	35	35	I5.0	I7.0	I7.0
I9	2I.5 - 46.5	45	45	58.0	57.0	57.0
20	I0 - 2I.5	45	45	82.0	78.0	78.0
2I	4.65- I0	37	37	I7I	I74.0	I74.0
22	2.I5- 4.65	20	20	0.54	0.54	0.64
23	I.0 - 2.I5	35	35	0.47	0.47	0.48
24	0.465- I.0	64	64	0.58	0.58	0.52
25	0.2I5- 0.465	I55	I55	0.90	0.90	0.76
26	0.0252	582	582	2.7I	2.7I	2.73

Table 2

Composition of Critical Assemblies ZPR-III
(nuclei/cm^3·10^{-22})

group of assemblies		U^{235}	U^{238}	Fe	Ni	Cr	Al	Na	C	O	Mo	Zr			
	A	235	238	55,87	58,7I	52,0I	26,98	22,99	I2,0I	I6,0	95,95	9I,22			
	γ g/cm^3	I8,75	I8,97	7,85	8,90	6,9I	2,70	0,84	I,67	2,55	I0,I9	6,44			
	$10^{-22}\cdot N$ nuclei/cm^3	4,80	4,80	8,47	9,I3	8,00	6,03	2,20	8,37	9,60	6,40	4,25			
	Assembly No.												reflector type	$M_{Cr.}$	$R_{Sph\ core}$
I	25	0,344	3,56	0,555	0,0840	0,I40							A	564	46,44
	24	0,363	3,50	0,566	0,0858	0,I43							A	456	42,49
	II	0,457	3,44	0,555	0,0840	0,I40							A	239	3I,75
	I0	0,569	2,78	I,I7	0,I78	0,296							A	I53	25,43
	32	0,445	0,03I7	4,92	0,747	I,24							A	2I3	30,83
2	9A	0,662	I,82	0,863	0,I3I	0,2I8	I,30						A	I5I	25,42
	20	0,292	0,9II	0,869	0,I32	0,220	I,52				0,322	0,I84	B	408	44,02
	3I	0,279	0,439	I,49	0,226	0,376	I,42						A	437	45,75
	6F	0,672	0,763	0,746	0,II3	0,I89	I,89						A	I33	22,96
	5	0,672	0,763	0,740	0,II2	0,I87	I,90						Ⓐ	I56	24,2I
	2A	0,67I	0,049	I,67	0,254	0,422	I,90						A	I44	23,58
	23	0,445	0,0336	0,55I	0,083I	0,I39	2,58						A	249	32,46
3	34	0,224	0,494	I,49	0,226	0,378	I,58		0,760				A	475	50,59
4	29	0,239	0,479	I,50	0,227	0,379	I,47			I,39			A	402	46,88
	30	0,284	0,434	I,49	0,226	0,376	I,4I			0,697			A	377	43,30
5	36	0,450	2,38	0,770	0,II7	0,I94		0,40I					A	2I7	30,90
	33	0,445	0,0326	3,86	0,586	0,976		0,400					A	225	3I,38
6	35	0,I95	0,0I39	3,0I	0,457	0,760		0,782		0,398			C	485	53,38
7	I6	0,450	2,4I	0,555	0,084	0,I40			I,52				A	202	30,I6
	I2	0,450	I,70	0,555	0,084	0,I40			2,68				A	I72	28,58
	I7	0,450	0,989	0,555	0,084	0,I40			3,82				A	I5I	27,37
	I4	0,450	0,0336	0,555	0,084	0,I40			5,35				A	I32	26,I7

REFLECTOR

type	U^{235}	U^{238}	Fe	Ni	Cr	Al	Na	Mo
A	0.00912	4.00	0.440	0.0667	0.II2			
B	0.00480	2.I8	I.I8	0.I79	0.298	0.608		0.I57
C	0.00432	I.90	I.I5	0.I74	0.290		0.7I5	0.I40
Ⓐ	0.00384	I.9I	0.444	0.0676	0.II2	I.48		
	0.00912	4.00	0.444	0.0676	0,II2	0,I37		

In all these cases the reflector density is 30 cm

Internal reflector, density 18.1cm

External reflector, density I8,I cm

Table 3

Results of Calculation of Critical Assemblies

groups of assemblies	№ assemblies	$\rho(U^{238})/\rho(U^{235})$	Volume fractions of the core materials							$R^{sph}_{акт. зоны}$, cm	$\Delta K_{eff.} = (K_{eff.} - 1)$, %				
			U^{235}	U^{238}	steel	Al	Na	C	O		$\Delta K^{*}_{eff.}$	series № 4	3	2	1
I	25	10,3	7,17	74,17	9,22					46,44	-0,44	-0,44	-1,41	-4,11	-0,25
	24	9,6	7,57	72,90	9,41					42,49	-0,55	-0,44	-1,28	-0,84	-0,03
	II	7,5	9,51	71,72	9,22					31,75	-0,08	-0,41	-0,94	-3,19	0,45
	10	4,9	11,85	57,90	19,47					25,43	0,44	0,09	-0,34	-2,17	1,33
	32	0,07	9,26	0,66	81,77					30,83	0,92	1,23	0,89	-0,06	3,36
2	9A	3,2	11,70	38,00	14,35	21,50				25,42	0,57	0,37	-0,07	-1,67	1,79
	20	3,1	6,09	18,97	14,45	25,14				44,02	0,22	-0,13	-0,65	-2,12	1,84
	31	1,6	5,81	9,14	24,76	23,49				45,75	1,85	1,41	0,90	-0,46	3,25
	6Ф	1,1	14,00	15,90	12,41	31,40				22,96	0,52	0,62	0,26	-0,98	2,20
	5	1,1	14,00	15,90	12,31	31,50				24,21	0,58	0,88	0,48	-0,52	2,68
	2A	0,07	13,97	1,02	27,77	31,44				23,58	0,51	0,81	0,48	-0,56	2,56
	23	0,07	9,27	0,70	9,16	42,82				32,46	0,34	0,84	0,44	-0,75	2,50
3	34	2,2	4,67	10,30	24,83	25,50		9,08		50,59	0,20	0,60	-0,16	-1,30	2,76
4	29	2,0	4,97	9,97	24,93	24,40			14,50	46,88	1,10	1,73	0,96	-0,18	3,94
	30	1,5	5,91	9,04	24,73	23,35			7,26	43,30	2,58	2,17	1,61	0,33	4,15
5	36	5,3	9,37	49,51	12,80		18,23			30,90	-0,14	-0,23	-0,71	-2,67	0,92
	33	0,07	9,27	0,68	64,20		18,20			31,38	1,09	1,54	1,22	0,21	3,55
6	35	0,07	4,06	0,29	50,02		35,56		4,15	53,38	1,78	1,46	1,14	0,54	4,07
	16	5,3	9,38	50,10	9,22			18,10		30,16	0,18	-0,02	-0,69	-2,59	1,24
	12	3,8	9,38	35,40	9,22			31,96		28,58	-0,57	-0,13	-0,87	-2,36	1,49
	17	2,2	9,38	20,60	9,22			45,68		27,37	-0,60	-0,10	-0,82	-1,96	1,73
	14	0,07	9,38	0,70	9,22			63,92		26,17	-1,27	-0,17	-0,55	-1,38	1,68

$\Delta K^{*}_{eff.} = \Delta K_{eff.}$ (of the 4th series) + corrections for the calculation inaccuracy of the formfactor and heterogeneity for the initial model, obtained by Zizin [4] and Baker [6].

Table 4

The Perturbation Theory Coefficients (R) of the 29th Assembly in Reference to U^{235} Fission and U^{238} Capture

$$\Delta\left(\frac{1}{K_{eff.}}\right)\% = R \cdot \frac{\Delta\sigma}{\sigma}\%$$

№ № groups	E_n				Coefficients R U^{235} fission	Coefficients R U^{238} capture
I	6.5	-	I0.5	MeV	0.00I73	0.00000
2	4.0	-	6.5		0.006I8	-0.00008
3	2.5	-	4.0		0.0I437	-0.0009I
4	I.4	-	2.5		0.02804	-0.00233
5	0.8	-	I.4		0.0398I	-0.00773
6	0.4	-	0.8		0.06978	-0.0I784
7	0.2	-	0.4		0.09937	-0.02773
8	0.I	-	0.2		0.09343	-0.03292
9	46.5	-	I00	kev	0.08886	-0.04005
I0	2I.5	-	46.5		0.04674	-0.0I928
II	I0.0	-	2I.5		0.02434	-0.00940
I2	4.65	-	I0.0		0.0I079	-0.00376
I3	2.I5	-	4.65			
I4	I.0	-	2.I5		0.00423	-0.00I50
I5	465	-	I000	ev		
I6	2I5	-	465		0.00I57	-0.00054
I7	I00	-	2I5			
I8	46.5	-	I00		0.00025	-0.00008
I9	2I.5	-	46.5			
20	I0.0	-	2I.5			
2I	4.65	-	I0.0		0.00003	-0.00000
22	2.I5	-	4.65			
23	I.0	-	2.I5			
24	0.465	-	I.0		0.00000	-0.00000
25	0.2I5	-	0.465			
26	thermal					

Table 5

Group Cross-Sections of U^{235}

(series 2, 3, 4)

group i	σ_t	σ_f	ν	σ_c	σ_{in}	σ_e	μ_e	ξ	$\sigma_{s(e)}$
I	6.30	I.630	3.40	0.0I9	I.03	3.62I	0.84	0.00I3	0.024
2	7.40	I.II5	3.04	0.029	I.92	4.336	0.80	0.00I7	0.025
3	7.70	I.200	2.79	0.038	I.9I	4.552	0.7I	0.0024	0.027
4	7.00	I.280	2.63	0.060	I.76	3.900	0.55	0.0038	0.026
5	6.60	I.2I0	2.52	0.II6	I.38	3.894	0.45	0.0046	0.03I
6	7.40	I.I60	2.46	0.I60	I.20	4.880	0.35	0.0054	0.039
7	9.20	I.3I5	2.47	0.233	I.00	6.652	0.23	0.0064	0.062
8	II.2	I.52I	2.45	0.358	0.60	8.72I	0.I3	0.0073	0.092
9	I2.5	I.802	2.44	0.5I5	0.I8	I0.00	0.07	0.0078	0.I0I
IC	I4.0	2.257	2.43	0.852	0.06	I0.84	0.04	0.008I	0.II4
II	I6.0	2.872	2.42	I.267	-	II.86	0.02	0.0082	0.I26
I2	I9.0	3.722	2.42	I.776	-	I3.50	0.0I	0.0083	0.I46
I3	23.0	4.968	2.42	2.530	-	I5.50	0.00	0.0084	0.I69
I4	27.0	6.838	2.42	3.560	-	I6.60	0.00	0.0084	0.I82
I5	32.0	II.0	2.42	6.3	-	I4.70	0.00	0.0084	0.I60
I6	38.0	I6.0	2.42	9.5	-	I2.5	0.00	0.0084	0.I36
I7	47.7	22	2.42	I3.5	-	I2.2	0.00	0.0084	0.I33
I8	69.0	35	2.42	22	-	I2	0.00	0.0084	0.I3I
I9	88.0	45	2.42	3I	-	I2	0.00	0.0084	0.I3I
20	III.	45	2.42	54	-	I2	0.00	0.0084	0.I3I
2I	93.0	37	2.42	44	-	I2	0.00	0.0084	0.I3I
22	39.0	20	2.42	7	-	I2	0.00	0.0084	0.I3I
23	6I.0	35	2.42	I3	-	I3	0.00	0.0084	0.I42
24	88.0	64	2.42	I0	-	I4	0.00	0.0084	0.I53
25	205	I55	2.42	35	-	I5	0.00	0.0084	0.I64
T	698	582	2.42	I0I	-	I5	0.00	-	-

Table 6

Group Cross-Sections of U^{238}
(series 3)

group i	σ_t	σ_f	ν	σ_c	σ_{in}	σ_e	μ_e	ξ	$\sigma_{3(e)}$
I	6.30	I.00	3.48	0.00	I.80	3.50	0.84	0.00I3	0.023
2	7.50	0.58	3.09	0.0I	2.5I	4.40	0.80	0.00I7	0.025
3	7.70	0.58	2.87	0.02	2.60	4.50	0.7I	0.0024	0.027
4	7.I0	0.49	2.67	0.06	2.25	4.30	0.53	0.0039	0.029
5	6.90	0.02	2.58	0.I3	2.I5	4.60	0.42	0.0049	0.040
6	7.80	-	-	0.I3	I.65	6.02	0.33	0.0056	0.049
7	9.60	-	-	0.I5	I.05	8.40	0.2I	0.0066	0.080
8	II.5	-	-	0.I8	0.55	I0.77	0.I2	0.0074	0.II6
9	I3.23	-	-	0.27	0.I9	I2.77	0.07	0.0078	0.I29
I0	I3.75	-	-	0.45	-	I3.30	0.04	0.008I	0.I40
II	I4.59	-	-	0.68	-	I3.9I	0.02	0.0082	0.I48
I2	I5.86	-	-	0.9I	-	I4.95	0.0I	0.0083	0.I6I
I3	I7.93	-	-	I.30	-	I6.63	0.00	0.0084	0.I8I
I4	2I.0I	-	-	2.00	-	I9.0I	0.00	0.0084	0.207
I5	22.7	-	-	3.40	-	I9.3	0.00	0.0084	0.2II
I6	22.I5	-	-	4.35	-	I7.8	0.00	0.0084	0.I94
I7	87.9	-	-	20.0	-	67.9	0.00	0.0084	0.74I
I8	42.2	-	-	I7	-	25.2	0.00	0.0084	0.275
I9	I34.7	-	-	57	-	77.7	0.00	0.0084	0.848
20	II0.8	-	-	78	-	32.8	0.00	0.0084	0.358
2I	I93.I	-	-	I74	-	I9.I	0.00	0.0084	0.208
22	9.54	-	-	0.54	-	9.0	0.00	0.0084	0.098
23	9.47	-	-	0.47	-	9.0	0.00	0.0084	0.098
24	9.58	-	-	0.58	-	9.0	0.00	0.0084	0.098
25	9.90	-	-	0.90	-	9.0	0.00	0.0084	0.098
T	II.7	-	-	2.7I	-	9.0	0.00	-	-

Table 7

Group Cross-Sections of U^{238}
(series 4)

group i	σ_t	σ_f	ν	σ_c	σ_{in}	σ_e	μ_e	ξ	$\sigma_3(\ell)$
I	6.30	I.00	3.48	0.00	I.80	3.50	0.84	0.00I3	0.023
2	7.50	0.58	3.09	0.0I	2.5I	4.40	0.80	0.00I7	0.025
3	7.70	0.58	2.87	0.02	2.60	4.50	0.7I	0.0024	0.027
4	7.I0	0.49	2.67	0.06	2.25	4.30	0.53	0.0039	0.029
5	6.90	0.02	2.58	0.I4	2.I5	4.59	0.42	0.0049	0.039
6	7.80	-	-	0.I3	I.65	6.02	0.33	0.0056	0.049
7	9.60	-	-	0.I4	I.05	8.4I	0.2I	0.0066	0.080
8	II.5	-	-	0.I8	0.55	I0.8	0.I2	0.0074	0.II6
9	I2.8	-	-	0.26	0.I9	I2.4	0.07	0.0078	0.I26
I0	I3.5	-	-	0.4I	-	I3.I	0.04	0.008I	0.I38
II	I4.0	-	-	0.6I	-	I3.4	0.02	0.0082	0.I43
I2	I5.5	-	-	0.8I	-	I4.7	0.0I	0.0083	0.I58
I3	I6.5	-	-	I.I6	-	I5.3	0.00	0.0084	0.I67
I4.	I8.0	-	-	I.84	-	I6.2	0.00	0.0084	0.I77
I5	23.0	-	-	3.2	-	I9.8	0.00	0.0084	0.2I6
I6	I8.5	-	-	4.4	-	I4.I	0.00	0.0084	0.I54
I7	80.0	-	-	20	-	60	0.00	0.0084	0.655
I8	40.0	-	-	I7	-	23	0.00	0.0084	0.25I
I9	I40	-	-	57	-	83	0.00	0.0084	0.906
20	I20	-	-	78	-	42	0.00	0.0084	0.458
2I	I90	-	-	I74	-	I6	0.00	0.0084	0.I75
22	9.54	-	-	0.64	-	9.0	0.00	0.0084	0.097
23	9.47	-	-	0.48	-	9.0	0.00	0.0084	0.098
24	9.58	-	-	0.52	-	9.06	0.00	0.0084	0.099
25	9.90	-	-	0.76	-	9.I4	0.00	0.9084	0.I00
T	II.7	-	-	2.73	-	8.97	0.00	-	-

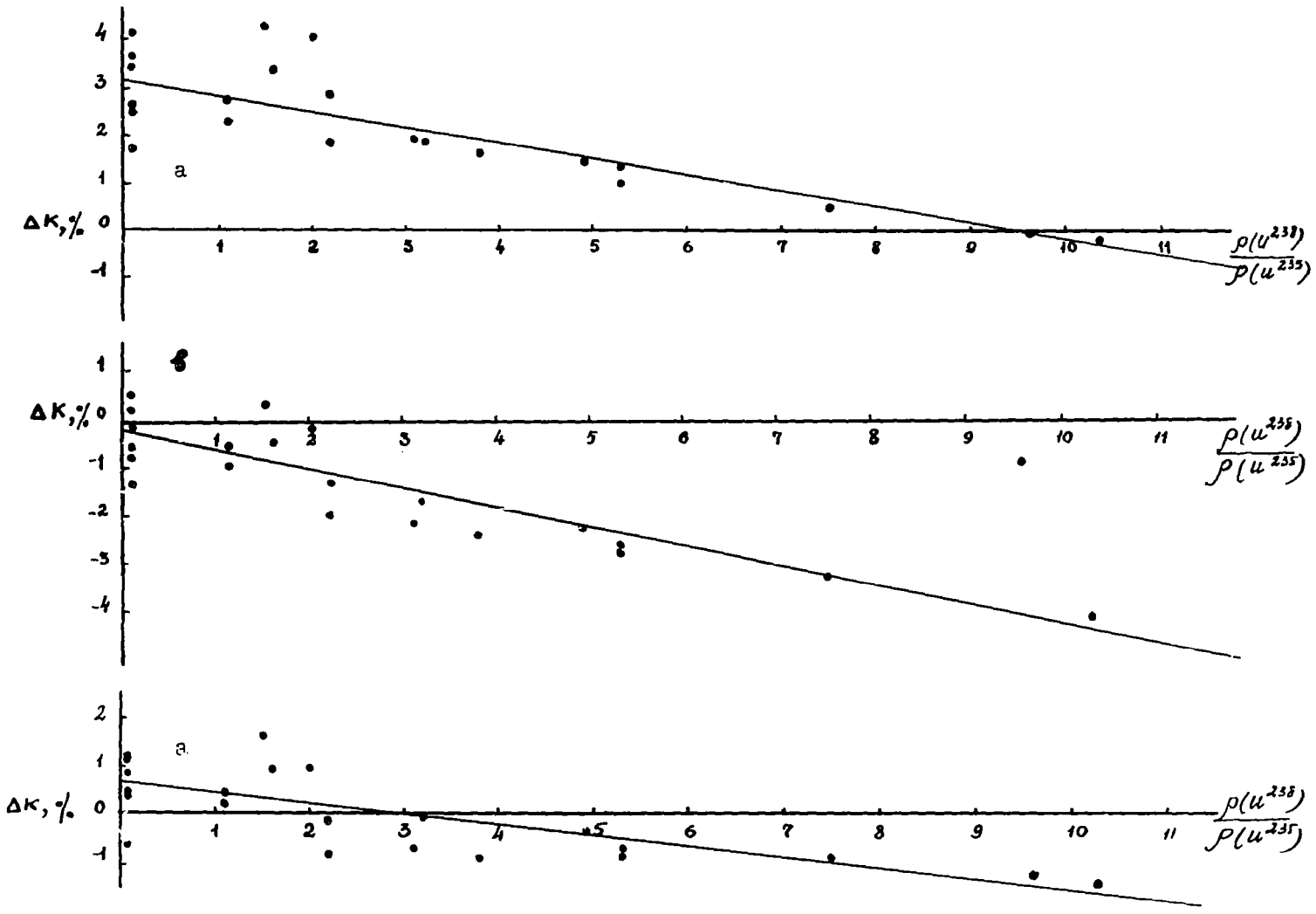

Fig. 1. $\Delta K_{eff.}$ dependence in calculation series 1,2,3 on ratio $\rho(U^{238})/\rho(U^{235})$

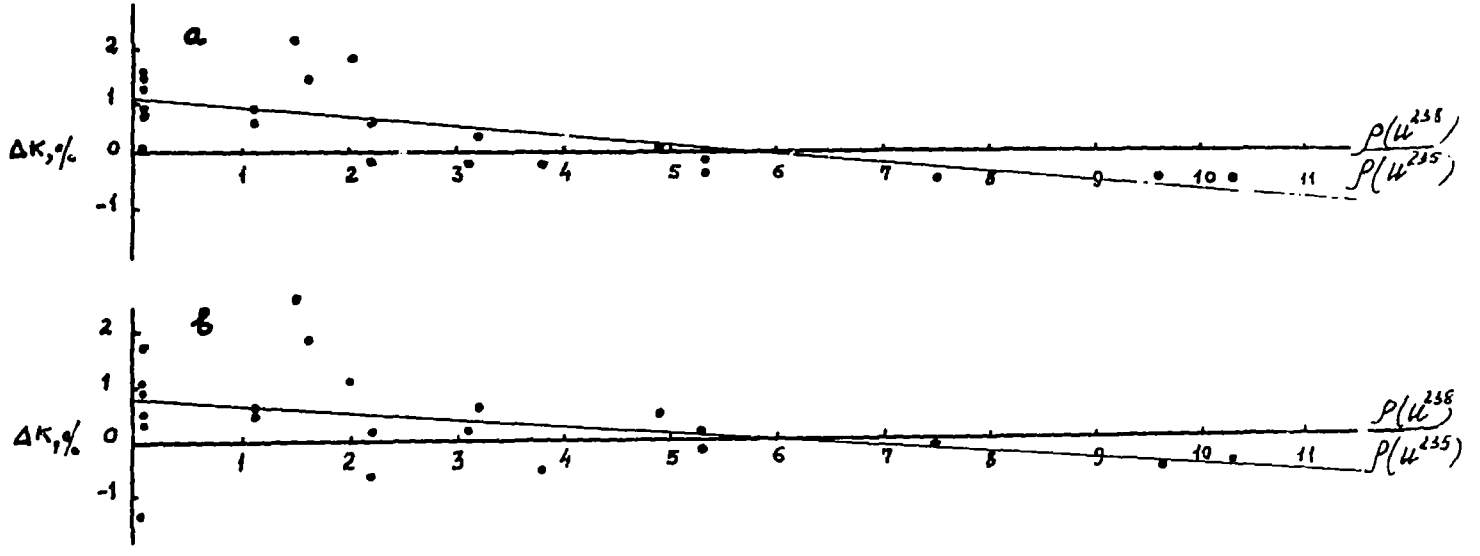

Fig. 2. $\Delta K_{eff.}$ dependence in 4th calculation series on ratio $\rho(U^{238})/\rho(U^{235})$